PHOTOLYSIS OF ALPHA AND BETA-TIN DI IODIDE

by

TITILAYO ADELAJA KUKU

A thesis submitted in partial fulfilment of the requirements

for the Degree of Doctor of Philosophy

of the University of London

Department of Electrical Engineering,
Imperial College of Science & Technology,
London, S.W.7.

June 1981

ABSTRACT

Powder samples of the two polymorphs of tin diiodide have been prepared. Thin films of both polymorphs prepared by vacuum evaporation have been photolysed with both narrow and broad band radiation. The effects of time, temperature, light intensity, doping, substrate type, oxygen or air ambient, film thickness, wavelength, crystal microstructure and oxygen uptake on the kinetics of the photolysis have been investigated. The kinetics have been followed by the use of a quartz crystal microbalance method (i.e. a mass decrease method).

The kinetics were found to divide into three main regimes,an initial regime in which the reaction extent is linearly dependent on time, t, a $\sim t^{+3/4}$ proportionality regime and finally a $t^{+\frac{1}{2}}$ regime. An anion vacancy diffusion mechanism has been proposed for the linear regime, while the $t^{+3/4}$ regime has been inferred to be due to tin metal cluster formation. The terminal regime has been related to bulk metallic tin properties.

Optical and electrical properties of both polymorphs of SnI_2 were also investigated. The optical transition in both polymorphs have been found to be characterised by direct and indirect allowed transitions.

The phase transition temperature from the α-(red) to the β-(yellow) polymorph has been correctly determined, while the crystal system of the β-polymorph has been derived from x-ray analysis of powder specimens.

The photolytic process has been applied to the formation of tin metal patterns of good resolution, and the production of transparent and semiconducting stannic oxide thin films.

LIST OF CONTENTS

		Page
1.	INTRODUCTION	1
	1.0 General Introduction	1
	1.1 Photocomposition of the Lead Halides	3
	1.2 Previous Knowledge of SnI_2	10
	1.2.1 Crystal Structure of Stannous Iodide	10
	1.2.2 Optical Properties of SnI_2	13
	1.2.3 Electrical Properties	14
	1.3 Choice of Experimental Technique for the Photochemical Reaction	15
	1.4 Range of Kinetic Data	17
	References	18
2.	THE POWDER FORM OF SnI_2	22
	2.1 Preparation of SnI_2 Powder	22
	2.2 X-ray Analysis of Powder Specimen	23
	2.3 Phase Change from α to β-SnI_2	29
	2.4 Types of Polymorphic Transformation	30
	2.4.1 Displacive Transformations	30
	2.4.2 Reconstructive Transformations	31
	2.4.3 Order-disorder Transformations	33
	2.5 Thermodynamics of Polymorphic Transformations	33
	2.5.1 First Order Transformations	34
	2.5.2 Second Order Transformations	36
	2.5.3 Third Order Transformations	38
	2.6 Mechanism of Phase Transition in SnI_2	39
	References	44

Page

3. OPTICAL AND ELECTRICAL PROPERTIES 46

3.1 Optical Properties 36

3.1.1 Determination of Optical Constants - Theory 46

3.1.2 Intrinsic Optical Absorption Band - Theory 49

3.2 Experimental Set-up for Optical Measurements 53

3.3 Results 56

3.4 Discussion 66

3.5 Electrical Conductivity 74

3.5.1 Experimental Set-up for Conductivity Measurements 75

3.5.2 Results and Discussion of Conductivity Experiments 76

3.6 Electrical Resistivity 79

References 82

4. EXPERIMENTAL 85

4.1 The Quartz Crystal Microbalance 85

4.2 Calibration of the Quartz Crystal Microbalance 90

4.3 Temperature Stabilisation 90

4.4 Thin Film Production 92

4.5 Light Source and Optical Filters 94

4.6 Photolysis Arrangement 99

4.7 The Vacuum Equipment 104

References 107

5. THE PHOTOCHEMICAL REACTION 108

5.1 Preliminary Studies 108

5.2 Kinetic Studies 113

5.2.1 Time Dependence of the Photolysis 113

5.2.2 Film Thickness Dependence 118

5.2.3 Temperature Effect 121

Page

5.2.4 Influence of Film Composition (doping) 121

5.2.5 Substrate Effect 126

5.2.6 Photolysis Ambient 126

5.2.7 Oxygen Uptake 128

5.2.8 Wavelength Dependence 128

5.2.9 Light Intensity 131

5.2.10 Crystal Microstructure 133

References 137

6. DISCUSSION OF KINETIC RESULTS 138

6.1 Photochemical Reaction Sites 138

6.2 Defect Nature of SnI_2 140

6.3 Qualitative Model for Photolysis in the Primary Regime 142

6.4 Quantitative Model for Photolysis in the Primary Regime 143

6.5 Reaction Mechanism 148

6.6 Model for Photolysis in the Intermediate Regime 157

6.7 Model for Photolysis in the Terminal Stage 163

References 165

7. TECHNOLOGICAL APPLICATION OF THE PHOTOLYTIC PROCESS 167

7.1 Transparent Tin Oxide Films 167

7.2 Production of SnO_2 Films 169

7.3 Physical Properties of SnO_2 Films 170

7.3.1 Optical Characteristics 170

7.3.2 Electrical Properties 171

7.3.3 X-ray Analysis 175

7.3.4 Discussion 176

Page

7.4 Metal Film Production 177

7.4.1 Evaporation of SnI_2 179

7.4.2 Photolysis of SnI_2 Films 179

7.4.3 Re-evaporation of SnI_2 Films 179

7.4.4 Reduction of SnO_2 Pattern to Sn Pattern 180

7.4.5 Discussion 184

References 186

LIST OF FIGURES

		Page
1.1	Tin (II) iodide projection on (010)	11
1.2	Coordination of Sn(1) projection on (100)	11
1.3	The coordination of Sn(2) viewed along (100)	11
2.1	Variation of structure energy with temperature for first order phase transitions	35
2.2	Variation with temperature of the structure energy, the specific heat and order	37
2.3	Layer structure of PbI_2 (2H)	42
3.1	Energy band structure for different forms of optical transition	51
3.2	Substrate holder arrangement for the evaporation of SnI_2 on glass substrates	55
3.3	Experimental arrangement for optical measurements	57
3.4	Room temperature transmission spectra of α- and β-SnI_2 thin films	58
3.5	Room temperature reflection spectra of α- and β-SnI_2 thin films	59
3.6	Room temperature optical transmission for yellow SnI_2 films	61
3.7	Variation of absorption coefficient with wavelength for α- and β-SnI_2 films	62

		Page
3.8	Variation of refractive index and extinction coefficient with wavelength for α-SnI_2 films	63
3.9(a)	Variation of refractive index and extinction coefficient with wavelength for β-SnI_2 films	64
(b)	Variation of refractive index and extinction coefficient with wavelength for PbI_2 films	65
3.10	Absorption edge structure for α-SnI_2 at room temperature	67
3.11	Absorption edge structure for β-SnI_2 at room temperature	68
3.12	$(n^2-1)^{-1}$ against the square of photon energy; for α- and β-SnI_2	71
3.13	Process steps in the preparation of a SnI_2 film for conductivity measurements	77
3.14	Diagram of a constant current source	78
3.15	Log (resistivity) against inverse temperature for thin films of SnI_2	80
4.1	Oriented quartz crystal cuts in relation to the natural crystal	87
4.2	Quartz crystal dimensions and defined gold electrode configuration	84
4.3	Evaporation source arrangement	93
4.4	Log of vapour pressure against reciprocal temperature for SnI_2, CuI and PbI_2	95

		Page
4.5	Radiance variation with wavelength for the 650 watts quartz halogen light source	97
4.6	Transmission of broad band copper sulphate solution filter	98
4.7	Photolysis arrangement	100
4.8	Circuit diagram for light intensity determination	103
4.9	Vacuum equipment diagram	103
4.10	Mass spectrometer analysis of residual gases in the vacuum equipment used for photolysis	106
5.1	Transmission spectra of photolysed and unphotolysed β-SnI_2 films	110
5.2	Time dependence of the photolysis of α and β-SnI_2	114
5.3	Time dependence of the photolysis of α and β-SnI_2	115
5.4	Long time dependence of the broad band photolysis of β-SnI_2	116
5.5	Plot of log (extent of reaction) against log (time) for data of Fig. 5.4	117
5.6	Time dependence of the photolysis of α-SnI_2	119
5.7	Film thickness dependence of photolysis of α-SnI_2	120
5.8	Temperature dependence of rate of photolysis for α- and β-SnI_2	122
5.9	Arrhenius plot of log (rate) against reciprocal temperature	123

		Page
5.10	Doping and substrate effects on photolysis of α-SnI_2	124
5.11	Doping effect on β-SnI_2 photolysis	125
5.12	Ambient effect on β-SnI_2 photolysis	127
5.13	Wavelength dependence of α-SnI_2 photolysis	129
5.14	Wavelength dependence of β-SnI_2 photolysis	130
5.15	Light intensity dependence of α- and β-SnI_2 photolysis	132
5.16	Effect of substrate temperature for film deposition on α- and β-SnI_2 film photolysis	136
6.1	Space charge region in the SnI_2 - W interface	153
6.2	Experimental set-up for the photolysis of powder samples of SnI_2	159
7.1	Room temperature optical transmission for SnO_2 films	172
7.2	Plot of α^2 against photon energy for SnO_2 films	173
7.3	Log (resistivity) against reciprocal temperature plot for SnO_2 films	174
7.4	Process stages in the production of tin metal patterns from SnI_2 films	178

LIST OF TABLES

		Page
1.1	Representative bond lengths and angles for SnI_2	12
2.1	Indexed x-ray powder data for the red (α-) polymorph of SnI_2	26
2.2	Indexed x-ray powder data for the yellow (β-) polymorph of SnI_2	27
3.1	Comparison of the energies of direct and indirect (allowed) transitions for SnI_2	69
4.1	Characteristics of optical interference filters	99
4.2	Characteristics of silicon photodiode type OSD-50-1	102
4.3	Calibration characteristics for diode type OSD-50-1	102
5.1	Features obtained from the x-ray analysis of photolysed and unphotolysed β-SnI_2 films	112
6.1	Calculation of mean diffusion length ℓ_D for the β-polymorph	147
6.2	d(A°) spacings calculated from the x-ray pattern of photolysed powder samples	161

LIST OF PLATES

		Page
2.1	X-ray diffraction patterns for α- and β-SnI_2 powder samples	25
2.2	Model of the α-SnI_2 structure	40
4.1	The quartz crystal plate and the ovens that surround it	91
4.2	The vacuum equipment used in the photolysis experiments	105
5.1	X-ray diffraction patterns for photolysed and unphotolysed thin films of β-SnI_2	111
5.2	Substrate temperature effect on the crystal microstructure of SnI_2 films	135
6.1	X-ray diffraction pattern for photolysed and unphotolysed α-SnI_2 powder samples	160
7.1	Patterns of SnO_2 and Sn generated on soda glass by the photolysis of SnI_2 in air	181
7.2	The experimental set-up for the reduction of SnO_2 film to Sn film	182
7.3	The grainy nature of the Sn film	183

ACKNOWLEDGEMENTS

I am most grateful to Dr. Mino Green for his wonderful guidance during the course of this work, and for the critical assessment of the contents of this thesis.

I would like to thank Professor J.C. Anderson for giving me the opportunity to study at Imperial College. Many thanks also to Drs. K.S. Kang, N.A. Radjy, Miss T.J. Giddings, Miss V.M. Heys, Messrs. D.M. Obaro and H. Egboh, for their wonderful comradeship. Thanks are also due to Mr. E.J. Weidmann, Miss C.D.M. Collins, and many other members of the department who were most helpful in the preparation of this text.

I would like to acknowledge the Ife University, Nigeria, for providing the bursary for the entire programme. Behind the scenes encouragement from Professor V.A. Williams, Dr. A. Odu, Mrs. C.O. Kuku and Miss D.M.A. Strachan of Ife University, is also much appreciated.

CHAPTER ONE

INTRODUCTION

1.0 General Introduction

The photolysis (i.e. the photodecomposition) of solids is a complex process, which exhibits most of the important features of solid-state reactions. The photolytic reaction in the solid can be resolved into three major steps:

(1) Creation and trapping of free carriers (holes and electrons) at defect centres or at lattice centres;

(2) Surface and/or bulk diffusion of atoms or vacancies away from the lattice site where charge trapping occurred;

(3) Phase separation: e.g. the removal of reaction products at the surface or the precipitation of material in the original material.

This complexity perhaps explains the scarcity of investigations of the mechanism of the photodecomposition of inorganic solids. Most studies of photodecomposition in solids have been done on the silver halides[1,2], but despite the technical importance of these compounds in photography[1], many of the details of the mechanism of photolysis are still unresolved[3]. The situation is not much better for the family of compounds with layer lattice structures, of which the lead halides are a notable example[4,5] (others include the halides of Cd, Bi, Cu, and Sb). It is not surprising, therefore, that no attempt has been made until now, to study the photodecomposition of stannous iodide, SnI_2 (which also has a layer lattice structure) in a quantitative

manner, let alone to understand the mechanism of the photolytic process.

The purpose of this work is to study the kinetics and mechanism of the photolysis of SnI_2. The originality of the work stems from the fact that no-one has ever attempted to do this. Stannous iodide has, however, been observed to be photosensitive[6], and photodecomposable[7,8].

SnI_2 exists in two polymorphic modifications identified by their colours, one being red (which we have labelled as the α-polymorph), the other yellow (we have labelled this as the β-polymorph)[6,9]. The literature is silent as regards classifying the reported physical or chemical properties of this compound as either being for the red or the yellow modification. Attempts have, therefore, been made in this work to identify the differences between these polymorphic forms, especially as regards their crystal structure, optical and electrical properties. These are as detailed in Chapters 2 and 3 respectively. Chapter 4 contains the description of the experimental set-up and processes connected with the photochemical studies. The results of the photolytic reaction are presented in Chapter 5, while the detailed mechanism of the process, based on the experimental results is presented in Chapter 6. The technological applications of the photochemical work are presented in Chapter 7.

1.1 Photodecomposition of the Lead Halides

Stannous iodide (probably both α and β) has a layer type lattice structure[10], and has been found to form a series of solid solution with the lead halides[11,12]. It has also been reported to share optical properties (excitonic spectra) in common with PbI_2[7]. A review of the photochemical properties of the lead halides would, therefore, be of considerable help in understanding the processes that could be involved in the photolysis of SnI_2.

The photochemical behaviour of the lead halides shows a great similarity to that of the silver halides. Like the latter, they decompose under the action of photons of suitable wavelength[4,13]. For the silver halides, a mechanism for the photolysis has been proposed[1], based on the Gurney-Mott principle[14], which states that photochemical decomposition of the silver halides consists of an electronic and an ionic part. Absorption of a photon by the crystal excites an electron into the conduction band. This electron moves to a suitable trapping site where it combines with an interstitial silver ion. By the movement and trapping of more electrons and interstitial ions to this site, an aggregate of silver atoms is formed. The holes can be trapped at surface halogen ions, followed by the desorption of halogen atoms as halogen molecules.

Dawood, Forty and Tubbs[4] were the first to study the photochemical decomposition of lead iodide either as single crystals or in thin film form. The photolysis was in air, and they followed the photochemical reaction by determining the change in the thickness of the specimen before and after decomposition by the measurement of the optical absorption of the resulting solution after the lead iodide specimen had been dissolved in water, at an absorption band of 225 nm. From their results, they were able to propose an exciton mechanism for the photochemical reaction. The mechanism involved

the production of excitons by the absorption of photons by the lattice. These excitons (electron-hole pairs) become trapped at negative ion vacancies, probably at edges of crystals, or edges of cracks, or at the free surface; and react there in pairs to produce free iodine molecules; and pairs of free electrons which may be trapped by the lead ions at the centre of decomposition. They were of the opinion that the time dependence they observed was due to the diffusion of halogen through a layer of lead and lead salts formed at the surface.

The kinetic study of Dawood et al[4] had a number of limitations, among which is the fact that the photolysis was in air where the production of lead oxide would occur at the temperature employed; adding to this is the fact that their kinetic work hinged on photolysing their specimen for a fixed period of time, rather than for a constant extent of reaction, which made their calculations of activation energy meaningless.

A study of the photolysis of lead chloride, $PbCl_2$, was made by Kaldor and Somorjai[15]. The kinetics of the photodecomposition was followed by measuring the reflection density (where reflection density D_r, is defined as $D_r = \log I/I_r$, where I is incident light intensity on specimen surface, and I_r is the intensity of the reflected beam) of irradiated films. The rate of photodecomposition (D_r) varied as $I^{0.17}$ for low light intensity (i.e. $I < 7 \times 10^4$ μW cm^{-2}), and as $D_r \geq I^{3.2}$, for $I \geq 7 \times 10^4$ μW cm^{-2}. The time dependence was similar to that of Tubbs[4a]. The photochemical reaction was reported[15] to be temperature independent within the range 25-150°C, while the mode of reaction was found to be the same in vacuum or inert gas ambient, but initially accelerated in oxygen, with a subsequent limiting of the reaction due to the formation of lead oxychlorides. The rate of

photodecomposition was suggested to be dependent on the trapping of charge by the lead and iodine ions. The mechanism proposed for the reaction is as follows:

$$Cl^-(\text{lattice}) + V_{Cl} \xrightarrow{h\nu} V_{Cl}^- + Cl \uparrow \qquad (1.1)$$

$$xPb^{2+}(\text{lattice}) + yV_{Cl}^- \rightarrow [\, Pb^{2+}_x \cdot V_{Cl}^{-y} \,] \rightarrow xPb \downarrow + yV_{Cl} \qquad (1.2)$$

where Cl^- (lattice) and Pb^{2+} (lattice) are the anion and cation in their lattice positions. The first step (Eqn. (1.1)) results in the removal of chlorine from the lattice while the second step (Eqn. (1.2)) leads to the precipitation of lead. Thus the mechanism is basically that of a vacancy motion.

The photolysis of $PbCl_2$ and $PbBr_2$ by Verwey[13] and Schnooman[16] also resulted in the production of colloidal lead particles, identified by x-ray work on photolysed samples. The photochemical reaction was followed by observing the change in the optical density, D, of irradiated films in air. The results were applied to the theory of Mie[17] for the photolysis of silver halides. This theory gives the extinction coefficient of a dispersion of colloidal metal particles in terms of its volume fraction of metal. The rate determining step was suggested to be the diffusion through a layer of increasing thickness of colloidal particles. A further experiment with doped crystals of $PbBr_2$ (dopants included AgBr, TlBr, and $BiBr_3$)[18] did show that the reaction was enhanced with the monovalent metal ions,

while it was retarded by the trivalent metal ions. This did suggest the influence of anion vacancies in the reaction process.

The study of the photodecomposition of $PbBr_2$ and PbBrCℓ by Pierrard[19] did indicate that the halides were surface generated. The reaction mechanism proposed was similar to that of Forty et al[4c] for PbI_2. The only difference occurred in the relative generation rate of chlorine to bromine gases in lead bromochloride, where more of bromine gas (∿60% of total gases) was generated. This was explained to be due to the higher affinity for electrons by chlorine, which did act as a deep trap for electrons.

Verwey[5] further studied the photolysis of single crystals of $PbBr_2$ and $PbCℓ_2$ cleaved under red light. The reaction was followed by the change in the optical density, D, of the irradiated crystals. The change in D was found to be proportional to t(time) initially, and $t^{\frac{1}{2}}$ for latter part of the reaction. The intensity dependence was in tune with those of Kaldor and Somarjai[15] for $PbCℓ_2$. The effect at higher intensities ($I > 6 \times 10^5$ μW cm^{-2}) was proposed to be due to photoenhanced evaporation. Verwey[5] concluded that the photolytic process in $PbCℓ_2$, $PbBr_2$ and PbI_2 are the same. He therefore proposed a mechanism for the photolysis of $PbCℓ_2$ and $PbBr_2$ described as the "dynamic" model. The model consisted of the transport of holes and anion vacancies to and from the surface respectively. At the surface, the holes, h^+, react with halogen ions X_s^-, according to

$$h^+ + X_s^- \rightarrow X_s \qquad (1.3)$$

A halogen atom thus formed may combine with another atom X_s, to give a halogen molecule, which can then desorb (the halogen atoms may also desorb directly). In any case, the halogen leaves the surface

and anion vacancies are left behind. These anion vacancies in turn are assumed to be transported into the crystal, resetting the halogen ion sites at the surface for subsequent trapping of a hole and desorption of halogen. Inside the crystal, electrons react with Pb^{2+} ions to give first Pb^{+} ions and then Pb atoms, which flock together in precipitates under annihilation of anion vacancies.

The photolysis of microcrystals of lead iodide suspeneded in binders like gelatin or polyvinyl alcohol, was studied by Jacobs and Corrigan[20]. The reaction was followed by measuring optical density changes on irradiation with semimonochromatic radiation. The optical density changes followed a $t^{\frac{1}{2}}$ law. The photon efficiency was evaluated between 350 nm and 560 nm. All meausrements were made at $100^{o}C$. The incorporation of potassium ions into the lead iodide microcrystals resulted in an increase of photon efficiency, while the incorporation of trivalent ions was found to depress the sensitivity. The importance of iodide ion vacancies was, therefore, underlined as being very contributary to the photolytic process.

Morantz et al.[21] photolysed disks (made of compressed powder) of lead iodide. They also observed a $\Delta D \propto t$ and $\Delta D \propto t^{\frac{1}{2}}$ relationship. The grain size of the specimens was observed to have a pronounced effect on the photolytic behaviour of the specimens. The behaviour of polycrystalline lead bromide was described on the assumption that $PbBr_2$ dissociated under irradiation to form a lead enriched region in each grain, and that the bromine species needed to diffuse through this region so as to form bromine gas in the intergrannular pores. Photolysis was reported to occur more rapidly in specimens formed from coarser powder than in finer powder; this effect was explained to be due to the relative increased hydrolysis of the finer powder specimen because of the larger surface area.

A spectral dependence of $PbBr_2$ layer photodecomposition was studied by Kostyshin et al.[22] in the wavelength range of 270-360 nm. A sharp increase in the decomposition rate (determined by optical transparency) was found under the effect of light from the exciton absorption region, i.e. 330-340 nm. The activation energy for $PbBr_2$ photolysis was determined from the temperature dependence of the light sensitivity. An exciton mechanism was suggested for the initial stage of lead bromide photolysis.

The kinetics of the photolysis of thin films of PbI_2 have also been followed by Albrecht and Green[23], using a quartz crystal microbalance method. They observed photolysis of PbI_2 in the temperature range 45-150°C, with an activation energy of 0.45 eV. The reaction was found to be non-activated above 150°C, and was found to be directly proportional to light intensity, over all the temperature ranges employed. The rate of the reaction was observed to be unaffected by grain size and gaseous ambient, but initially accelerated by the inclusion of AgI or CuI within the film. Three ranges of kinetics were observed, an "initial" part, which was interpreted to be due to nucleation (Pb^+ ion production) and surface reaction. In the "intermediate" region, the rate of reaction was found to be directly proportional to time, this was associated with the main photolysis without the intervention of optically absorbing product. The third and "terminal" part, gave a $t^{-\frac{1}{2}}$ dependence of reaction rate, and was taken to be due to the produced lead particles. They were able to establish that iodine was generated at the solid vacuum interface, and the lead particles were generated within the bulk of the film. They also proposed a mechanism for the photolytic reaction, this was similar to that proposed by Verwey[5] for $PbBr_2$ and $PbCl_2$, known as the "dynamic" model. Theirs was however more explicit.

Buckman and Hong[24] were able to suggest that the cause of the large refractive index change[25] in the photolysis of PbI_2 films by measuring the photoconductivity and x-ray diffraction patterns of a photolysed film. They were able to suggest that the large refractive index change was due to the introduction of localised electron states in the band gap. These states were suggested to be associated with the inclusion of isolated PbO and/or $PbCO_3$ in the film rather than I^- vacancies or neutral Pb clusters. The grain boundaries in the polycrystalline films were suggested to provide entrances for ambient gases as well as exits for I_2 gas during photolysis. These gases form bonds with the Pb left behind, greatly inhibiting Pb clustering. The reaction leading to lead salt formation was reported to proceed strongly at 150-175°C, while lead clustering due to increased mobility did not compete significantly with these reactions until the temperature exceeded 180°C.

From the review, two mechanisms appear to have been considered for the photolysis of the lead halides. These are the exciton mechanism proposed for PbI_2 by Dawood et al[4], and the dynamic model of Verwey[5] for $PbC\ell_2$ and $PbBr_2$, which has been applied in a considerably modified and extended form to PbI_2 by Albrecht and Green[23]. Most of the reports suggested that the halogen was surface generated, except in the work of Dawood et al[4] and Morantz et al[21], where it was suggested that the $t^{\frac{1}{2}}$ rate dependence was because of the outdiffusion of halogen gas through the layer of lead and lead salts photolytically produced at the surface. The surface generation of I_2 was however successfully established by Albrecht and Green[23] for PbI_2 in their kinetic work.

The photodecomposition of the lead halides was generally reported to result in the production of lead particles. The bulk generation of the lead particles was implied in the mechanism of Verwey for $PbC\ell_2$ and

$PbBr_2$, but was more fully established in the work of Albrecht and Green on PbI_2. The evidence from the sensitisation of single crystals or films of the lead halides accumulated from monovalent metal ion doping[4,18,20,23] adsorbed dyes[25] and fogging[26] did give a lot of credence to the fact that holes are the majority carriers of photocurrent in the photolysis of the lead halides.

1.2 Previous Knowledge of SnI_2

Since this work covers a wide range of measurements, the relevant previous knowledge of SnI_2 will be reviewed.

1.2.1 Crystal Structure of Stannous Iodide

SnI_2 has a layer structure[10], in which there is a layer stacking of I-Sn-I on top of each other. Bonding between molecules within a layer are of covalent and ionic type, while bonding between layers is of the molecular or Van der Waals type. SnI_2 occurs in two modifications, one being red, the other yellow[6,9]. The yellow is the stable from above $100^{o}C$[6]. Percentage ionicity in both types is estimated to be 20%[9].

Aylett[27] suggested that SnI_2 and PbI_2 have the same structure (CdI_2 type) while Belotski et al.[28] found that SnI_2 and PbI_2 form a series of solid solutions of PbI_2 (CdI_2 type) structure, pure SnI_2 having a "different structure". In these reports no mention was made of the polymorphic type studied, i.e. either red or yellow.

A recent study by Howie et al.[11] has classified red SnI_2 as a monoclinic crystal of space group C^2/m, with a = 14.17, b = 4.535, C = 10.87Å, and β = 92.0. The compound has a unique layer structure in which the metal atoms occur in two distinct sites as shown in Fig. 1.1, in the (010) projection of half of the unit cell.

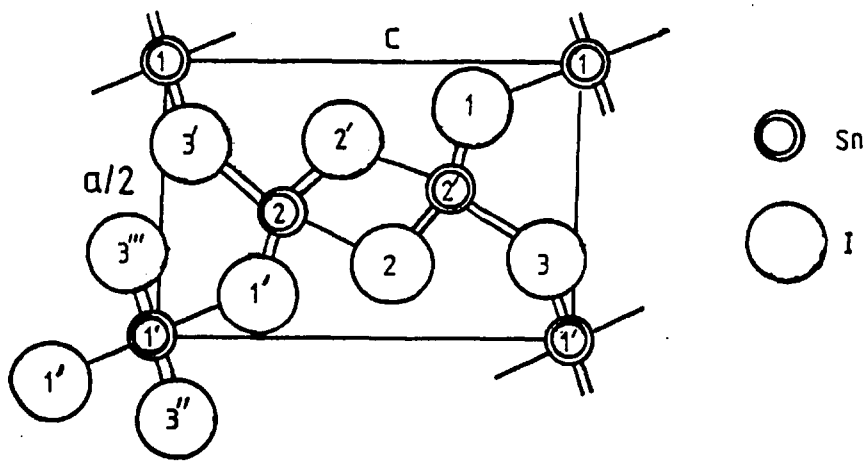

Fig 1·1 Tin(II) iodide projection on (010). Single lines joinning atoms indicate atoms in the same layer perpendicular to b. Double lines indicate contact between tin and iodine atoms in adjacent layers. The projection is for one half of the unit cell of α-SnI_2 (after Howie et al [11]).

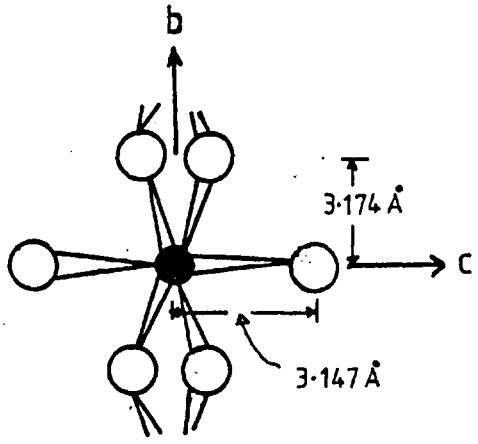

Fig 1·2 Coordination of Sn(1), projection on (100). The dark circle is tin atom while the larger open circles are iodine atoms.

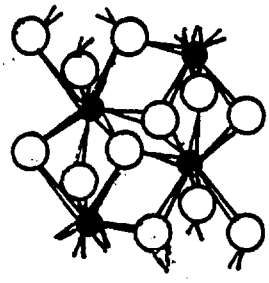

Fig 1·3 The coordination of Sn(2) viewed along (100) with the positive direction of b tipped towards the observer through 20°. The atoms are joined by tin-iodine vectors, to demonstrate the coordination of both tin(small dark circles) and of iodine (larger open circles) atoms.

TABLE 1.1: Representative bond length and angles for SnI_2 (after Howie et al.[11]).

Atom designations are as in Fig. 1.1

(a) Coordination of Sn(1) (distorted octahedron)

Iodine-Iodine and Tin-Iodine Coordinate	Bond Length (Å)	Iodine-Tin-Iodine Coordination	Bond Angle
Sn(1') - I(1')	3.147	I(1') - Sn(1') - I(3''')	89.4°
Sn(1') - I(3")	3.174	I(1') - Sn(1') - I(3")	90.6°
I(1') - I(3")	4.495	I(3") - Sn(1') -*I(3")	91.2°
I(1') - I(3''')	4.445	I(3") - Sn(1') - I(3''')	88.8°
I(3") - I(3''')	4.441		
I(3") -*I(3''')	4.535		

(b) Coordination of Sn(2)

Tin-Iodine and Iodine-Iodine Bonds	Bond Length (Å)	Iodine-Tin-Iodine Coordination	Bond Angle
Sn(2') - I(1)	3.198	I(1) - Sn(2') -*I(1)	90.3°
Sn(2') - I(2)	3.251	I(1) - Sn(2') - I(2)	87.3°
Sn(2') - I(3)	3.718	I(1) - Sn(2') -*I(2)	160.3°
Sn(2') - I(2')	3.004	I(1) - Sn(2') - I(3)	77.5°
I(1) -*I(1''')	4.535	I(1) - Sn(2') -*I(3)	130.4°
I(1) - I(2')	3.988	I(1) - Sn(2') - I(2')	80.0°
I(1) - I(2)	4.451	I(2) - Sn(2') -*I(2)	88.5°
I(1) - I(3)	4.348	I(2) - Sn(2') - I(3)	68.0°
I(2') - I(2)	4.040	I(2) - Sn(2') -*I(3)	118.4°
I(2) - I(3)	3.915	I(2) - Sn(2') - I(2')	80.4°
I(3') - I(3''')	3.999	I(3) - Sn(2') -*I(3)	75.2°
I(1') - I(2")	4.193	I(3) - Sn(2') - I(2')	141.6°

*Indicates that that the atom is translated by b.

Sn(1), lying on a centre of symmetry, is surrounded octahedrally by iodine atoms. Table 1 shows that there is no significant distortion of octahedral bond angles around this tin atom, and the differences in bond length are less than 1%. Four iodine atoms I(3), are 3.174Å distant, in layers above and below that containing the tin atom. The octahedron is completed by two iodine atoms I(1) at 3.147Å in the same layer as the tin atom. Infinite chain of edge sharing octahedra thus extend normal to (010) as shown in Fig. 1.1. The octahedrally coordinated tin atoms account for one-third of the total tin atoms in the unit cell.

Sn(2) atoms have nearest neighbour iodine atoms which occur in pairs related by a two-fold screw axis along (010) as shown in Figs. 1.1 and 1.3. Each Sn(2) is surrounded by seven iodine atoms. Six in layers above and below that containing the tin atom, lie at the corners of a trigonal prism. The seventh and closest, lies in the same layer as the tin. The prisms extend infinitely normal to (010), and have iodine atoms I(1) and I(3) in common with the octahedron chains described above.

The I--I distance between sequence of layers is 4.535Å. There are six formula units per unit cell.

1.2.2 Optical Properties of SnI_2

The studies of the optical properties of SnI_2 have been carried out on thin films and single crystals of unspecified polymorphic type. The reported works were on the transmission and reflection spectra. SnI_2 was reported[29] to have an absorption spectrum characterised by indirect transition, with the bandwidth for indirect transition at $300^{o}K$, being 2.068 eV[29], and phonon energy of 54 meV. There is a

shift of the forbidden bandwidth for indirect transitions to higher energies with reduced temperature, being typically 2.110 eV at 86°K.

Photoluminescence was not observed at room temperature, but at 86°K two wide bands did emerge with maxima at 6294Å, which were observed to be the same whether emitted from a cleaved plane of a single crystal or from an end surface[29].

Exciton spectra of SnI_2 investigated by transmission on thin films at 86°K have shown exciton spectra similar to that of PbI_2. Gorban et al.[29] have observed exciton spectra with lines at 4992, 4832, 4804, 4795, 4789Å, which have been attributed to the Wannier exciton series. All the observed lines fitted very well to a hydrogen-like $1/n^2$ series. The dissociation energy and the forbidden bandwidth for direct transitions calculated from the exciton lines gave R = 0.108 eV and Eg = 2.592 eV respectively. Batsanov et al.[30] had earlier quoted the band gap to be 2.4 eV, the temperature, specimen type, and method of determination were not stated.

1.2.3 Electrical Properties

Not much is known about the electrical properties of SnI_2. The only thermoelectric power measurement on the compound did indicate that SnI_2 is an ionic conductor in the temperature range 339-440°C[31]. The mode of conduction in the temperature range employed in this work is not known for certain, but is believed to be mostly ionic, since SnI_2 in pressed disk form has found application as either an anode[32], or a cathode[3] in the construction of solid state batteries incorporating solid electrolytes.

1.3 Choice of Experimental Technique for the Photochemical Reaction

From the review of work on the photolysis of the lead halides (Section 1.1), a number of experimental methods have emerged by which the photolysis of SnI_2 can be followed, namely:

(a) determination of the change in the optical density of an irradiated film[16]. The optical density, D is defined as

$$D = \log_{10} \frac{I_o}{I}$$

where I_o is the incident light intensity on the film surface*, and I, that of the transmitted beam. The increase in the optical density ΔD, that would be obtained (due to new absorption bands created by the tin metal particles produced) can be monitored in a part of the spectrum where SnI_2 is non-absorbing

(b) the rate of evolution of photolytic iodine gas can be determined by placing a mass spectrometer gauge head close to the irradiated sample, and detecting the gas relative to the mass spectra[34]

(c) a technique could involve measuring the pressure increase in an enclosed vessel due to the evolution of photolytic gas[35]

(d) the rate of photolysis can also be followed by dissolving irradiated films of SnI_2 in a suitable solvent, so as to be able to measure the optical absorption and then calculate the tin (II) iodide concentration from Beer's law[4]

---

* I_o is corrected for reflection.

(e) the photochemical reaction could equally be followed by a measurement of the reflection density of the film[15], where reflection density, D_r, is defined as

$$D_r = \log_{10} \frac{I_o}{I_r}$$

where I_o is the incident light intensity, and I_r is the reflected beam from the surface of the irradiated film

(f) an ellipsometric set-up could also be employed[36], and the reaction monitored by observing the change in the index as well as the extinction coefficient with time for a film irradiated with monochromatic radiation

(g) lastly, one can employ the mass change method of Albrecht and Green[23]. This involves the use of a quartz crystal microbalance. The technique is based on the fact that molecules of iodine gas are produced and escape from the film, thus leading to a mass reduction of the film at a rate determined by the reaction mechanism.

Techniques (a) to (f) have a lot of unacceptable limitations in terms of sensitivity, reproducibility, continuity, and the successful monitoring of the initial stages of the reaction. Since the quartz crystal microbalance technique could readily overcome these shortcomings, we have employed this technique in all the photolysis experiments carried out in this work.

1.4 Range of Kinetic Data

The photochemical reaction has been followed by shinning filtered light on evaporated films of SnI_2 on quartz crystal substrates, and observing the change in the resonant frequency of the quartz oscillator, due to mass change. The experimental results are presented in Chapter 5, as extent of reaction (i.e. number of molecules of SnI_2 photolysed cm^{-2}) against time. Attempts have been made to study the effect of the relative influence of,time, temperature, film microstructure, film composition (doping with impurities), environment (ambient), thickness, substrate type, light intensity, oxygen uptake and wavelength, on the rate of the photochemical reaction.

REFERENCES

1(a) C.E.K. Mees, T.H. James, "The Theory of Photographic Process", Macmillan, New York (1966)

(b) J.F. Hamilton, The Photographic Process in Prog. Solid State Chem. 8, 167 (1973)

2. J.W. Mitchell, Phot. Sci. 5 49 (1957)

3. F.A. Kroger, "The Chemistry of Imperfect Crystals", vol. 3, North-Holland, Amsterdam (1974)

4(a) M.R. Dawood, A.J. Forty, M.R. Tubbs, Proc. Roy. Soc. A. (GB), 280 (1383), 566 (1964)

(b) R.I. Dawood, A. J. Forty, M.R. Tubbs, Proc. Roy. Soc. A. (GB), 284 (1397), 272 (1965)

(c) A.J. Forty, R.I. Dawood, M.R. Tubbs, J. Sci. Instrum. (GB) 41(5), 274 (1964)

5. J.F. Verwey, J. Phys. Chem. Sol. 31(1), 163 (1970)

6(a) P. Freundler and (Mille) Y. Laurent, Compt. rend. 179, 1049 (1924)

(b) F. Wohler and F. Dunhaupt, Liebig's Ann. 85, 374 (1853)

7. V.M. Kosarev, V.S. Kostko, and N.N. Karpuk, J. Appl. Spectr. (USA), p.1282, Oct. (1978)

8. V.M. Kosarev, V.S. Kostko, A.I. Ivakha, V.F. Nadtochii, T.N. Sushkevich and S.F. Chepur, Zhurn. Prikl. Spekr. 27(3), 549 (1977)

9. K.S. Pitzer and J.H. Hildebrand, J. Amer. Chem. Soc. 63, 2472 (1941)

10. M.W. Lister and L.E. Sutton, Trans. Faraday Soc. 37, 406 (1941)

11. R.A. Howie, W. Moser, I.C. Trevena, Acta Cryst. B28, 2965 (1972)

12. D.P. Belotskii, I.N. Antipov, V.H. Nadtochi and S.M. Sosik, Inorg. Mater. 5, 1583 (1969)

13. J.F. Verwey, J. Phys. Chem. Solids 27, 468 (1967)

14. N.F. Mott and R.W. Gurney, "Electronic Processes in Ionic Crystals (2nd ed.), New York (1964)

15. A. Kaldov, G.A. Somorjai, J. Phys. Chem. 70, 3538 (1966)

16. J.F. Verwey, J. Schonman, Physica (Netherlands) 35 (3), 386 (1967)

17. G. Mie, Annln. Phys. 25, 377 (1908)

18. J. Schoonman and J.F. Verwey, Physica 39, 244 (1968)

19. J. Pierrard, Envir. Sci. and Tech. 3, 48 (1969)

20. J.H. Jacobs, R.A. Corrigan, J. Phot. Sci. 21, 193 (1973)

21. D.J. Morantz, R.A.M. Scott, J.J. Shortland, J. Phys. and Chem. Solids (GB) 33 (6), 1235 (1972)

22(a) M. Kostyshin, E.Mikhailovskaya,V.M.Sharyi, Toim. Eesti. Nsv. Tead. Akad. Fuus. Mat. (USSR), 23(1) 79 (1974)

(b) M.Kostyshin, E. Mikhailovskaya, V.M. Sharyi, Ukr. Fiz. Zh. (USSR) 19(8), 1327 (1974)

(c) M.T. Kostyshin, E.V. Mikhailovskaya, Ukr. Fiz. Zh. (USSR) 19(3), 507 (1974)

23. M.G. Albrecht and Mino Green, J. Phys. Chem. Solids 38, 297 (1977)

24. A.B. Buckman, N.H. Hong, J. Opt. Soc. Am. 67(8), 1123 (1977)

25. H.E. Spencer, J.P. Darlak, J. Phys. Chem. 72, 2384 (1967)

26. J. Malinowski, Phot. Sci. and Eng. 15(3), 175 (1971)

27. B.J. Aylett.,Prog. Stereochem. 4, 231 (1969)

28. D.P. Belotskii, I.N. Antipov, V.H. Nadtochi and S.M. Dodik, Inorg. Mater. 5, 1583 (1969)

29. I.S. Gorban, V.F. Gorchev and T.N. Sushkevich, Sov. Phys. Solid State 18 (7) (1976)

30. S.S. Batsanov, Izv. Akad. Nauk, SSSR. Neorg. Mater. 2(12), 2251 (1966)

31. U. Trolle, A. Kvist, Z. Naturfosch. 249, 469 (1969)

32. L.C. Chi, Ger. Offen. 2, 254, 415 (Cl.Holm) 1974. Appl. P.2254415.6, 7, Nov. (1972)

33. P.R. Mallory, Fr. Demande 2, 205, 750 (Cl.Hokm), May, 1974. Appl. P.7239,447, 8, Nov. (1972)

34. M.G. Albrecht, Ph.D. Thesis, Imperial College, University of London (1975)

35(a) G.W. Luckey, J. Phys. Chem. 57, 791 (1953)

(b) G.W. Luckey, J. Chem. Phys. 23, 882 (1955)

36. J.F. Reber, R. Steiger, Surf. Sci. 49(1), 236 (1975)

CHAPTER TWO

THE POWDER FORM OF SnI_2

In this chapter the preparation procedure for the powder samples of both polymorphs of SnI_2 is outlined, the structural detail of our prepared specimens are compared with those of published works on SnI_2. Our novel structural analysis of the yellow specimen is also discussed, while attempts have been made to outline the mechanism for the polymorphic transformation from the red to the yellow polymorph.

2.1 PREPARATION OF SnI_2 POWDER

The basic materials used in the preparation of Stannous iodide, SnI_2, were Analar grade hydriodic acid (66% w/v), supplied by Hopkins and Williams, and tin metal powder (150 μm particle size, and 99.75% purity) supplied by Goodfellow Metals. The hydriodic acid (∿40 ml) was placed in a three necked, ground joints, round bottomed flask, and was initially deaerated by passing through it a stream of nitrogen gas (≦5 ppm O_2). The tin metal (∿10g) was then added in small bits at a time. This was necessary because of the frothing that resulted with the addition of the metal to the acid. When all the metal had been added, the mixture was refluxed for three hours with a constant passage of oxygen free nitrogen gas through the refluxing mixture. A heating mantle provided the uniform heating during the reflux stage. After three hours the reflux arrangement was usually quickly converted to a distillation arrangement, the flask and the content being heated in a paraffin bath, so as to distill off the excess hydriodic acid and water that might have been left over from the reflux stage. There was still a continuous passage of oxygen free nitrogen through the distilling mixture. When all the excess HI had been

distilled off there was always left a mass of reddish SnI_2. During both the distillation and reflux stages, the glassware was usually wrapped in aluminium foil so as to protect the contents from being decomposed by light, since SnI_2 is highly photosensitive as will be made more evident in Chapter Five.

The SnI_2 residue from distillation was usually recrystallised from a suitable hot solvent. The solvent from which the prepared compound was crystallised was found to control the polymorphic form that could be obtained. Tin diiodide exists in two polymorphic forms, differentiated by their colours, one being red, the other yellow[1,2]. Recrystallisation from hot ethyl alcohol (Analar grade) resulted in the red (α-SnI_2) low temperature modification, while changing the recrystallisation medium to either hot Analar grade methyl alcohol (methanol) or trichloromethane (chloroform) resulted in the yellow (β-SnI_2) high temperature modification. Earlier production of SnI_2 from a solution of stannous chloride and potassium iodide by Freudler and Laurent[2] gave a mixture of the red and yellow polymorphs. An excess of stannous chloride favoured the red, while an excess of potassium iodide in the base mixture favoured the yellow. In our case we believe it is a subtle solvent - SnI_2 nucleus interaction that determines the polymorphic type that is obtained. As detailed below, (section 2.3), the yellow polymorph is the high temperature form, and is therefore expected to be of a slightly larger unit cell volume than the low temperature red modification.

2.2 X-RAY ANALYSIS OF POWDER SPECIMEN

The powder specimens of SnI_2 (both polymorphs) were x-rayed, and the x-ray pattern recorded on photographic films supplied by Kodak Limited (double screen type). We used a Debye Scherrer (114.6 mm diameter) x-ray powder camera arrangement. Beam voltages of 25 to 30 kV were found

sufficient with beam currents of 15 to 20 mA. We used a CuKα filtered radiation. Prior to the exposure to x-ray radiation, the powder samples were put in 0.4 μm capillary tubes, and sealed at both ends, because of the relative atmospheric sensitivity of SnI_2[2].

Shown in plate 2.1 are the photographs of the diffraction patterns obtained for exposed powder forms of both polymorphs to x-ray radiation at a beam voltage of 30 kV and beam current of 20 mA for 2 hours.

The d-values calculated from the Bragg equation

$$\lambda = 2d \sin \theta \qquad (2.1)$$

for λ(copper filter) = 1.5418 A°, are as detailed in table 2.1 and 2.2 for the red (α-SnI_2) and yellow (β-SnI_2) polymorphs respectively.

The d-values obtained from the powder samples of α-SnI_2 were found to be in accord with those earlier obtained by Howie et al[3] for red SnI_2. This is confirmation of the correctness of our preparative procedure.

There has been no report in the literature of characteristic d-values for β-SnI_2. Our d-values, detailed in table 2.2, are therefore the first to be reported for this polymorph.

Since nothing is known about the unit cell dimensions of the β-polymorph as well as its structural system, we tried to determine these and have therefore employed the powder photograph indexing method described by Henry, Lipson and Wooster[4]. This involves the calculation of the $Sin^2\theta_{h\,h\ell}$ for the d-values obtained from the powder photograph, and to relate these with some set equations for the different crystal systems like the cubic, the tetragonal, hexagonal, trigonal, orthorhombic, monoclinic, or the triclinic systems. For the hexagonal and trigonal systems for example,

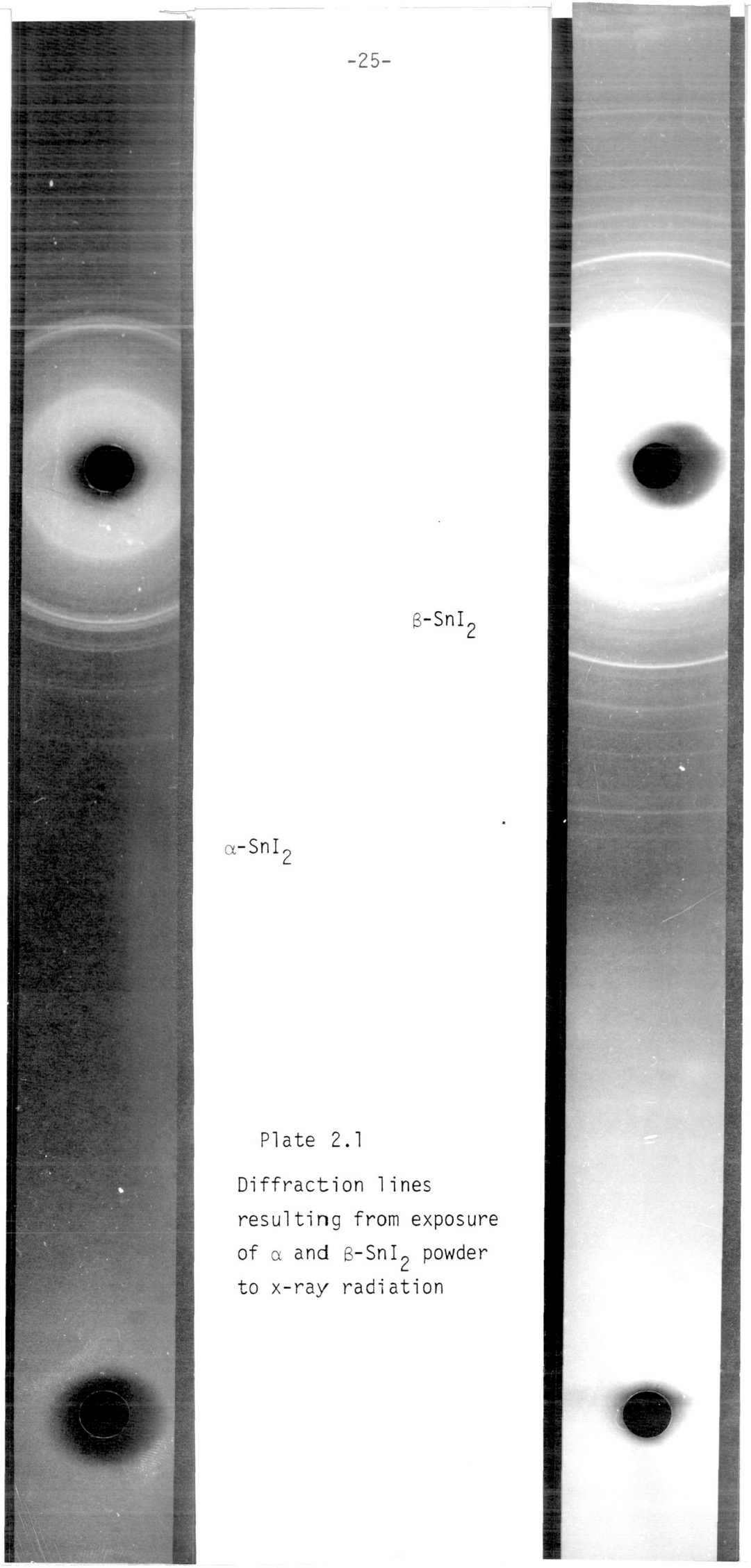

Plate 2.1

Diffraction lines resulting from exposure of α and β-SnI_2 powder to x-ray radiation

Table 2.1: Indexed x-ray powder data for the red (α-) polymorph of SnI_2, obtained in this work. The hkℓ values have been taken from the published work of Howie et al[3] for α-SnI_2

Line No.	d(A°)	hkℓ	I/I_0
1	5.99	$20\bar{1}$	15
2	5.691	201	40
3	4.40	$20\bar{2}$	20
4	3.65	003	35
5	3.55	400	40
6	3.32	401	40
7	3.27	310	100
8	3.18	203	80
9	3.08	311	60
10	3.02	$40\bar{2}$	22
11	2.747	113	25
12	2.695	004	15
13	2.448	$31\bar{3}$	10
14	2.292	601	40
15	2.236	$51\bar{2}$	10
16	2.166	512 or 005	20
17	2.137	602	20
18	2.071	$20\bar{5}$	15
19	1.965	513	15
20	1.927	115	6
21	1.870	$40\bar{5}$	6
22	1.844	223	11
23	1.784	711 or $42\bar{2}$	10
24	1.636	$51\bar{5}$ or $40\bar{6}$	20
25	1.605	$31\bar{6}$	10
26	1.566	025 or 316	10

Table 2.2: X-ray powder data for the yellow (β-) polymorph of SnI_2 obtained in this work.

Line No.	$d_{obs.}$ (A°)	$d_{calc.}$ (A°)	hkℓ	I/I_o (%)
1	7.378	7.384	100	7
2	7.084	7.082	001	7
3	5.108	5.111	101	7
4	3.481	3.541	002	70
5	3.316	3.274	201	25
6	3.210	3.193	102	12
7	2.798	2.791	120	10
8	2.691	2.724	112	10
9	2.360	2.361	003	100
10	2.318	2.325	301	10
11	2.235	2.248	103	12
12	2.184	2.192	212	15
13	1.962	1.967	131	33
14	1.850	1.846	400	7
15	1.790	1.786	401	7
16	1.773	1.770	004 or 132	30
17	1.726	1.722	104	5
18	1.694	1.694	230	7
19	1.648	1.648	231	15
20	1.601	1.596	204	10
21	1.578	1.582	223	5
22	1.469	1.467	142	25
23	1.416	1.416	005	40
24	1.398	1.395	240	7
25	1.369	1.362	224	6
26	1.338	1.339	134	6
27	1.324	1.326	150	18
28	1.256	1.252	503	10

$$\text{Sin}^2\,\theta_{hk\ell} = A(h^2 + hk + k^2) + C\ell^2 \qquad (2.2)$$

where h, k and ℓ are lattice indices, A and C are constants, they are related to the lattice constants a and c as follows:

$$A = \lambda^2/3a^2$$

and

$$C = \lambda^2/4c^2 \qquad (2.3)$$

λ is the wavelength of the incident x-ray radiation.

According to Henry et al[4], it is possible to examine the relationship between the experimental $\text{Sin}^2\,\theta_{hk\ell}$ values in order to determine the crystal system present.

Our $\text{Sin}^2\,\theta_{hk\ell}$ values, and subsequent indexing gave us the indication that the β-SnI_2 polymorph is either of the hexagonal or trigonal system, since we had a good fit to eqn. (2.2), as detailed in table 2.2. The values of the cell constants obtained by the above procedure are

$$a = 8.526\ A°$$
$$c = 7.082\ A°$$

The work of Howie et al[3] on α-SnI_2 showed that this polymorph was monoclinic with a = 14.17, b = 4.535 and c = 10.87 A°, while β = 92°. On comparing our results with those of Howie et al, there appears to be an appreciable increase in the unit cell volume (∿9% per molecule of SnI_2) with phase change to the β-polymorph. The increase in volume is in conformity with the fact that β-SnI_2 is a high temperature polymorph (discussed later in section 2.3), and hence expected to be of increased unit cell volume. We are therefore of the opinion that the crystal lattice dimensions, and the crystal system obtained for β-SnI_2 are in order.

per hour). The temperature being monitored by the use of two "Chromel-Alumel" thermocouples attached to the front ends of the glass substrate, these were held in position by the use of "Silver Dag".

The red colour of the film was observed in low intensity white light to be quite stable until a temperature of 108°C, when shades of yellow colour started to appear across the film. The transformation of the entire film to the yellow form was not complete at this instant, but lingered on for another 12 minutes, when the red film was observed to be completely transformed to the yellow form. It has therefore been possible to characterise the transition temperature from the α to the β-polymorph to be 108 ± 2°C.

2.4 TYPES OF POLYMORPHIC TRANSOFRMATION[5-7]

The rate of transformation between one polymorph of a substance and another can vary widely depending upon the type of transformation, the mechanism involved and the stability of the resulting structure. The different forms of polymorphic transformations include displacive (α-β, or high-low inversion), reconstructive (or diffusive) and order-disorder transformations. The mechanism and characteristics of these different types of polymorphic transformations are as detailed below.

2.4.1 Displacive Transformations

This is called high-low inversions, or α-β inversions. Displacive transformations occur with great rapidity, the structure 'snapping' over into that of a second polymorph immediately upon entering the second's pressure or temperature field of stability. Before and after such transformations, near neighbours remain near neighbours, in other words no bonds between atoms are broken during a displacive transformation. However bond directions may change as near neighbours shift slightly, that is, they are displaced relative to each other.

Some of the principal characteristics of displacive or high-low polymorphism as cited by Sosman[5] are:

(1) A high-low inversion is completed promptly, often within a few seconds after attaining the inversion temperature (or inversion pressure).

(2) It is reversible, proceeding in the opposite direction if the temperature (or pressure) is returned to its pre-inversion value.

(3) Little difference in heat content exists between the high and low polymorphs.

(4) The presence of any other phases in external contact with the crystal will neither alter nor catalyse its high-low inversion.

(5) A temperature hysteresis exists, i.e. for falling temperatures the inversion occurs at a slightly lower temperature than for the reverse situation of rising temperature, the average of these two temperatures usually being quoted as the inversion temperature.

Buerger[6] observed that in displacive transformations the high temperature form, as compared to the low, will be the more open structure, its atoms being packed less compactly and less tightly bonded to each other. It will also have the larger heat capacity and the higher symmetry, the low temperature form usually being a derivative structure of the high. The high temperature form may never be "quenched" in, i.e. made to exist within the P, T field of the low temperature form.

2.4.2 Reconstructive Transformation[7]

This is also known as diffusive transformation or sluggish inversions. Reconstructive transformations involve the transformation of

one polymorph into another by means of two steps:

(1) The breakage of bonds, and a general disruption of the old structure.

(2) The reorganisation and diffusion of the atoms into their position in the newly stable structure.

Step (1) requires the introduction of considerable energy to break the bonds and thus constitutes a high-energy barrier that opposes the progress of any reconstructive transformation, causing it to be slow and sluggish. In fact some reconstructive transformations are so slow that the old polymorph may persist unstably even when held in the P,T field of the new. The energy barrier inherent in step (1) permits its metastable existence beyond its own stability field. Reconstructive transformations are particularly deterred by rapid cooling. Brought suddenly to a temperature at which the low temperature polymorph is stable, but so low that breakage of bonds (step 1) is difficult and rate of diffusion (step 2) is very slow, a high temperature polymorph will transform to the low-temperature structure at a negligible rate. Thus it survives metastably at this low temperature and is said to be "quneched in".

Reconstructive transformations have the following principal characteristics:

(1) The transformation occurs sluggishly.

(2) Considerable difference in the heat content between the two polymorphs may exist.

(3) The temperature (or pressure) of transformation may be considerably undershot or overshot, so that a polymorph may persist, sometimes indefinitely, within a P,T field for which it is unstable.

2.4.3 Order-disorder Transformations[7]

These are divisible into two subtypes: (1) rotational transformations and (2) interchange transformations. Rotational transformations may occur in crystal structures containing NO_3^-, CO_3^{2-}, or CN^- groups. Interchange transformations on the other hand are illustrated by the polymorphs of $KA\ell Si_3O_8$, or Cu-Zn alloy, and are characterised by a change in the relative occupancy of the available cation sites by either Aluminium (Aℓ) or Silicon (Si) in the case of $KA\ell Si_3O_8$. In the case of Cu-Zn alloy, Cu or Zn atoms occupy each other's cubic sublattice in conformity with the relative state of order of the system. Both forms of order-disorder transformation are characterised by the fact that they take place over a wide temperature margin, and leading to a more disordered state from a more ordered system, with temperature increase.

Interchange transformations involve a breakage of bonds and an exchange of position. As a consequence, they can be as sluggish as reconstructive transformations. With falling temperature they may not occur at all.

2.5 THERMODYNAMICS OF POLYMORPHIC TRANSFORMATIONS

A polymorphic transformation, that is equilibrium change of phase of fixed composition to another of identical composition, is thermodynamically one of the simplest types of phase equilibrium. Thermodynamically, transformations are characterised by their order, the order of transformation being the order of the first derivative of free energy that displays a discontinuity. Three modes of thermodynamic transformation are known, and differentiated as first, second and third order transformations respectively.

2.5.1 First Order Transformations[8,9,11]

If we assume a situation in which the pressure is negligibly small, so that the work, $P\Delta V$, of changing the volume from one polymorphic form to another is negligible, under these conditions the relative stabilities of two polymorphs can be studied by comparing their Gibbs free energies.

$$G = H - TS \tag{2.4}$$

where H is the enthalply or heat content of the polymorph, S its entropy, and T the temperature under consideration. The most stable polymorph has the smallest free energy G (i.e. the most negative). In general, two polymorphs, 1 and 2, have different enthalpies and entropies. They are equally stable when their free energies are equal, i.e. according to eqn. (2.4)

$$H_2 - H_1 = T(S_2 - S_1) \tag{2.5}$$

or

$$\Delta H = T\Delta S \tag{2.6}$$

These relations are graphically illustrated in Fig. 2.1. Each polymorph has a specific energy H at zero T. At this temperature G = H, according to eqn. (2.4). At zero T therefore,the stable polymorph is the one with the most negative enthalpy. With increasing T, the free energy G decreases, i.e. becomes more negative. Certain forms with high internal energy,especially the less dense forms, have relatively high entropy because of larger void space, for example such forms (as form 2 in Fig. 2.1) have a rapidly declining G curve which may cross that of the form which is stable at zero T. Beyond the crossing point, $G_2 < G_1$, so that form 2 becomes stable relative to form 1. The transition requires an increase in the

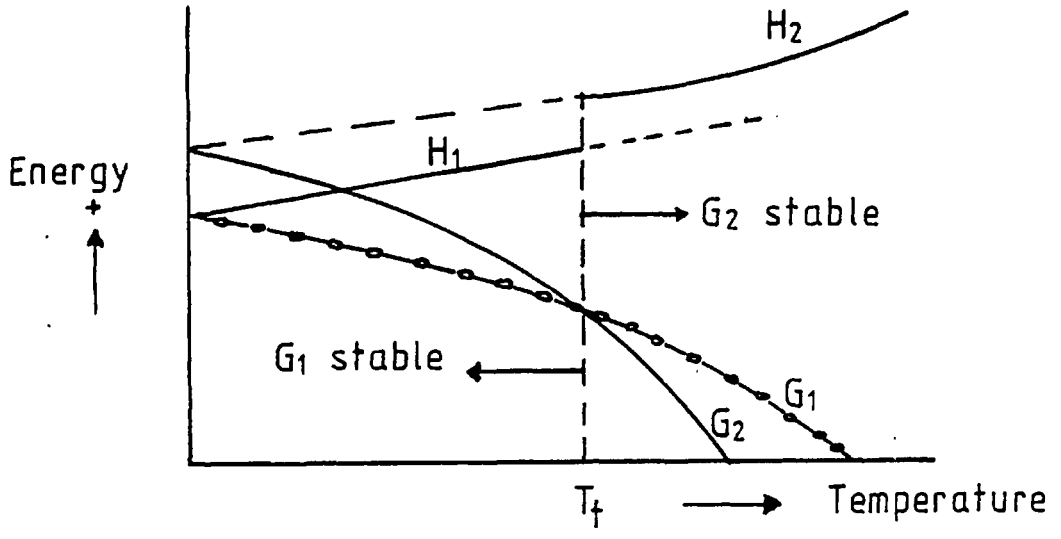

Fig 2·1 The relation between the structure enthalpy, H, and the free energies, G, for two polymorphs, 1 and 2, as a function of temperature [8].

internal energy H, of the system. The difference, ΔH, is the latent heat of transformation. Phase transformation may therefore entail a stepwise increase in energy with increasing temperature.

The type of transition just described is the classical one, and is known as a first-ordertransformation. This implies that G is continuous across the transformation whereas the first derivatives of G, i.e. $S = (\partial G/\partial T)$ and $V = (\partial G/\partial P)_T$ exhibit discontinuities at the transformation as do higher derivatives. Since there is discontinuity in S, while G is continuous, there is discontinuity in H.

2.5.2 Second Order Transformations[8,9]

Second order phase transitions are those in which there are continuities in the Gibbs function and its first derivatives, but which are discontinuous in the second derivatives. Thus there would be no discontinuities in S, V, or H (which are first derivatives in G), but there would be discontinuities in heat capacity C_p, compressibility β_T and coefficient of thermal expansion, α. Thus

$$\left(\frac{\partial^2 G}{\partial T^2}\right)_p = -\left(\frac{\partial S}{\partial T}\right)_p = -\frac{C_p}{T} \tag{2.5}$$

$$\left(\frac{\partial^2 G}{\partial p^2}\right)_T = \left(\frac{\partial V}{\partial P}\right)_T = -\beta_T V \tag{2.6}$$

$$\frac{\partial}{\partial T}\left[\frac{\partial(G/T)}{\partial(1/T)}\right]_p = \left(\frac{\partial H}{\partial T}\right)_p = C_p \tag{2.7}$$

Second order transformations have zero latent heat of transformation since ΔG and ΔS are both zero. Some of the properties of this transformation are as shown in Fig. 2.2[9]. The energy is seen to increase gradually until a certain temperature, T_c, is reached, at which point the rate of increase abruptly declines. As a result, there is discontinuity in C_p, the

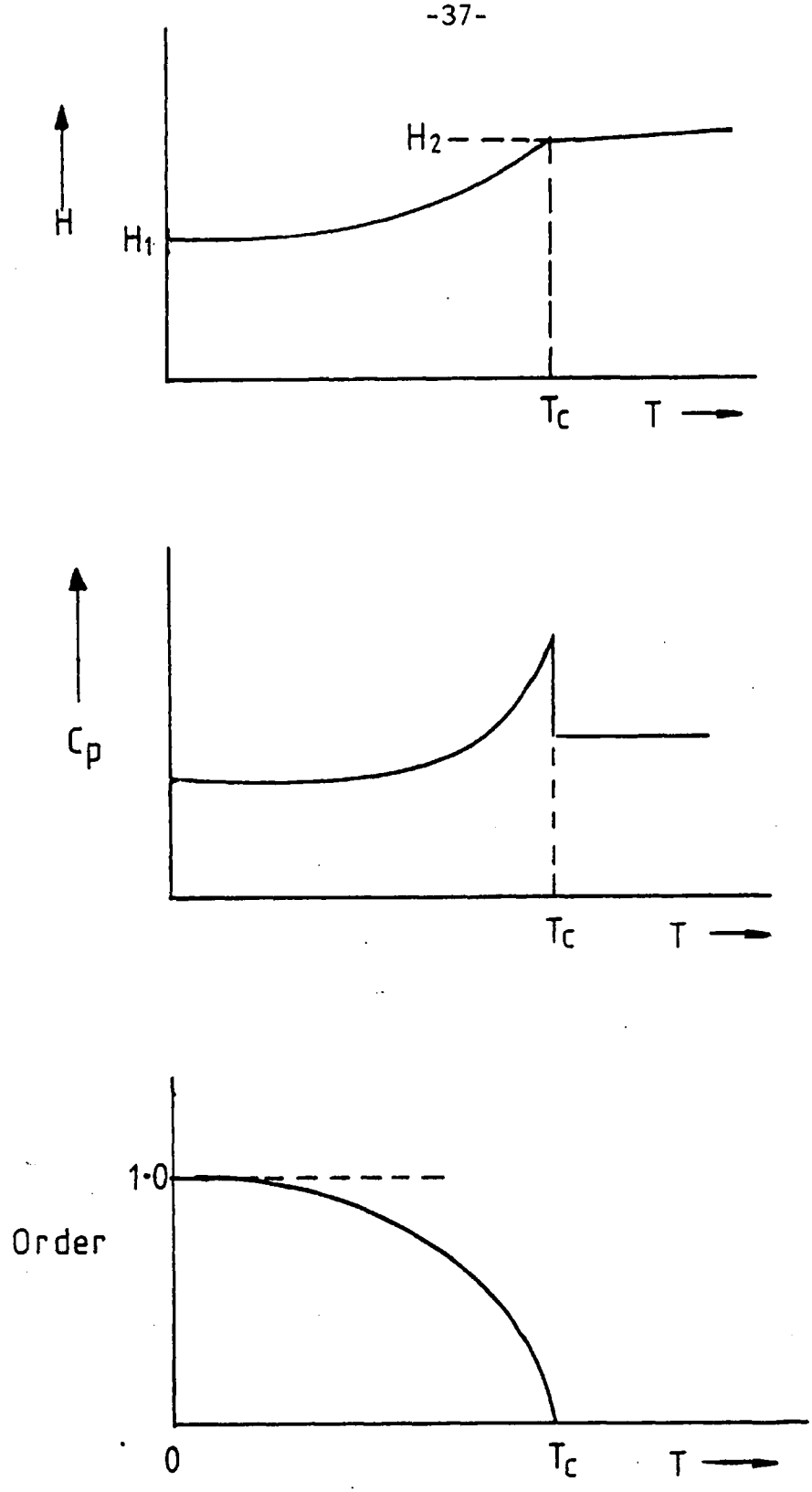

Fig 2·2 The variation with temperature of the structure enthalpy, H, the specific heat, C_p, and order, in a second order transformation [9].

specific heat. The resulting Lamba-shaped specific heat curve gives rise to the alternative name Lambda - point transformation.

Examples of second order transitions are order-disorder transformations in alloys and ferroelectric-paraelectric transitions.

2.5.3 Third Order Transformations[9]

This has the specific heat, C_p, continuous, but dC_p/dT discontinuous at the transformation point. Third order transformations are exemplified by the Curie point of a variety of ferromagnetic substances.

As the order increases, the discontinuity in properties becomes decreasingly significant and it is no longer appropriate to think in terms of a phase change. Transformations of order greater than three have not been recognised with certainty[9].

2.6 MECHANISM OF PHASE TRANSITION IN SnI_2

We do not know the crystal structure of β-SnI_2, it has only been possible to determine the symmetry of the unit cell. Based on the information gathered from the powder lines, we can usefully speculate upon models for how the α-form might transform to the β-form.

From our visual observation of the phase transformation in thin films and powder samples in sealed up capillary tubes (evacuated) it was possible to deduce that the transformation from α to the β-polymorph was not instantaneous, but lingered for a few minutes. The mode of transition can therefore be inferred to be a reconstructive transformation.

Based on the unit cell dimensions obtained for the β-polymorph, we were able to calculate the density of this polymorph to be 4.81 g/cm^3, while the unit cell was found to contain four SnI_2 molecules as against a density of 5.285 g/cm^3 and six molecules per unit cell for α-SnI_2. The change in density was considered reasonable if one considers that this is a high temperature modification. The increase in volume is about 9% per molecule.

From the $Sin^2 \theta_{hk\ell}$ values, we were able to infer that the β-SnI_2 molecule could be of either a hexagonal or trigonal system. The calculation of the number of molecules in the unit cell, based on the experimentally determined cell volume gave four molecules per unit cell. For an hexagonal system the number of molecules per unit cell could be either four or six or multiples of both[7], while for the trigonal system the number of molecules per unit cell could only be three or multiples of this[7]. Our derivation that there were four molecules in the unit cell of β-SnI_2 therefore indicates that the crystal system is hexagonal.

The study of the structure of α-SnI_2 by Howie et al[3] revealed that this polymorph is monoclinic, with the tin atoms occupying two distinct lattice sites, and therefore possess two types of lattice coordination. One-third of the tin atoms (at the corners of the unit cell) are octahedrally coordinated (Figs. 1.1 and 1.2), while the other two-thirds of the tin atoms occupy trigonal prism sites, and are coordinated to seven iodine atoms three in layers above and below the tin atom, while the seventh occupies the same layer as the tin atom (Figs. 1.1 and 1.3).

Taking the β-polymorph to be hexagonal would require an octahedral coordination about the tin atoms. To achieve this from the structure of the α-form, there must be a breakage of bonds, displacement of atoms, and an overall rearrangement of the structure of the red form. This rearrangement however must be such that it would have the minimal distortion of the initial lattice, and the least energy. From Fig. 1.1 and the picture of our model for the unit cell structure of the α-polymorph shown in plate 2.2, we can observe that the tin atoms labelled as tin (1) or tin (2) in Fig. 1.1 are in distinct continuous columns in the b-direction. The tin (1) atoms are octahedrally coordinated, while tin (2) are of trigonal prism coordination. To achieve an hexagonal structure from this we propose that the tin-iodine bonds between tin (2) and the iodine in the same layer with

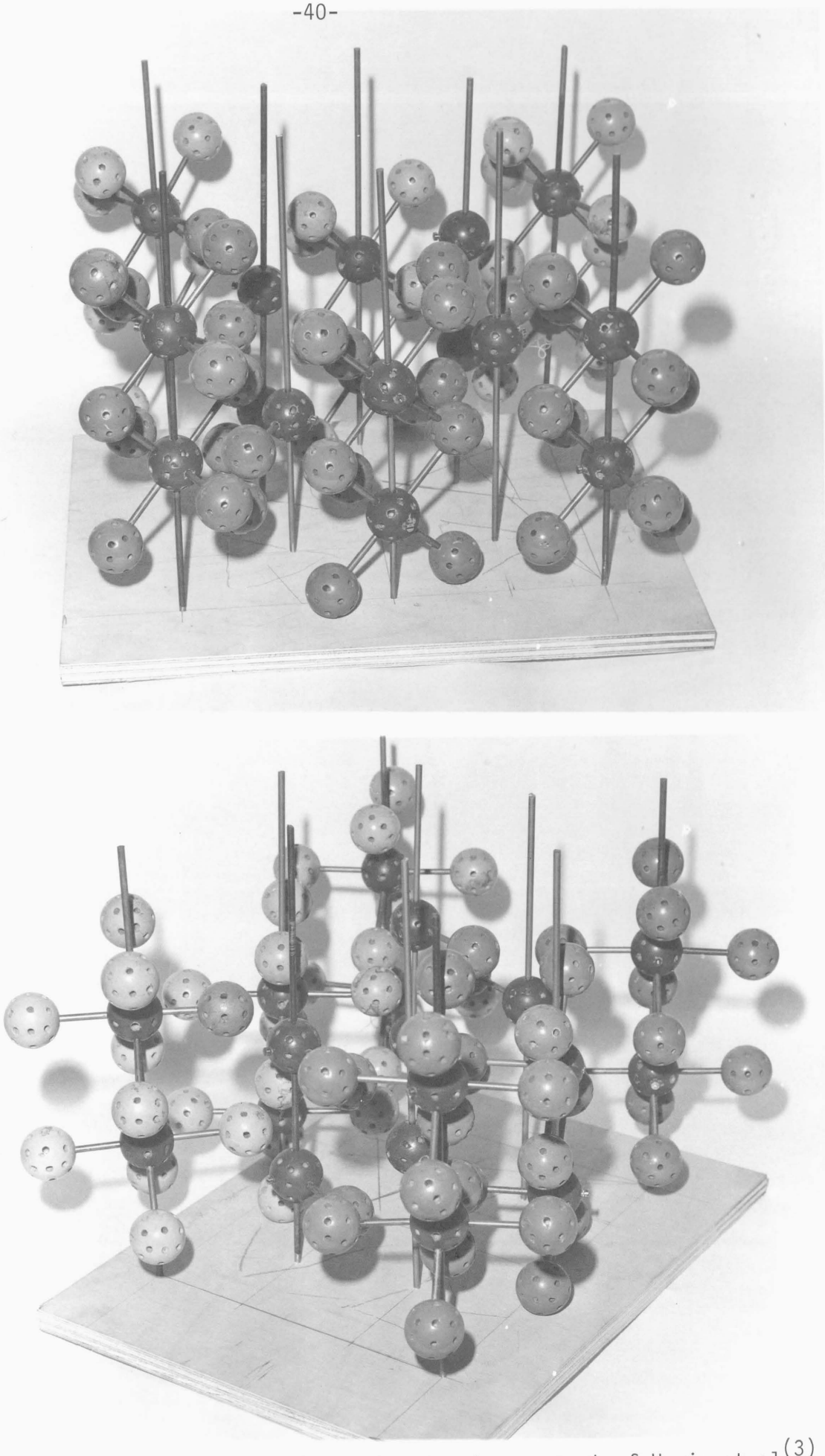

Plate 2.2: Built up model for α-SnI_2 from the structure report of Howie et al[3]. (a) is for the projection in the $\underline{b}$ direction perpendicular to the base plate, while (b) shows the $\underline{a}/2 - \underline{c}$ projection. The black balls are tin atoms, while the lighter balls are iodine atoms.

it are broken, leaving tin (2) with an octahedral coordination. There is then a translation of the tin (2) atoms by ½b in an upward direction (tin (2)) and downward direction (tin (2")), so that the tin atoms can now lie in the same plane as the tin (1) atoms. This we believe would lead to a lateral displacement of the column of tin (1) atoms and a consequent lengthening of the a-axis, such that ½a (α-SnI_2) would be the same as the a-value obtained for β-SnI_2 (i.e. a = 8.526 A°). There is the possibility of the translation of the c-axis in the α-polymorph to the b-direction in the β-polymorph, and this would therefore account for the values obtained for a- and b- from our powder data. A shift in the orientation of the system would lead to a generation of a stacking of I-Sn-I layers in the c-direction of β-SnI_2, with the layer sequence being separated by the Van der Waal distance of about 4A°. To obtain this from our values of 7.082 A° for the c-axis, it means that the a and b axis must be fairly deviated from the vertical direction as is the case in the lead iodide, PbI_2, structure shown in Fig. 2.3[10]. We are of the opinion that the resulting structure for the β-SnI_2 after the phase transformation would be very much like the PbI_2 structure, which is also of the hexagonal system[11]. There are four PbI_2 molecules per unit cell, and the lead atoms occupy octahedral sites only between every two layers of iodine atoms[11].

More credence is given to the above deduction by the fact that SnI_2 and PbI_2 have been observed to form a continuous series of solid solutions, $Pb_xSn_{(1-x)}I_2$ ($0 \leq x \leq 1$), the resulting solution having a PbI_2 structure[3,12]. It must be noted that the preparation of these solid solutions took place at high temperatures (usually >>108°C) at which the β-SnI_2 has the derived hexagonal lattice structure. We would therefore expect the two compounds to mix quite freely.

It is interesting to note that if we assume that β-SnI_2 has the same molecular volume as PbI_2 (since we assume the same crystal structure which is hcp) then the density of SnI_2 would be 4.97 gm/cc. We found that

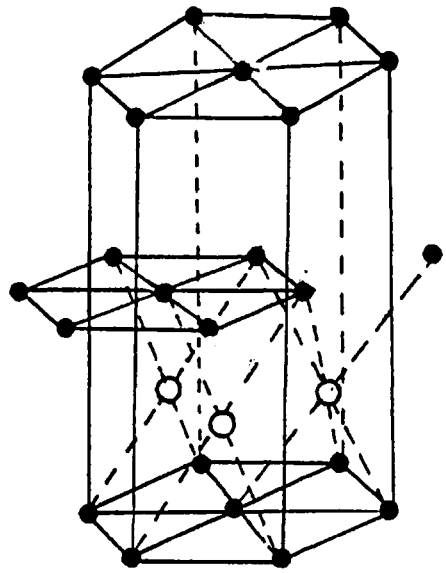

Fig. 2.3: Layer structure of PbI_2 (2H)[10]. The open circles represent Pb atoms, while the dark circles represent iodine.

the x-ray density was 4.81 gm/cc which is close to the calculated value.

SnI_2 is able to form polymorphic forms which differ in their crystal density because of the electronic configuration of tin (2+) ion ([Kr] $4d^{10}$ $5S^2$). The outermost s-orbital is easily polarisable and because of its shape can be "squashed in" to form a more condensed structure, as appears to be the case for SnI_2. More evidence in support of this model has been obtained from our optical work as reported in Chapter Three. The unique characteristic of the s-orbital in being able to be squashed in to form a more condensed crystal lattice has also been observed in iron, Fe, when it transforms from the more dense γ phase to the less dense δ phase at a temperature of 1390°C[13].

We have only been able to establish the phase transformation temperature, the unit cell dimensions and the crystal system of the β-polymorph of SnI_2. We have attempted to justify the transformation by a fairly crude transformation mechanism. More work would be needed to enable the full characterisation of the detailed structural arrangement of this

compound (i.e. in terms of bond lengths, interlayer spacings, bond angles etc.) which have not been considered in this work. With the achievement of the above the postulation of a more detailed mechanism for the phase transformation might be possible.

REFERENCES

1. K.S. Pitzer and J.H. Hildebrand. J. Am. Chem. Soc. 63, 2472 (1941)

2. P. Freudler and Y. Laurent. Comp. rend. 179, 1049 (1924)

3. R.A. Howie, W. Moser and I.C. Trevena. Acta Cryst. B28, 2965 (1972)

4. N.F.M. Henry, H. Lipson and W.A. Wooster. "The Interpretation of X-ray Diffraction Photographs", London,Macmillan & Co. Ltd. 1960, chapt. 12

5. R.B. Sosman. "The Phases of Silica", New Brunswick, Rutgers Univ. Press, 1965, p.75

6. M.J. Buerger. "Phase Transformations in Solids". (R. Smoluchowski, ed.), New York, Wiley, 1951, p.105

7. F.D. Bloss. "Crystallography and Crystal Chemistry - An Introduction", Holt Rinehart and Winston Inc., New York, 1971, chapt. 10

8. M.J. Buerger. Fortschr Mineral 39, 9 (1961)

9. D. McKie and C. McKie. "Crystalline Solids", Thomas Nelson, Exeter, 1974, p.476

10. M.G. Albrecht. Ph.D. Thesis, Imperial College, London (1975)

11. National Bureau of Standards, Circular 439, 5, 35 (1955)

12. D.P. Belotskii, I.N. Antipov, V.F. Nadtochic and S.M. Dodik. Izv Akad Nauk SSSR, Neorg. Mater. 5(10), 1852 (1969)

13. V.K. Grigonovich. The D.I. Mendeleyev Periodic System and Electron Structure of Metals, "Nauka", 1966

CHAPTER THREE

OPTICAL AND ELECTRICAL PROPERTIES

In this Chapter the optical and electrical properties of SnI_2 are investigated. The relationship of the main optical constants, n, the refractive index, and K, the extinction coefficient to photon energy are investigated for the two modifications of SnI_2. The nature of the excitation of electrons between the valence and the conduction bands have also been looked into. The variation of the resistivity with temperature has been determined and attempts have been made to distinguish between the electronic and ionic conductivities of the two modifications of SnI_2.

3.1 OPTICAL PROPERTIES

3.1.1 Determination of Optical Constants - Theory

Data on the optical constants, n and K of thin films are obtained by investigating the transmission and reflection of light, by the test material. The complete formulae for the transmission, $T = \frac{I_t}{I_o}$, or reflection, $\mathcal{R} = \frac{I_r}{I_o}$, (i.e. the ratio of the intensities of the incident and transmitted (I_t) or reflected (I_r) light beams) of a sample with monochromatic radiation of wavelength λ can be expressed as[1]

$$T = \frac{I_t}{I_o} = e^{-\alpha x} \frac{[(1-R)^2 + 4R \sin^2 \theta]}{(1-Re^{-\alpha x})^2 + 4Re^{-\alpha x} \sin^2(\theta+\phi)} \qquad (3.1a)$$

$$\mathcal{R} = \frac{I_r}{I_o} = \frac{R[(1-e^{-\alpha x})^2 + 4e^{-\alpha x} \sin^2\phi]}{(1-Re^{-\alpha x})^2 + 4Re^{-\alpha x} \sin^2(\theta+\phi)} \qquad (3.1b)$$

where x is the sample thickness, α the absorption coefficient, and R is the surface reflectance. The values of the angles θ and ϕ are given by the formulae:

$$\theta = \tan^{-1} \frac{2K}{n^2 + K^2 - 1} \quad \text{and} \quad \phi = \frac{2\pi n x}{\lambda}$$

ϕ indicates the phase change on one traverse of the sheet of thickness x, while the second term in the denominator of Eqn. (3.1) is an interference term which can be used advantageously to determine n from the interference fringes which result when α is small enough to allow the light wave to traverse the sample several times.

If no interference fringes are observed because,for example, of surface roughness, or high absorptivity of the film, we can average over the interference term and use the simple relationships, namely

$$T = \frac{(1-R)^2 \; e^{-\alpha x} \; (1 + K^2/n_2)}{1 - R^2 \; e^{-2\alpha x}} \tag{3.2a}$$

$$\mathcal{R} = \frac{R(1 - e^{-2\alpha x})}{1 - R^2 \; e^{-2\alpha x}} \tag{3.2b}$$

These equations show that n and K can be found from T and $\mathcal{R}$.

For most transmission experiments, $K^2 \ll n^2$, hence Eqn. (3.2a) reduces to the form[2]

$$T = \frac{(1-R)^2 \exp(-\alpha x)}{1 - R^2 \exp(-2\alpha x)} \tag{3.2c}$$

The above formula (Eqn. (3.2c)) allows for multiple internal reflections from the sample surface.

The transmission coefficient, T, and reflectance, R, are directly measurable quantities, hence the absorption coefficient of the thin films of thickness x can be calculated from the relationship[3]

$$\alpha = \frac{1}{x} \ln \left[\frac{(1-R)^2}{2T} + \sqrt{\frac{(1-R)^4}{(2T)^2} + R^2} \right] \qquad (3.3)$$

which also allows for multiple internal reflection from the sample surface[2].

Equations (3.2) and (3.3) are valid for all angles of incidence. For the simplest case of the normal incidence, the reflectivity is given as

$$R = \frac{n^2 + K^2 - 2n + 1}{n^2 + K^2 + 2n + 1} \qquad (3.4)$$

where n and K are the real and imaginary parts of the index of refraction $N = n - iK$, when K is expressed as[3]

$$K = \frac{\alpha\lambda}{4\pi} \qquad (3.5)$$

Equation (3.4) can be rearranged to the form,

$$n = \frac{1 + R + \sqrt{4R - (1-R)^2 K^2}}{1-R} \qquad (3.6)$$

from which the values of n as a function of wavelength can be determined from the experimental values of R, and K is calculated from experimental values of α, using Eqn. (3.5).

3.1.2 Intrinsic Optical Absorption Band - Theory

The existence in all ionic or covalent materials of a wide spectral region of very intense absorption, limited on the long wavelength side by a sharp edge, is due to the fact that the absorption of photons of sufficiently high energy is accompanied by electron transitions from the valence to the conduction band. The readily observed increase in the absorption coefficient for photons of energy $h\nu > Eg$ (where Eg is the band gap energy) allows us to estimate the value of the forbidden band width, i.e. the shape of the absorption band edge is governed by the electron energy-band structure of the material.

The expression for the absorption coefficient corresponding to an electron transition from a state i in the valence band to a state f in the conduction band (see Fig. 3.1) without phonon participation has the form[1]

$$\alpha = \frac{c}{\nu} |P_{i,f}|^2 N(h\nu) \tag{3.7}$$

where c is a constant, representing the medium and $N(h\nu)$ is the density distribution of the final states over an interval of unit energy. The matrix element representing transitions of this type is

$$P_{i,f} = -i\hbar \int \psi_f e_K \operatorname{grad} \psi_i \, d\tau \tag{3.8}$$

where e_K is the polarization vector of radiation with the wave vector K, $i = \sqrt{-1}$. The wave functions of electrons in a crystalline solid can be written in the following form

$$\psi_{Kn} = e^{iK.r} U_{Kn}(r) \tag{3.9}$$

where U_{Kn} are periodic functions with the same period as the lattice. P_{if} vanishes at any point where the following selection rule is not satisfied.

$$K_i + K = K_f \tag{3.10}$$

which can be expressed as

$$K_i \approx K_f \tag{3.11}$$

since the wave vectors of an electron in the initial and final states are much greater than the wave vector of a photon.

In accordance with the above selection rule, Herman[4] derived that the energy threshold for the vertical (direct) transitions should correspond to the frequency

$$h\nu' = E_C' - E_V \tag{3.12}$$

which is considerably higher than

$$h\nu = E_C - E_V \tag{3.13}$$

as shown in Fig. 3.1a.

Experimental results on absorption edge measurements on silicon and germanium[5] show that the absorption increased strongly at $h\nu \approx Eg_i$. This phenomena was explained by Barden, Blatt and Hall[6] to be due to the relaxation of the selection rule of Eqn. (3.10) in the regions of photon energies insufficient for direct transitions. This was because of the interaction of electrons with phonons. Thus in the energy band structure shown in Fig. 3.1a, we can follow Herman[4]

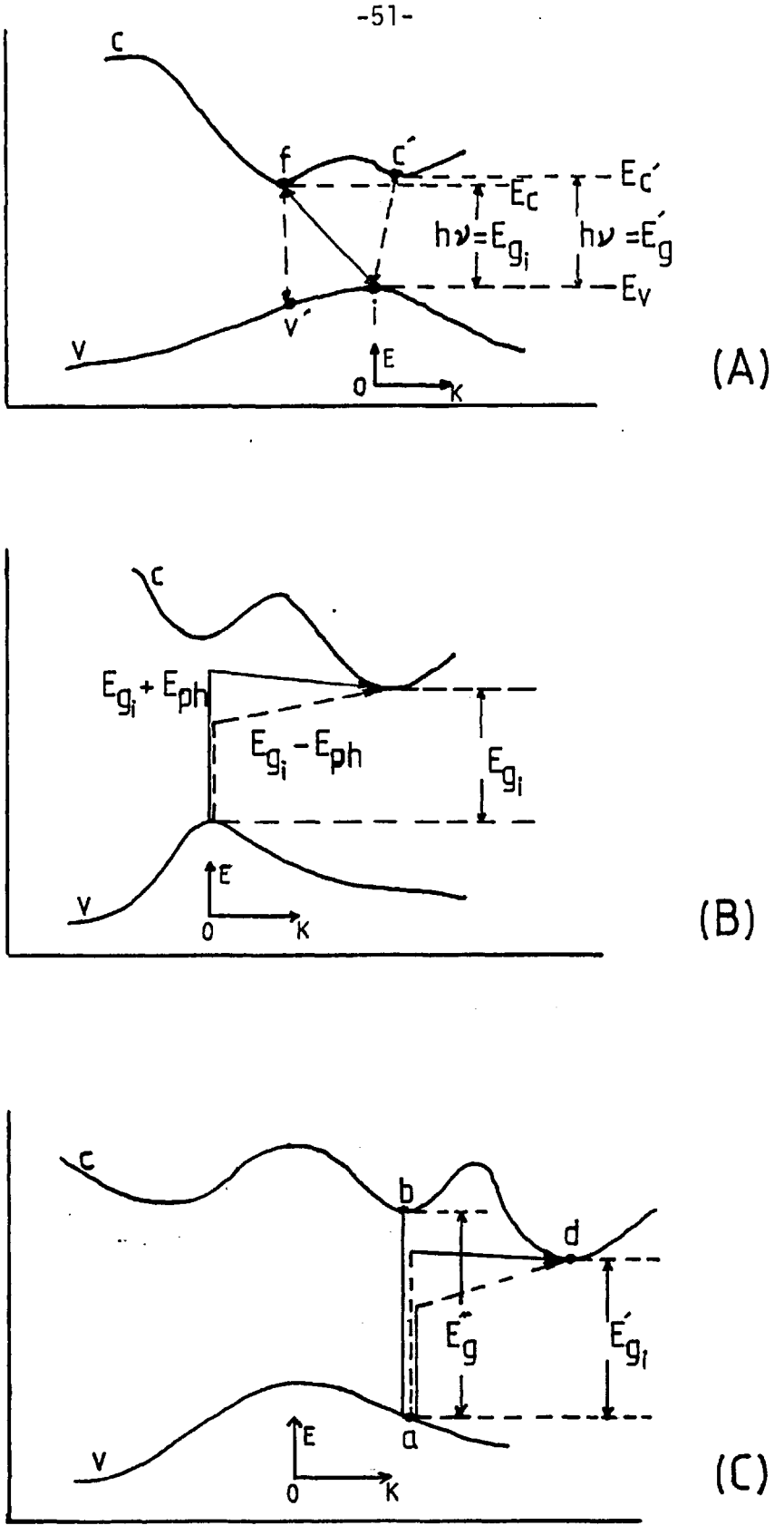

Fig 3·1 Energy band structure for different forms of optical transitions in some hypothetical semiconductors. v denotes valence band, while c denotes conduction band. A and B represent the case for allowed transitions at K=0 while C represents that for forbidden transition at K=0.

in assuming that an electron is excited optically (with phonon assistance) from a state i to c' and is then transferred from c' to f, thus emitting a phonon. As a result of this, the electron wave vector changes considerably and the whole process can be considered as a "non-vertical" or "indirect" transition from i to f with the absorption of a photon of energy $h\nu = Eg_i$.

Assuming that the phonon matrix elements are constant, and that $E_{v'} - E_i \approx E_{c'} - E_f$, Barden et al.[6] have shown that the wavelength dependence of the absorption coefficient for an indirect transition should be

$$\alpha_i = A(h\nu - Eg_i \pm E_{ph})^2 \qquad (3.14)$$

in the case when transitions are possible for K = 0. E_{ph} is the phonon energy.

The indirect transition with phonon absorption is expressed as

$$\alpha_{ia} = A(h\nu - Eg_i - E_{ph})^2 \qquad (3.14a)$$

while

$$\alpha_{ie} = A(h\nu - Eg_i + E_{ph})^2 \qquad (3.14b)$$

represents indirect transition with phonon emission. These transitions are shown more clearly in Fig. 3.1b.

For direct transitions, beginning with threshold energy Eg', the absorption coefficient α_d increases according to the theory as follows:

$$\alpha_d = A'(h\nu - Eg')^{\frac{1}{2}} \qquad (3.15)$$

as shown in Fig. 3.1a.

Equations (3.14) and (3.15) are for indirect or direct transitions respectively, allowed by the selection rule at K = 0. There are some compounds that are characterised by forbidden transitions, i.e. transitions which are not possible at K = 0, become possible at $K \neq 0$. The spectral variation of absorption coefficient for compounds of this type characterised by forbidden indirect transition has been shown also by Barden et al.[6] to be

$$\alpha_{fi} = A(h\nu - Eg_i' \pm E_{ph})^3 \qquad (3.16)$$

while that of forbidden direct transition is

$$\alpha_{fd} = A'(h\nu - Eg'')^{3/2} \qquad (3.17)$$

These transitions are schematically represented in Fig. 3.1c.

The considerable difference between Eqns. (3.14) to (3.17) can be used to analyse the experimental data on the form of the absorption band edge, and to explain the nature of electron transition.

3.2 EXPERIMENTAL SET-UP FOR OPTICAL MEASUREMENTS

Room temperature optical transmission and reflection measurements were made on thin films of SnI_2 evaporated on clean glass slides (substrate cleaning procedure in Chapter 4). The evaporation took place in a vacuum of about 1.7×10^{-6} torr. The evaporation set-up and the description of the vacuum equipment are as detailed in Chapter 4.

The temperature at which the glass substrate is kept during evaporation was found to determine the type of SnI_2 obtained. This effect is similar to the effect of the solvent on the modification type that can be obtained during preparation as described in Chapter 2.

In the thin film form as well as in the powder form (Chapter 2), SnI_2 has been found in this work to change polymorphic form from the red to the yellow form, at a temperature of 108°C. Evaporating SnI_2 on a substrate held at room temperature resulted in the yellow (high temperature) form. However on evaporating SnI_2 on 'hot' substrates, i.e. substrates kept at a temperature of about 100°C, and then allowed to cool down to room temperature after the evaporation was completed, resulted in a film which was the red modification. The two polymorphs of SnI_2 are henceforth referred to as α-SnI_2 (red) and β-SnI_2 (yellow) polymorph.

The thickness of the film was directly determined during evaporation by the use of a quartz crystal thin film monitor, housed in the same jig, and next to the glass substrate as shown in Fig. 3.2. The operational mode of the thin film monitor (quartz crystal microbalance) is fully documented in Chapter 4. To determine the film thickness most accurately, there was need for calibration. This was achieved by evaporating films of SnI_2 onto glass substrates held in a substrate jig (see Fig. 3.2) and through a metal mask in contact with the substrate. This enabled well defined patterns to be detailed on the substrate with well defined edges. Gold was later uniformly evaporated on the glass slides with the mask removed, to give a good reflecting surface. The thickness of the SnI_2 film was then conveniently measured on a multiple beam interferometric microscope (Varian Vacuum division). The thickness was correlated

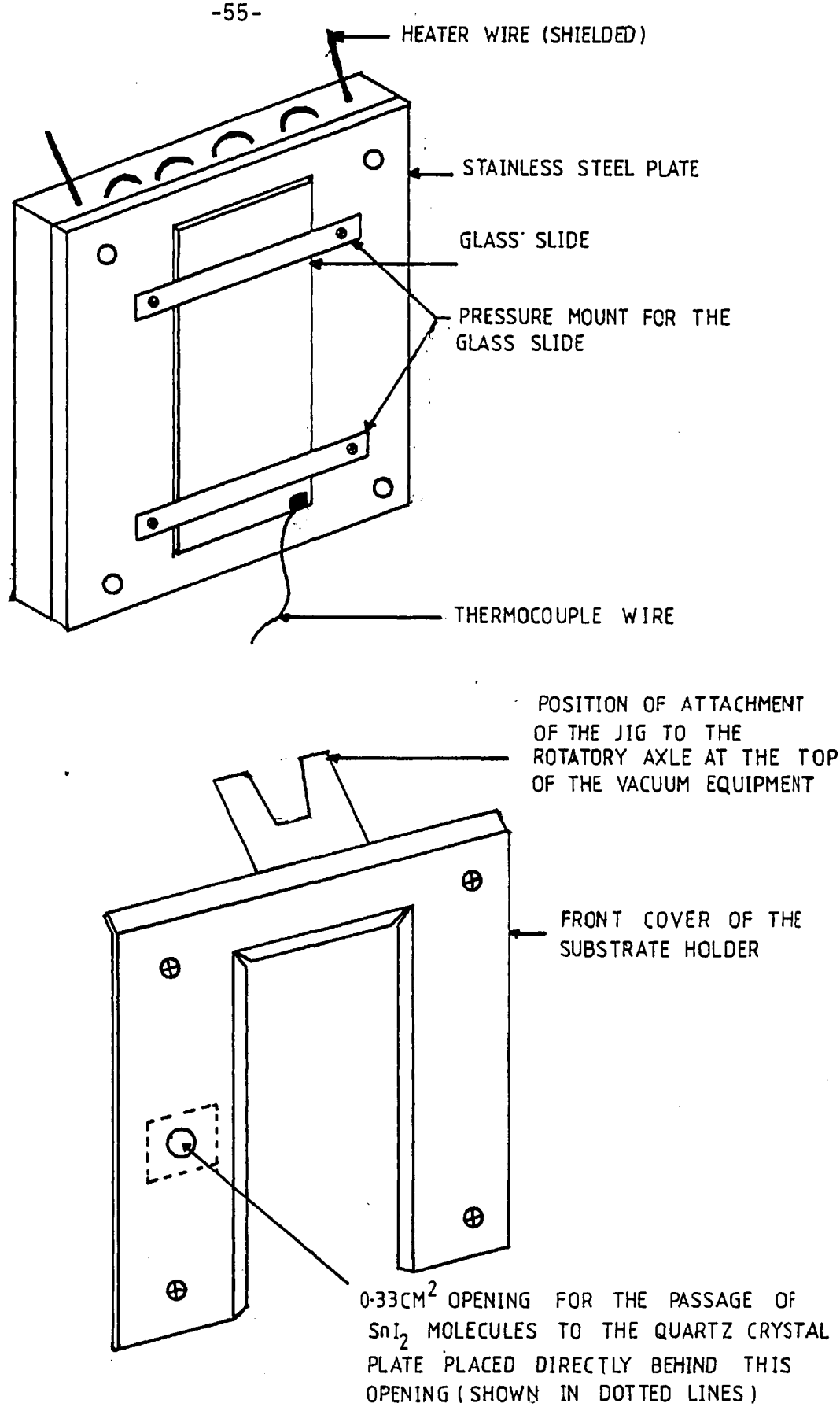

Fig 3·2 Substrate holder arrangement for the evaporation of SnI_2 on glass substrates. This arrangemt is also used during the photolysis of thin films on glass substrates.

to the change in the resonant frequency of the quartz crystal microbalance, and was therefore an index of the film thickness. This is a most accurate method, since the inherent error in the film thickness determination is well within 5%. Results obtained from the above thickness determination were checked against "Tallysurf" measurement of the same set of films. The agreement between the two modes of film thickness measurement was very good, i.e. within 2%.

Transmission measurements on the thin films were made at room temperature in a Bechman DK2A double beam spectrometer, over the wavelength range 0.36 to 2.5 μm. The experimental arrangement is as shown in Fig. 3.3. Transmission spectrum was obtained in two parts. In the infra-red region, (0.65 to 2.5 μm), a lead sulphide detector was used above the integrating sphere, this was replaced by a photomultiplier tube for the scan in the visible below 0.75 μm.

The reflection spectrum was taken relative to the reflecting surfaces of ceramic plates (of known reflectivity) as shown in Fig. 3.3, but with the sample and reference being held in front of the two ceramic tiles, in such a way that they "look" into the integrating sphere. The same set of detectors were employed as in the transmission measurements, covering the wavelength range 0.36 to 2.5 μm.

3.3 RESULTS

Transmission and reflection measurements were made at normal incidence (0.36 to 2.5 μm) for thin films of the two modifications of SnI_2. In Fig. 3.4 are presented the transmission results for both types of SnI_2, using films of about the same thickness (~8000Å), while in Fig. 3.5 are presented the reflectivity data for the same set of films. Both types of SnI_2 are observed to be appreciably transparent in the

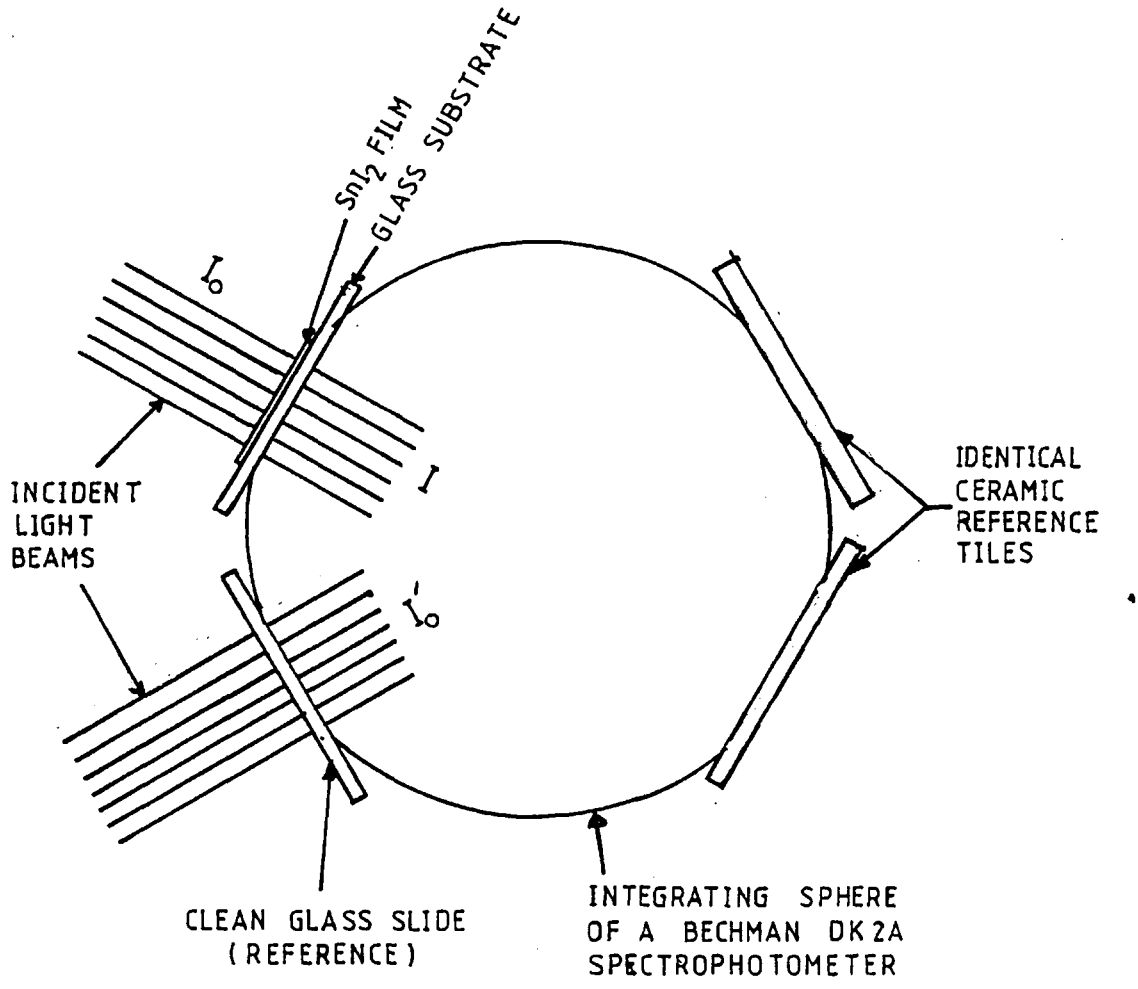

Fig 3·3 Experimental arrangement for the measurement of the transmission spectrum of SnI_2 films.

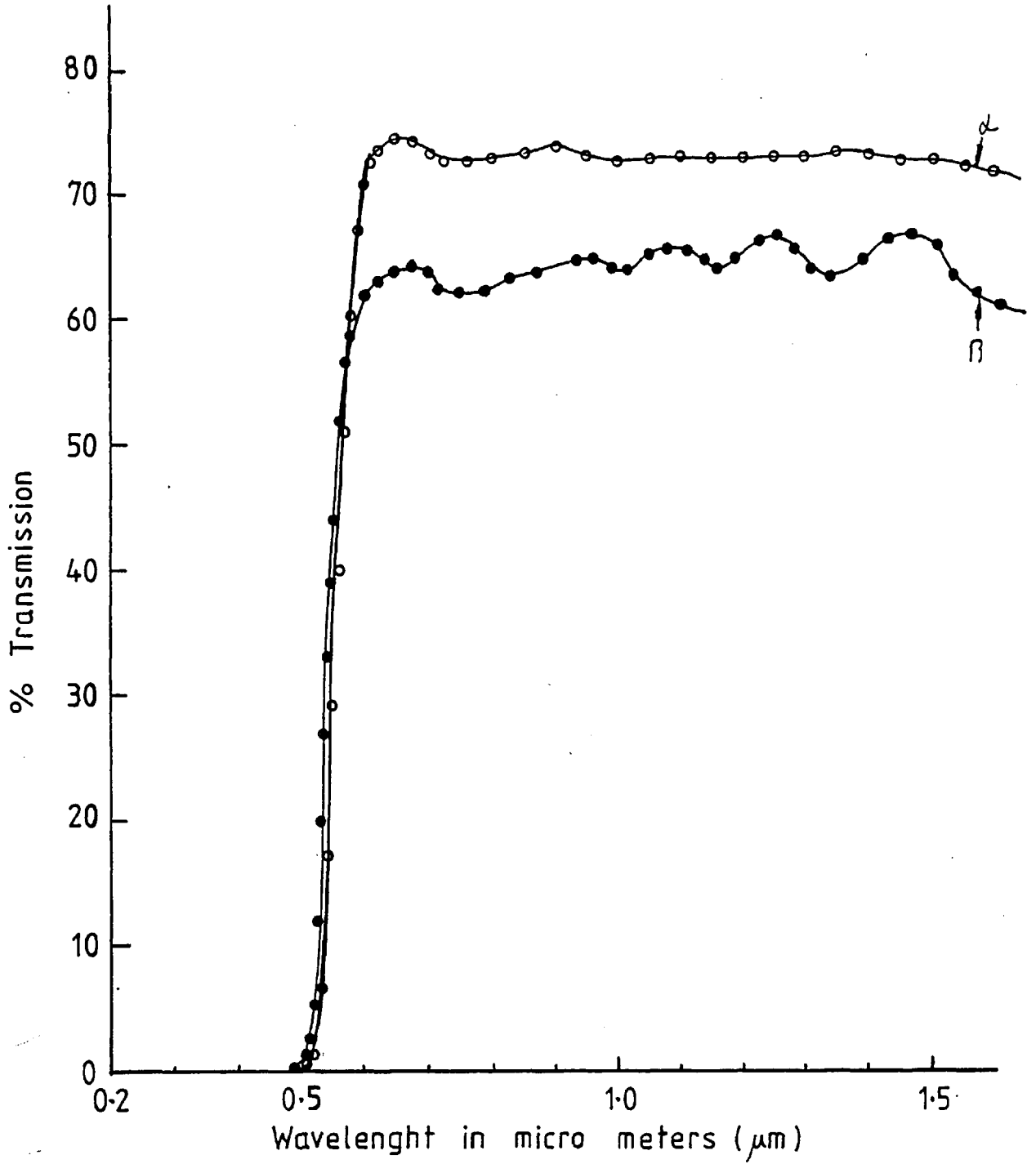

Fig 3·4 Room temperature transmission spectra of thin films of the red(α) and yellow(ß) polymorphs of SnI_2. Film thickness ≈ 8000 Å.

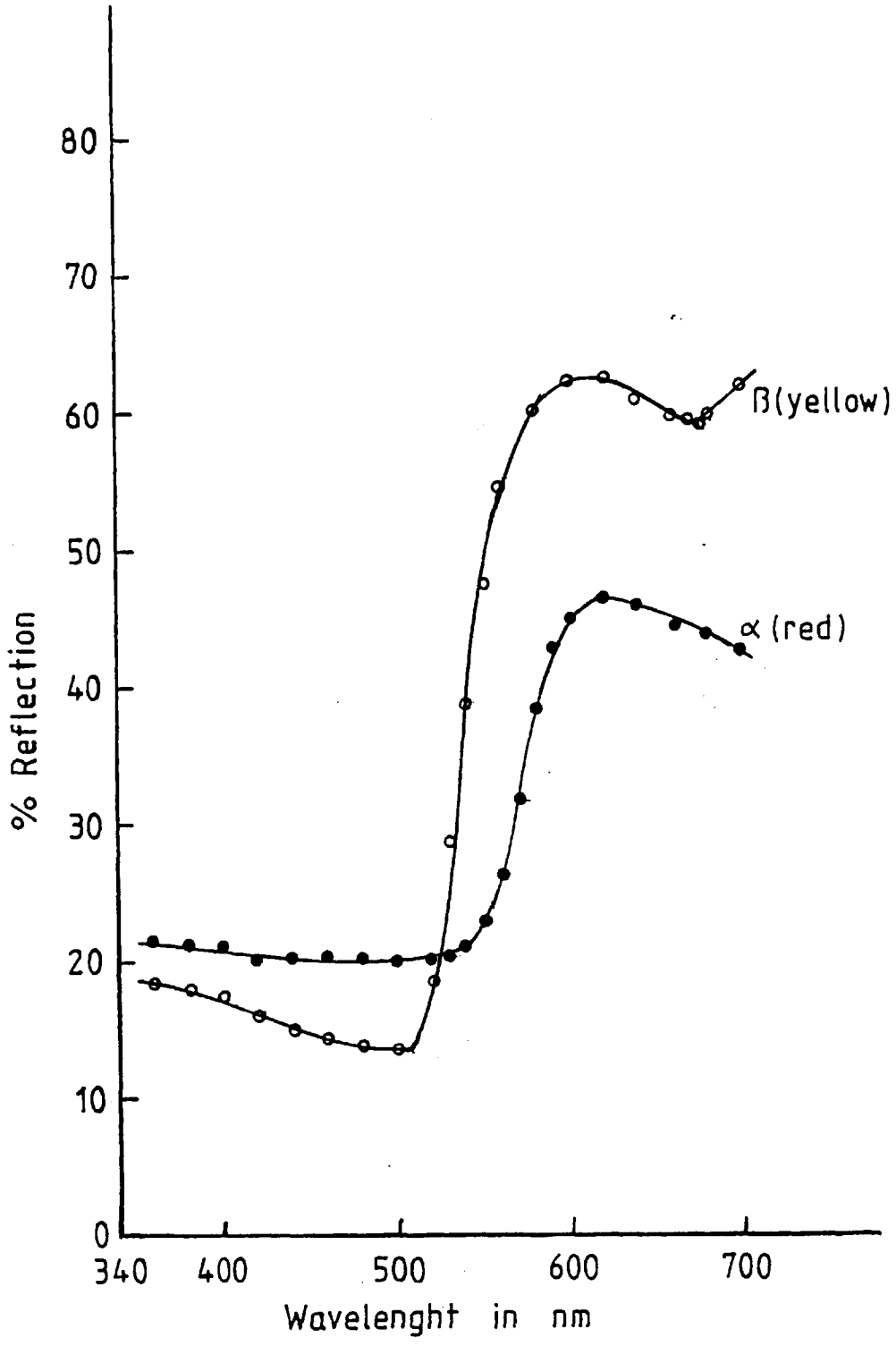

Fig 3·5 Room temperature reflection spectra of the red(∝) and yellow(ß) polymorphs of SnI_2. Film thickness ≈8000 Å.

infra-red, the absence of reproducible absorption peaks within this region did indicate a lack of impurity absorption effects. The regions of the band edge are very well defined in both types of polymorphs. The transmission spectra of this region is presented in Fig. 3.6 for thinner films of both specimens ($\sim$5000Å). These show much more evidence of structure than was possible in the thicker films of Fig. 3.4. In the β-SnI_2, transmission peaks are observed at 623 nm (1.99 eV), and 542 nm (2.287 eV), with a shoulder in the transmission spectrum at 500 nm (2.48 eV). Peaks that are not very strong are observed in α-SnI_2 at 594 (2.088 eV), 632 (1.962 eV) and 660 nm (1.879 eV) respectively. The above set of peaks were observed to be very reproducible for all samples of thickness $x \leq 7000$Å. These peaks were tested for interference effects[2], but were found not to be due to interference effects in the films.

The variation of absorption coefficient, α, (obtained from Eqn. (3.3), with wavelength for both types of SnI_2 in the high absorption regions are as presented in Fig. 3.7. Both α-, and β-SnI_2 are characterised by high absorption coefficients, $\alpha > 10^4$ cm^{-1}, while β-SnI_2 appears to be the more absorbing of the two. β-SnI_2 also shows more evidence of structure for $\alpha > 5.8 \times 10^4$ cm^{-1}.

The refractive index n, and the extinction coefficient, K, for both polymorphs of SnI_2 were calculated using Eqns. (3.5) and (3.6). The variation of n and K with wavelength are quite similar to those obtained by Tubbs[7] for thin films of PbI_2. The variation of n and K wth wavelength are as shown in Figs. 3.8 and 3.9 for α- and β-SnI_2 respectively. Fig. 3.9b also indicates the variation of n and K with wavelength as obtained by Tubbs for PbI_2. The n values rose from a value of 2.00 in the very absorbing region to a value of about 5.97 in the fairly

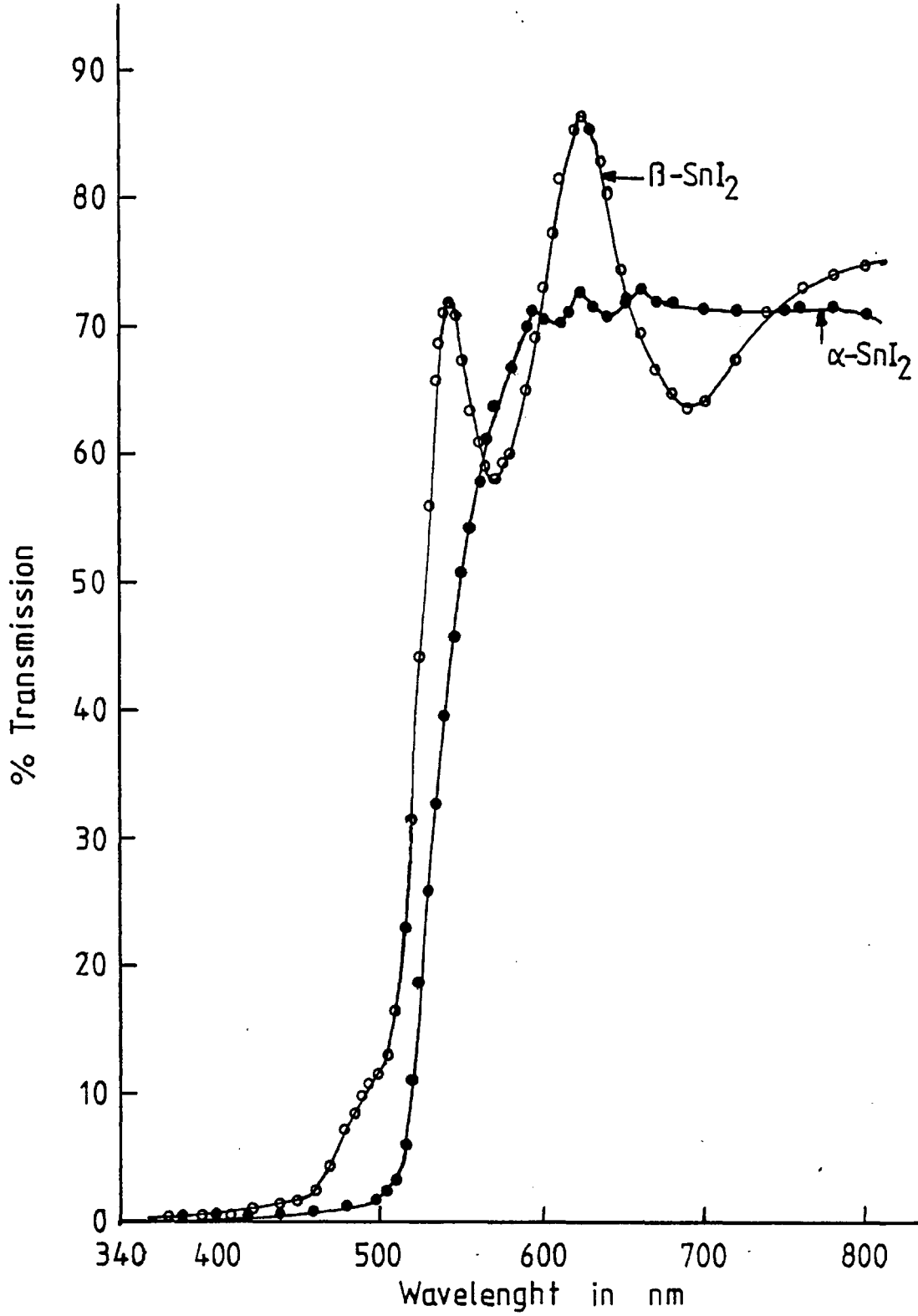

Fig 3·6 Room temperature transmission spectra for yellow and red thin films (0·48 and 0·55 μm thickness respectively) of SnI_2 .

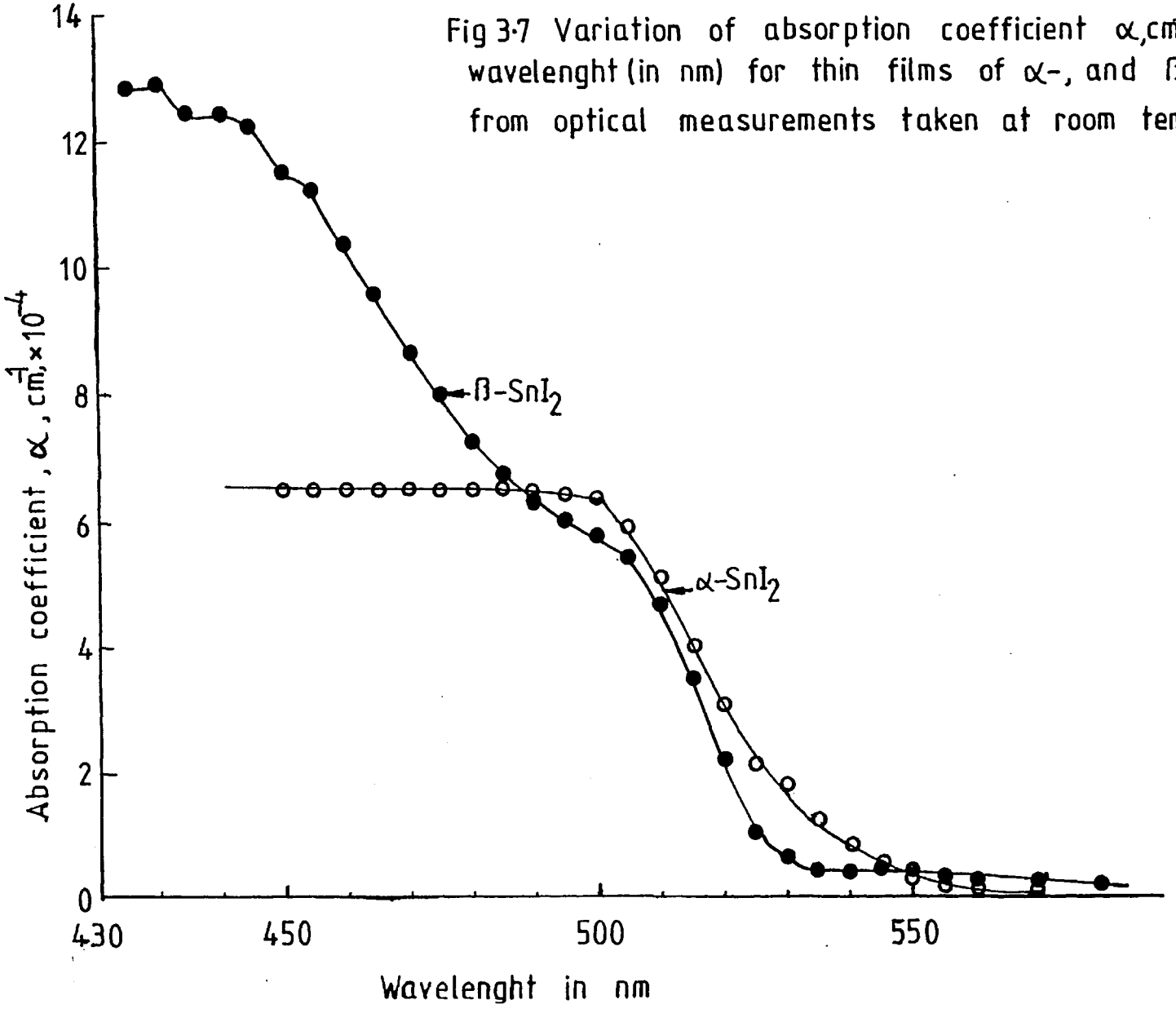

Fig 3·7 Variation of absorption coefficient α, cm^{-1} with wavelenght (in nm) for thin films of α-, and β-SnI_2 from optical measurements taken at room temperature.

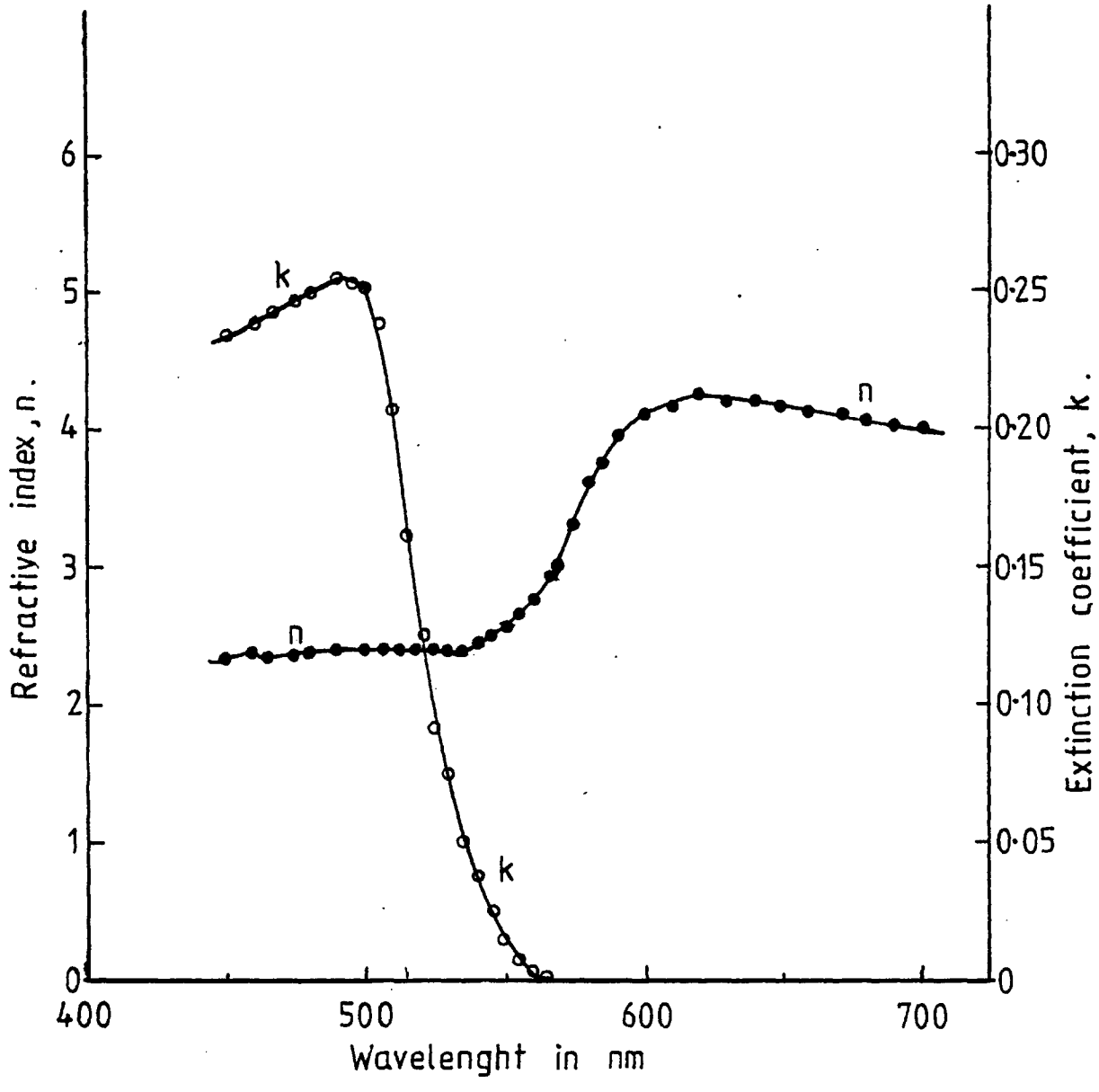

Fig 3·8 Variation of refractive index, n, and extinction coefficient, k, with wavelenght for thin films of α-SnI_2 in the absorption edge region.

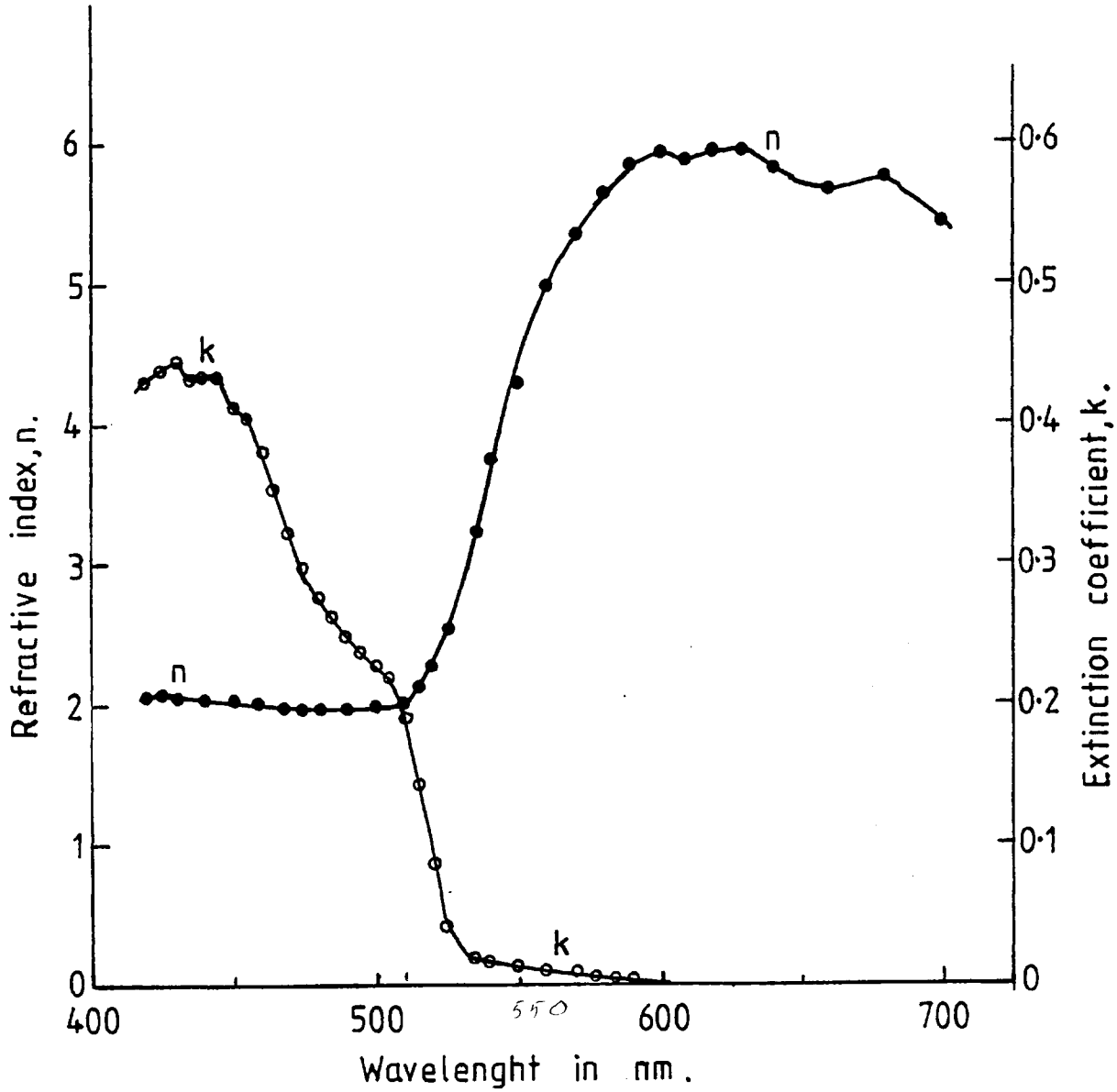

Fig 3·9(a) Variation of refractive index, n, and extinction coefficient, k, with wavelenght in the absorption edge region for thin films of β-SnI_2

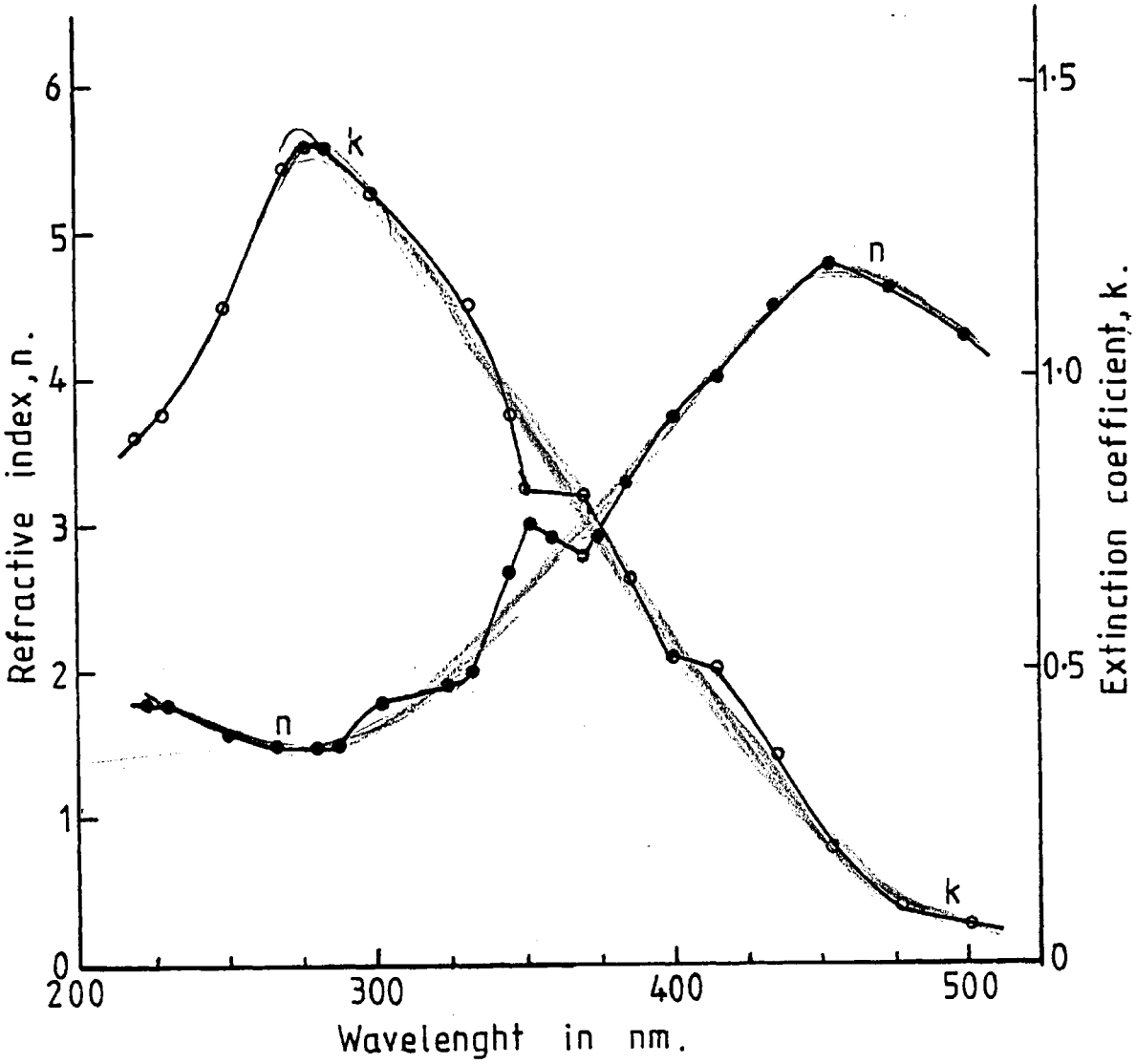

Fig 3·9(b). Variation of refractive index, n, and extinction coefficient, k, with wavelenght for PbI_2 as given by Tubbs [7].

transparent region for the β-SnI_2 films, while there was an increase from 2.40 in the absorbing region to 4.52 in the fairly transparent region for the α-SnI_2 films. The n and K values are estimated to be correct to 5% as the only possible source of error in their calculation could only have come from the sample thickness measurement.

3.4 DISCUSSION

In accordance with the analysis of optical absorption data discussed by Barden et al.[6], the region of high absorption was investigated for evidence of either direct allowed or direct forbidden transitions in tune with Eqns. (3.15) and (3.17) for both polymorphs of SnI_2. For values of $\alpha > 10^4$ cm^{-1}, no region in the photon energy range greater than 1.9 eV showed any evidence for a fit in either polymorph, for forbidden direct transition dependence of photon energy, hν of $\alpha \propto (h\nu - Eg_o)^{3/2}$ where Eg_o is the direct forbidden transition band gap energy. However as shown in Fig. 3.10, and Fig. 3.11, for α- and β-SnI_2 respectively, there appears to be a good fit for allowed direct transitions where $\alpha \propto (h\nu - Eg')^{\frac{1}{2}}$, for both modifications. The extrapolated values of the allowed direct transition energy Eg′ are 2.358 ± 0.071 eV for α-SnI_2, and 2.495 ± 0.075 eV for β-SnI_2.

The α values were also examined for evidence of either allowed or forbidden indirect transition as given by Eqns. (3.14) and (3.16). Our data would not fit into Eqn. (3.16) for forbidden indirect transitions. There was, however, a good fit for allowed indirect excitation with a plot of $\alpha^{\frac{1}{2}}$ against photon energy as shown in Figs. 3.10 and 3.11 for the α-, and β-SnI_2 polymorph respectively. The fit is for $\alpha \leq 10^4$ cm^{-1}, since there is considerable deviation for $\alpha > 10^4$ cm^{-1}. The good fit (for $\alpha \leq 10^4$ cm^{-1}) gives a clear indication that the mode of excitation in

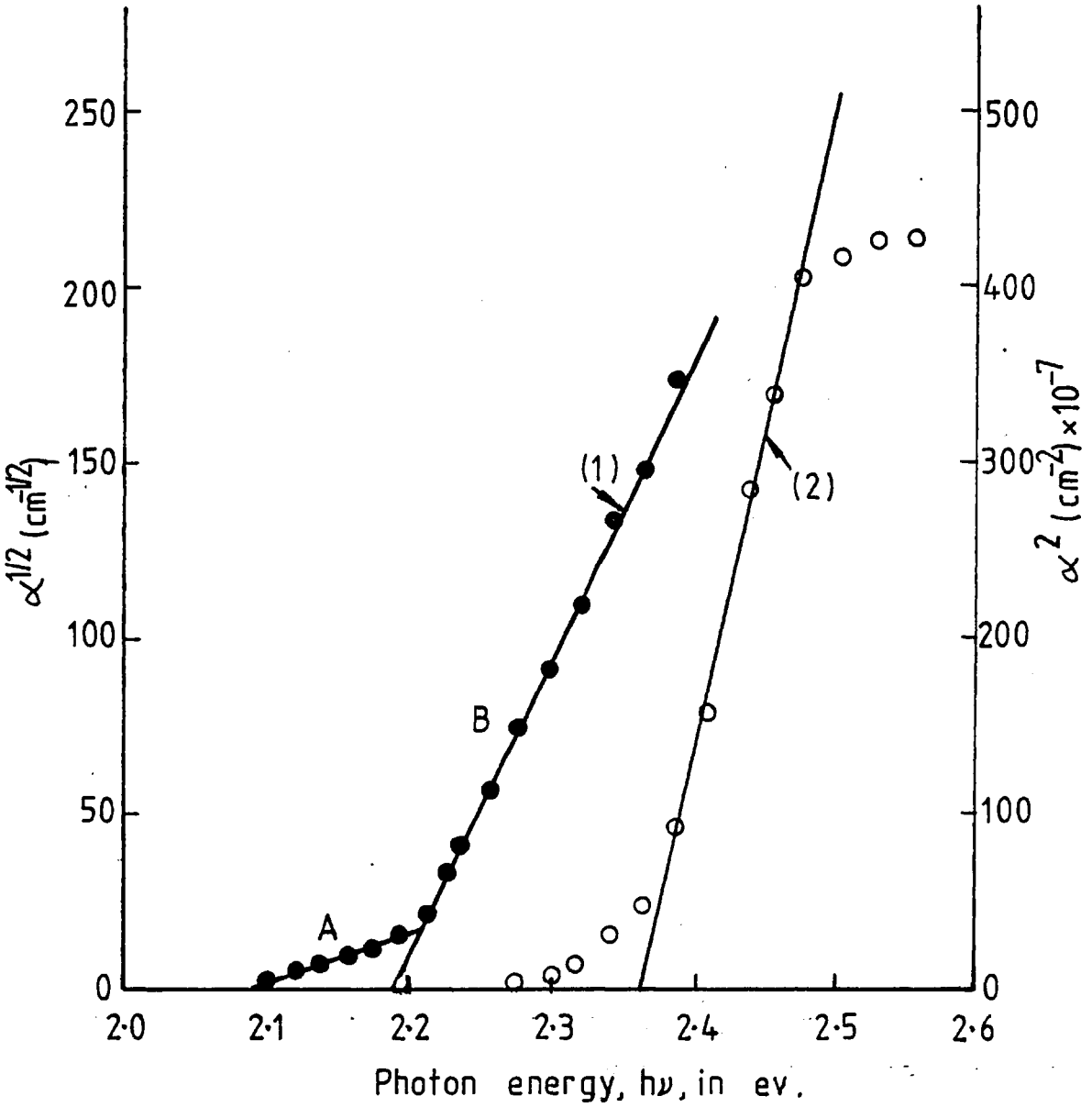

Fig 3·10 Absorption edge structure for α-SnI_2 at room temperature. Curve (1) is the variation of $\alpha^{1/2}$ with photon energy, while (2) is the variation of α^2 with photon energy.

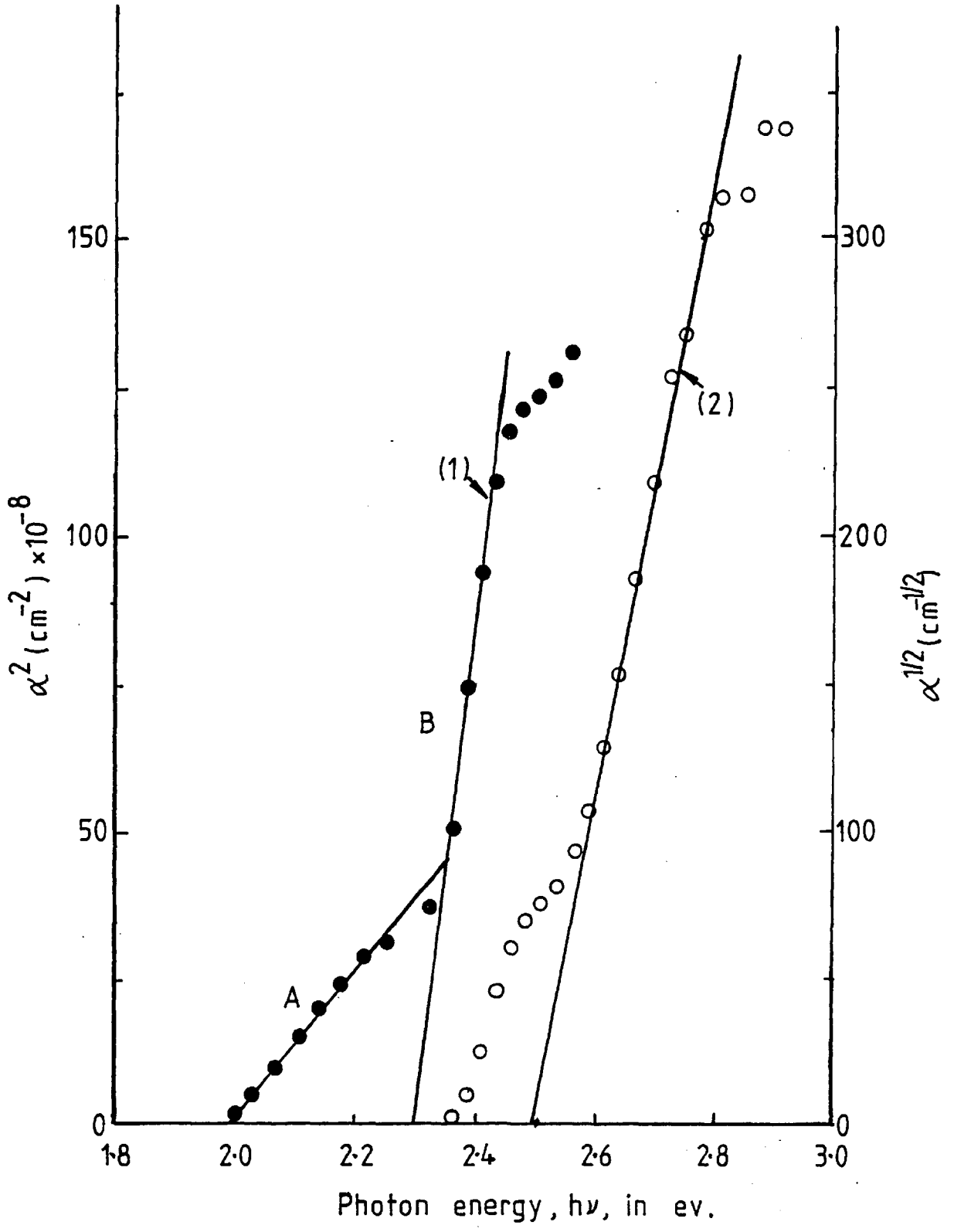

Fig 3·11 Absorption edge structure for ß-SnI_2 at room temperature. Curve (1) shows the variation of $\alpha^{1/2}$ with photon energy while curve (2) shows the variation of α^2 with photon energy.

this absorption coefficient regime is mostly due to allowed indirect transitions. The transitions are taken to be due to phonon interaction with lattice electrons, hence the two linear regions labelled A and B in the $\alpha^{\frac{1}{2}}$ against $h\nu$ plot of Figs 3.10 and 3.11, can be interpreted to be due to phonon absorption, and phonon emission respectively. An extrapolation of the lines result in an allowed indirect transition energy Eg_i of 2.136 ± 0.045 eV for α-SnI_2, and Eg_i of 2.153 ± 0.045 eV for β-SnI_2. The phonon interaction energies have also been estimated to be 0.051 ± 0.002 eV and 0.152 ± 0.005 eV for α and β-SnI_2 respectively.

An earlier report on the optical properties of SnI_2 by Gorban et al.[8] did indicate that the compound was characterised by an indirect absorption, and a nearby direct one. The polymorphic type was not stated, but is believed to be the yellow polymorph, since the films were produced on room temperature substrates. Their results are compared in Table 3.1 along with the results obtained in this work for experiments carried out at room temperature.

Eg'	Eg_i	E_{ph}	Polymorphic type	Reference
2.495	2.143	0.152	Yellow	This work
2.358	2.136	0.051	Red	This work
2.592	2.068	0.054	Unspecified	8
2.40	-	-	Unspecified	9

Table 3.1: Comparison of the energies of direct and indirect (allowed) transitions for SnI_2 obtained in this work and earlier works.

The values of the energy for direct or indirect transition obtained in references 8 and 9 differ from those obtain in this work, although the E_{ph} values compare quite favourably. Phonon interaction energies obtained in this work compare equally favourably with those obtained for CdI_2[10], PbI_2[11] and BiI_3[12], which are isoelectronic with SnI_2, and share the layer type lattice in common with SnI_2, which tends to show that our results are in order.

The experimentally determined values of Eg_i and Eg' compare favourably with the corresponding energies of the different peaks observed in the transmission or reflection spectrum of either of the polymorphs. For β-SnI_2, the peaks at 1.990 and 2.287 are well related to the Eg_i values of 1.99 and 2.29 eV respectively, while the shoulder at 2.48 eV corresponds with the band gap energy Eg' of 2.495. The shoulder at 2.48 eV can according to Tubbs[7] be deduced to be due to exciton transition. This is further supported by the energy obtained for the first and most intense of the exciton series of SnI_2 obtained by Gorban et al.[8], which was at 2.484 eV. There are no low temperature experimental data to give further weight to this deduction. However a plot of $(n^2-1)^{-1}$ against $(h\nu)^2$ did give a straight line with deviations in the high energy range as shown in Fig. 3.12. The deviations at high energies are ascribed to an exciton contribution near the absorption energy[13]. Since this effect is common to both polymorphs of SnI_2, the mode of transition can therefore be concluded to be due to allowed excitation directly or indirectly to exciton states in the conduction band. The peaks at 1.99 and 2.287 eV in β-SnI_2 can therefore be suggested to be due to indirect exciton transitions, while the shoulder at 2.48 eV can be taken to be due to direct exciton transitions near the absorption

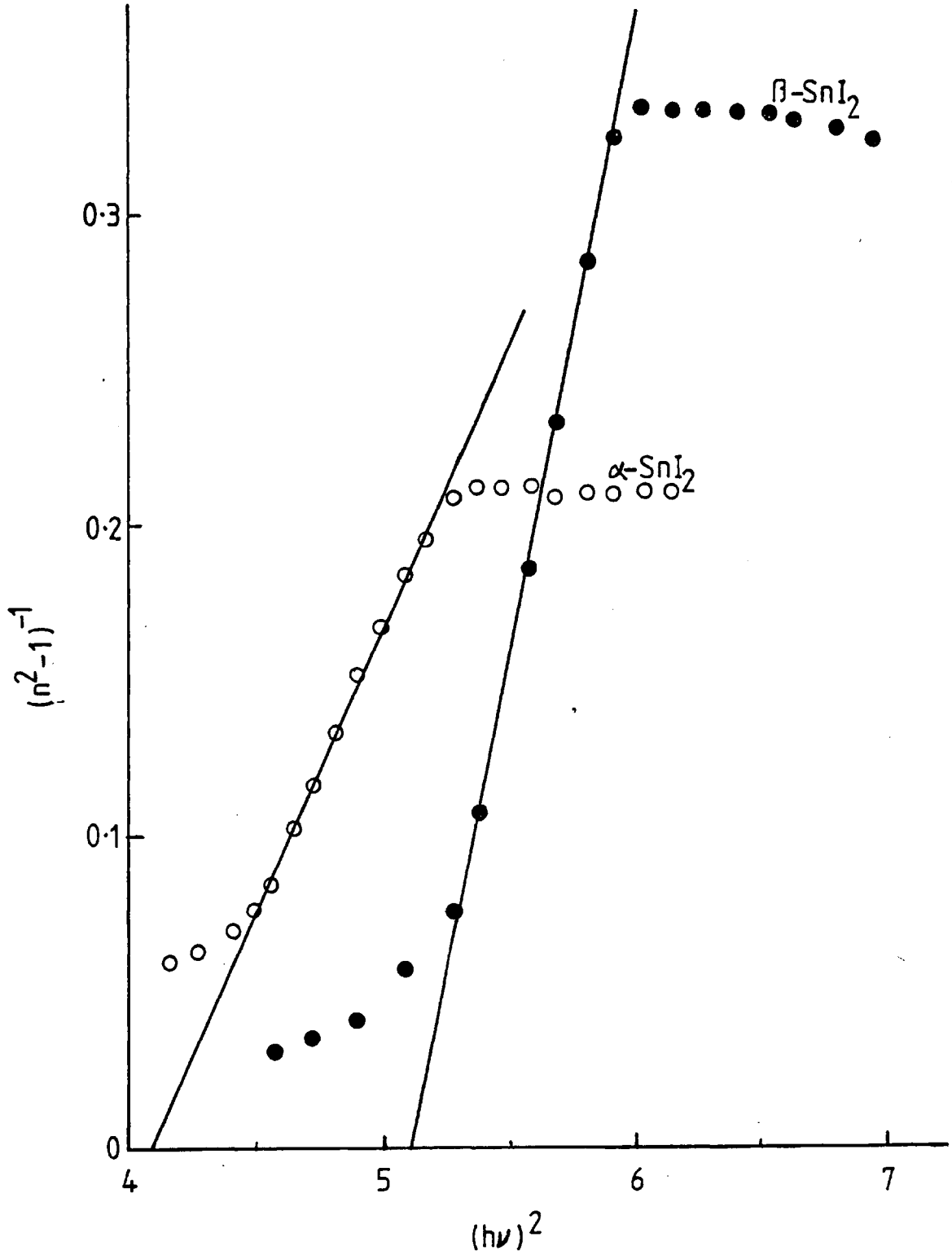

Fig 3·12 A plot of the value $(n^2-1)^{-1}$ against the square of the photon energy, $(h\nu)^2$, for α-, and ß-SnI_2.

edge. The peaks in the α-SnI_2 specimens at 2.088, 1.962, and 1.879 eV are also interpreted to be due to indirect exciton transitions. These peaks are not as resolved as is the case in β-SnI_2. The loss in resolution is attributed to the probable higher density (as discussed below) of this polymorph, which might also account for the obscuring of the direct exciton peak or shoulder in the spectrum of the specimen.

The denser polymorph of a material always has a higher refractive index than the less dense one[14]. A comparison of the refractive index for both α- and β-SnI_2 in the region of the band edge shown respectively in Figs. 3.8 and 3.9, indicates that the α-SnI_2 polymorph is denser. This conforms with the observation that the β-SnI_2 polymorph is the high temperature form, and is therefore expected to be of larger unit volume due to thermal expansion, which is probably upheld on cooling. This has been found to be correct as detailed in Chapter 2.

From studies of the room and liquid nitrogen temperature absorption spectra of many metal iodides with layer structure, Tubbs[15] assigned the main absorption peaks to excitonic transitions in anions situated in the strong electric field due to oppositely charged neighbours. The model predicts four strong exciton peaks that is, a low energy halogen doublet (called X_1 and X_2 by Tubbs) occurring near the absorption edge, and a high energy halogen doublet (X_3 and X_4) about one or two electron volts above the edge. The anionic exciton model has provided a useful zero-order scheme which allows interpretation of the observed excitonic absorption bands, especially the variation of the first exciton peak position with interionic distance in many metal iodides with layer structures such as CdI_2, ZnI_2, MnI_2, PbI_2 and BiI_3. However, the model is not favourable for SnI_2 in view of the present results. Firstly, if we associate the peaks at 1.99 and 2.29 eV in β-SnI_2 with the low

energy doublet, X_1 and X_2 respectively, as outlined by Tubbs,then the separation of the low energy doublet would only be 0.3 eV (which is still lower in α-SnI_2). Tubbs' model predicts a much higher value. Therefore, to interpret such a small doublet separation, it would be necessary to consider an admixture of metal 5s states and the halogen 6p valence states. Secondly, there is complete absence of the high energy doublet X_3, X_4, in the spectrum of either polymorph of SnI_2. Thus the four exciton peaks expected from the Tubbs' model are not quite defined in the spectrum of both polymorphs of SnI_2.

The metal ions in SnI_2 have the outer electronic configuration $4d^{10}\ 5s^2$, which make them isoelectronic with Tl^+ and Pb^{2+} ions. In the intrinsic absorption spectra of TlCl and TlBr, a single exciton peak near the absorption edge was interpreted as a localised excitation of Tl^+ - ions[16]. This cationic model was supported by two independent calculations of the band structures of TlCl, and TlBr[17,18], in which both the top of valence band and the bottom of conduction band are located at the X zone edge in the Brillouin Zone and are mainly described with Tl6s and 6p wavefunctions respectively. In PbI_2, anomalous behaviours of band edge excitons have been explained by a repulsive central cell correction due to the cationic character of the excitons[19]. The cationic nature has been confirmed by a pseudopotential calculation of the band structure[20].

From the results of the optical work on SnI_2 (of unspecified polymorphic type) by Gorban et al.[8], they were able to associate the excitonic transitions with the cations. But in a recent computation of the band structure of SnI_2 by Dori et al.[21] (by a semiempirical tight binding method) based on the experimental data of Gorban et al.[8], a

reduced cationic character of the exciton was deduced. This was attributed to the fact that apart from the metal s-orbitals contributing to the excitation, there were also contributions from the iodine $P_{x,y,z}$ orbitals as well as the metal $P_{x,y}$ orbitals. As deduced earlier, α-SnI_2 is denser than β-SnI_2. The decrease in the direct band-gap energy Eg', with increased crystal density (Eg'_{α} = 2.358 eV and Eg'_{β} = 2.495 eV) observed in this work compares favourably with that reported for the layer structure materials like GaS and GaSe[22], CdI_2 and SnS_2[23]. The tin ion (Sn^{2+} - ion) in SnI_2 has an outer electronic configuration of $5S^2$. The above effect is characteristic of a conduction band which is predominantly S-like in character[23]. The p- or d-like states do not change appreciably in energy with increasing density, while the S-states, with their spherical symmetry are influenced strongly and move nearer the core, i.e. in this case, all valence-conduction band energy gaps decrease. It can, therefore, be deduced that the differences between the optical properties of the two polymorphs of SnI_2 are due to the relative densities of the crystals, while the two retain their basic layer type lattice structure. We can equally conclude that the mode of excitation in the two polymorphs of SnI_2 are due mainly to the cations.

3.5 ELECTRICAL CONDUCTIVITY

SnI_2 of unspecified modification has found application as either an anode or as a cathode in solid state batteries[24], while both the α- and β- modifications have been found to be influenced by monovalent iodide dopants, in the vacuum photolysis of these compounds, as outlined in Chapter 5. These two effects do show that SnI_2 is a mixed conductor,

most probably within the temperature range of the photolysis experiments reported in Chapter 5. Attempts were therefore made to measure both ionic and electronic conductivities independently on the same specimen.

The difficulty in obtaining non-polarisable iodide ion reversible electrodes for passing an ionic current through the specimen led to the use of a four point d.c. technique, in which a constant ionic current could be passed through the specimen between two further thin films of SnI_2 acting as reservoirs of I^- ions, and electronically isolated from the specimen by a thin film of an iodide ion conducting solid electrolyte (e.g. AgI, used in this work). The voltage (set up due to the electrochemical effect of the ionic current between the two probes) could be measured using voltage probes of the same construction as above, i.e. a sandwich of an electrolyte, AgI, in thin film form, between a SnI_2 thin film (sample) and another SnI_2 thin film as reservoir. This technique of measuring simultaneously the ionic and electronic conductivities of mixed conductors has occasionally found application in silver and copper ion mixed conductors[25-28] and in potassium ferrites[29].

3.5.1 Experimental Set-up for Conductivity Measurements

Thin films of SnI_2 were employed in conductivity measurements. The evaporation procedure is as detailed in Section 3.2. The films were evaporated on clean high resistivity "Corning" 7059 glass slides. Thin films of AgI were evaporated on the SnI_2 film, through a molebdenum metal mask, so as to define electrode areas for the d.c. ionic current and voltage probes, which are symmetrically arranged about the centre of the SnI_2 film. Using the same mask as above, SnI_2 film, to act as a reservoir for the conducting species, was eventually evaporated. Lastly, electronic contacts were made to the ionic current electrodes and voltage probes by the evaporation of gold through another metal mask,

on top of the SnI_2 reservoirs. Because of the construction of the mask, electrodes for electronic current input, and electronic voltage probes, were also defined on the SnI_2 film sample during the above gold evaporation. Fig. 3.13 shows the steps involved with the preparation of a typical sample. All evaporations were made using the substrate holder arrangement shown in Fig. 3.2. The holder has provisions for raising the temperature of the sample to any desired level. Thermocouples were usually attached to the front end of the glass slide, so as to measure the real temperature of the film. Contacts were made between the gold films and external measuring devices by the use of 'silver dag', while an Edward's TL4 lead through incorporating Teflon, provided adequate electrical connections outside the vacuum equipment. Both ionic and electronic currents were supplied by a simple constant current source, shown in Fig. 3.14. Typical current input was about 67 nA. All voltages between the electronic or ionic probes were read on high impedance 'Solatron' digital voltmeters. A chart recorder was interfaced with the voltmeters, so as to record the voltage excursions, especially in determining the switching and equilibrium conditions. All measurements were made on heated films in the vacuum, at a pressure of 1.7×10^{-6} torr.

3.5.2 Results and Discussion of Conductivity Experiments

Attempts to measure the electrical conductivity of SnI_2, by the use of a d.c. four-point probe technique proved difficult. Instability of the readings, and non-reproducible results are related to the unsuitability of the solid electrolyte employed in the work. There is no known solid electrolyte which is an all iodide ion conductor, and which can be made compatible with the thin film approach. Silver iodide is mainly a silver ion conductor, although it has found application in solutions, as an iodide ion exchange membrane[30], this however has not

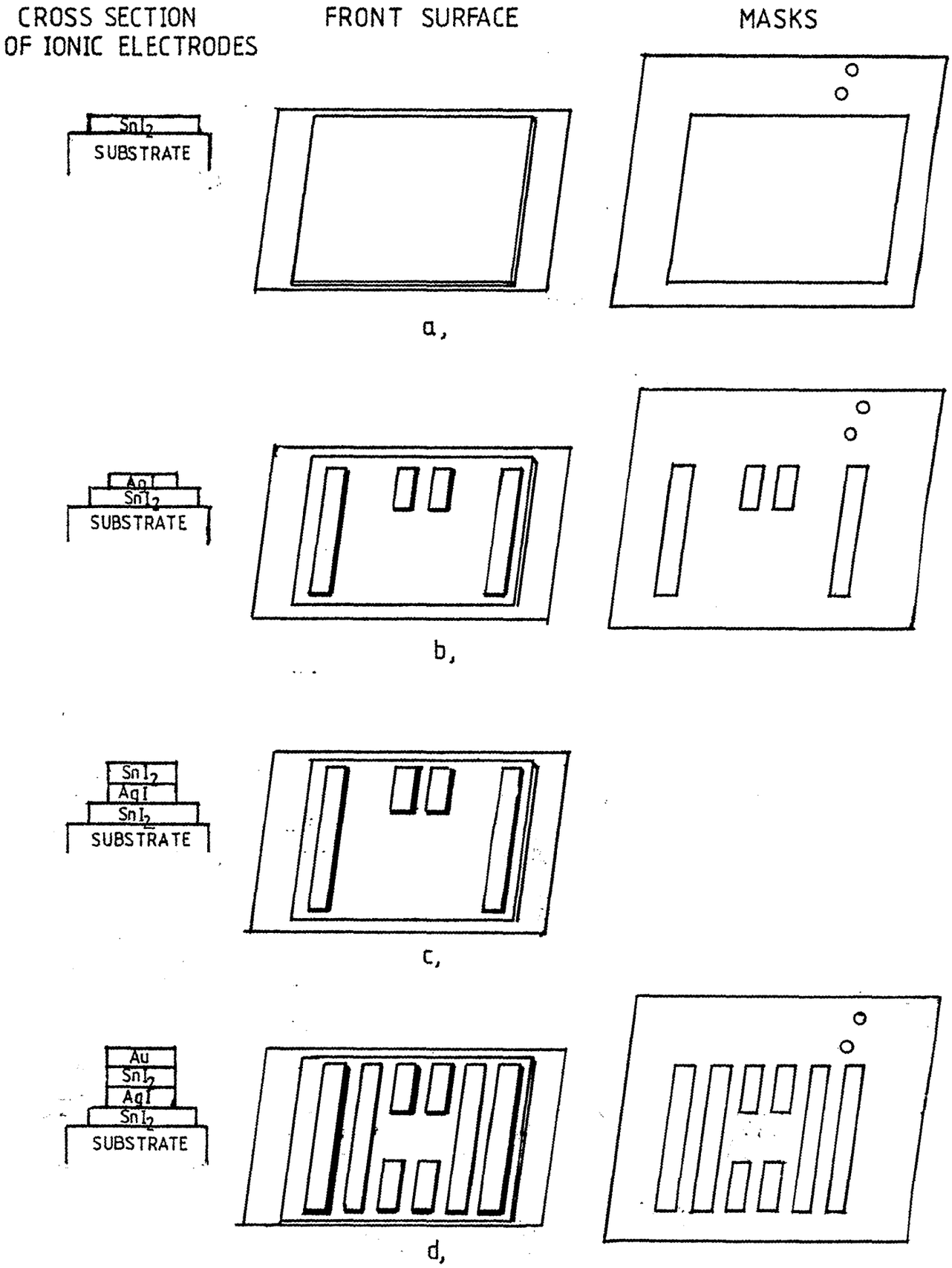

Fig 3·13 Process steps in the preparation of a thin film of SnI_2 for the measurement of ionic and electronic conductivities.

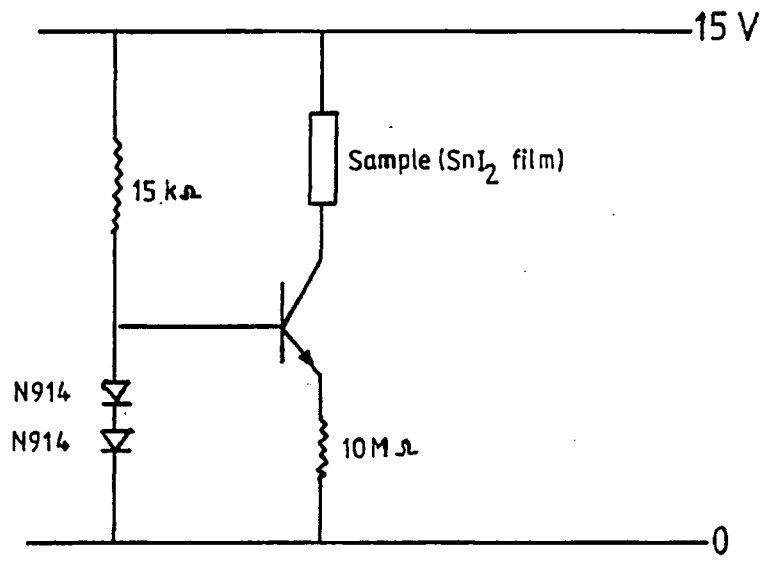

Fig 3·14 Schematic diagram of a simple constant current source.

been realised in the solid state. The above technique is highly versatile, if only a suitable iodide ion conducting solid electrolyte can be found, and which would be compatible with the thin film process.

3.6 ELECTRICAL RESISTIVITY

Since no reliable results could be obtained from the conductivity experiments, attempts were then made to determine the resistivity of thin films of SnI_2, and see how this changed with temperature. Thin films were prepared as earlier outlined. Gold films were evaporated on the film through a metal mask, to define electrode areas. Electrical contacts were then made to the gold film using 'Silver-dag'. The films were placed in a jig, as in Fig. 3.2, and kept in vacuum. Electrical contacts were made to equipments outside the vacuum system by the use of an Edward's TL4 lead through. The resistance measurements were read on a high impedance Keithley 616 digital electrometer. Films were heated using a Solatron power supply, while the film temperature was determined by means of a thermocouple fixed to the front end of the Corning 7059 glass substrates. All measurements were on films kept in vacuum of 1.7×10^{-6} torr. Shown in Fig. 3.15 are the results obtained for different films of SnI_2 which were initially red at room temperature. Thin films of the red modification were used as the starting material, since it was observed that on raising the temperature of the yellow (β-) film from room temperature, it soon changed into the α-form, only to revert to the β- form above $108^{o}C$. The obtained results are usually in the form shown in Fig. 3.15, irrespective of starting with either a yellow or a red film.

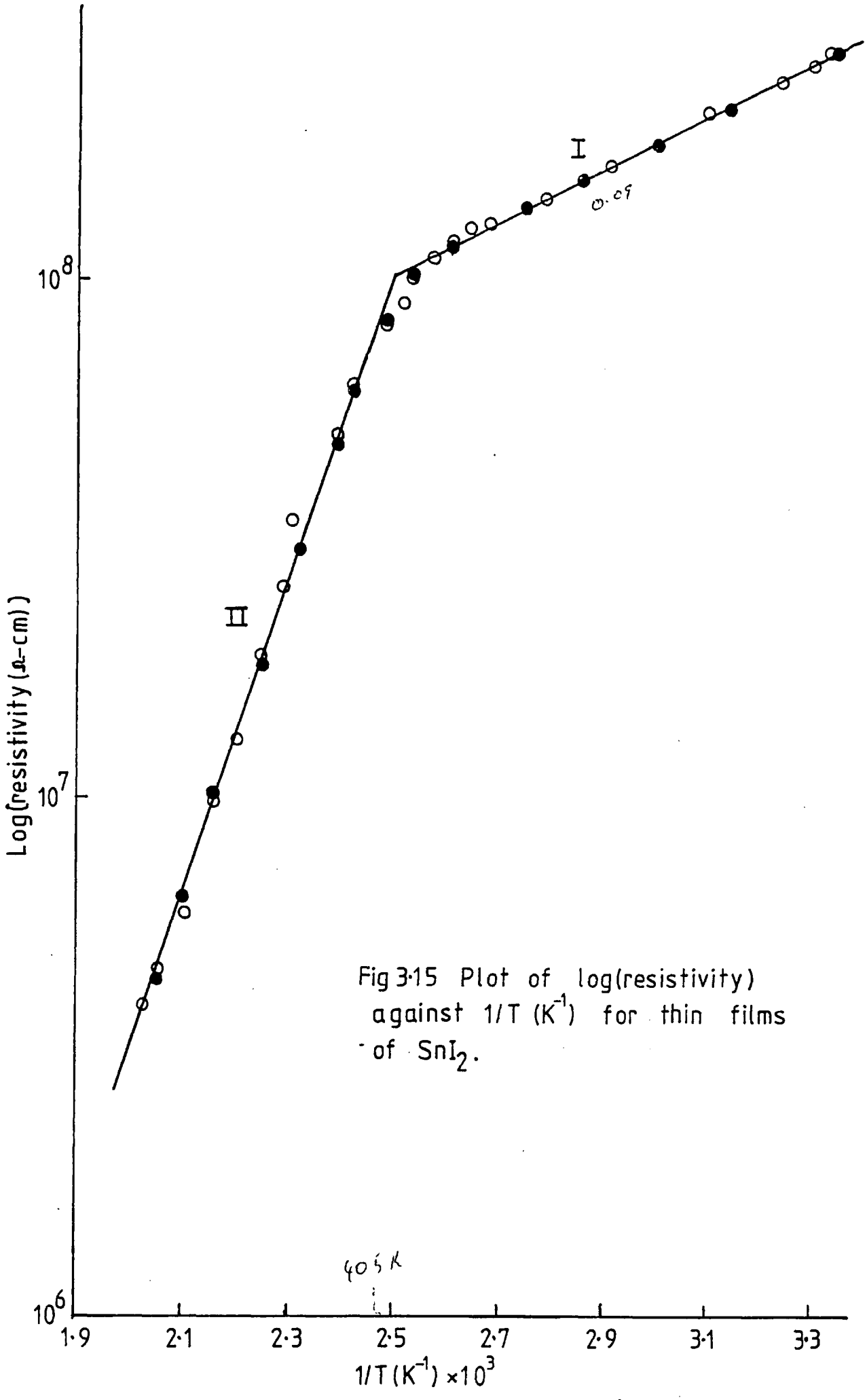

Fig 3·15 Plot of log(resistivity) against 1/T (K^{-1}) for thin films of SnI_2.

The log(resistivity) against inverse temperature (in ^{o}K) plot in Fig. 3.15 give two distinct regions, with two different activation energies, which are 0.099 eV for region I, and 0.595 eV for region II. The shapes of the plots were retained for experiments carried out in low pressures ($\sim 10^{-5}$ torr) of air or oxygen, although the values of the resistivities varied considerably, the activation energies remained about the same.

In the light of the above observation, the mode of electrical conduction in both regions of Fig. 3.15 remain the same in all ambients. The change from region I to region II is due to structural effect. The transition begins at a temperature of 111.6^{o}C, which is not much higher than the phase transition temperature of 108^{o}C. The nature of conductivity in both phases is believed to be intrinsic, and is taken to result from the movement of defects produced by thermal activation. The lower energy of region I is, therefore, a measure of the energy required to form the defects, while the higher activation energy in region II, is related to the sum of the energies required to form the defect, and the energy required to effect a phase change. As would be made more evident in Chapter 6, the defect nature in regions I and II is anionic.

REFERENCES

(1) V.S. Vavilov, "Effects of radiation on Semiconductors", Consultant bureau, New York, 1965.

(2) J.I. Pankove, "Optical processes in semiconductors", Dover Publications, Inc., New York, 1971.

(3) M.P. Lisitsa, Soviet Physics - Doklady, 1, 716, 1956.

(4) F. Herman, Phys. Rev. 95, 847, 1954.

(5) H.Y. Fan, "Infrared absorption by semiconductors", Usp Fiz Nauk, 64, 316, 1958.

(6) J. Barden, F. Blatt, L. Hall, Proceedings of a conference on photoconductivity, John Wiley & Sons Inc., New York, 1954.

(7) M.R. Tubbs, Proc. Royal Soc. 280A, 566, 1964.

(8) I.S. Gorban, V.F. Gorchev, T.N. Suskhevich, Sov. Phys. Solid State, 18(7), 1220, 1976.

(9) S.S. Batsanov, Iz. Akad Nank SSSR, Neorg. Matter., 2(12), 2251, 1966.

(10) Ya, O, Dovgii, M.S., Pridzyrailo, Ukr. Fiz. Zh. 14, 1805, 1969.

(11) G. Harbeke, E. Tosatti, Phys. Rev. Lett. 28, 1567, 1972.

(12) V.I. Vaschkhenko, V.B. Timofeev, Sov. Phys. - Solid State, 9(6), 1242, 1967.

(13) T. Komatsu, Y. Karifu, J. Phys. Soc. Japan, 40(4), 1062, 1976.

(14) F.D. Bloss, "Crystallography and crystal chemistry - an introduction", Holt, Rinehart, and Winston Inc., New York, 1971.

(15) M.R. Tubbs, J. Phys. Chem. Solids, 29, 1191, 1968.

(16) B.Z. Bachrach, F.C. Brown, Phys. Rev. Lett. 21, 685, 1968.

(17) H. Overhof, J. Treusch, Solid State Commun. 9, 53, 1971.

(18) M. Inoue, M. Okazaki, J. Phys. Soc. Japan, 31, 1313, 1971.

(19) G. Harbecke, E. Tosatti, J. Phys. Chem. Solids, 37, 126, 1976.

(20) Ch. Schlutter, M. Schluter, Phys. Rev. B9, 1652, 1974.

(21) E. Doni, G. Grosso, and I. Ladiana, Physica 99B, 281, 1980.

(22) F. Bassani, G. Fischer, D.L. Greenway, Proc. Int. Semiconductor Conference, Paris, 1964.

(23) D.L. Greenway, R. Nitsche, J. Phys. Chem. Solids 26, 1445, 1965.

(24) (a) L.C. Chi, Ger. Offen, 2,254,415, (Cl.H01m) 1974, Appl. p.2254415.6, 07, Nov. 1972.

(24) (b) P.R. Mallory, Fr. Denande, 2,205,750 (Cl.H01m), May 1974, Appl. P7239,447, 08 Nov. 1972.

(25) J. Yokota, J. Phys. Soc. Japan 16, 2213, 1961.

(26) H. Rickert, Z. Phys. Chem. N.F.23, 355, 1960

(27) N. Valverde, Z. Phys. Chem. N.F.70 128, 1970.

(28) T. Kakahashi, O. Yamamoto, F. Matsuyama and Y. Nada, J. Solid State Chem. 16, 35, 1976.

(29) G.J. Dudley, B.C.H. Steele and A.T. Howe, J. Solid State Chem. 18, 141, 1976.

(30) J. Koryta, "Ion-selective electrodes", Cambridge Univ. Press, London, 1975.

CHAPTER FOUR

EXPERIMENTAL

In this Chapter, the experimental arrangement for the photolysis of SnI_2 is discussed, along with the equipment and processes involved in the experiments. A brief description is also given of the quartz crystal microbalance employed in the photochemical experiments.

4.1 The Quartz Crystal Microbalance

The quartz crystal microbalance technique has been employed in this work since it is one of the most sensitive mass balance techniques available[1]. We are interested in monitoring the rate of evolution of molecular iodine gas, resulting from the photodecomposition of our films. Our requirement therefore is an equipment capable of monitoring very small changes in mass. The quartz crystal microbalance, as used by us, has a maximum sensitivity of 1×10^{-12} g[2]. The technique incorporates the use of piezoelectric thin quartz crystal plates[3]. According to size, shape and crystallographic cut, the quartz crystal can be excited into a particular mechanical resonance, when excited by an alternating voltage. With the alternating voltage, an alternating stress results, and electrical energy is converted to mechanical energy. Changes in the environment of the vibrating quartz plate can cause the resonant frequency to change. With the deposition of mass on the crystal surface, a decrease in the resonant frequency of the plate results. It is by monitoring the shift in the resonant frequency of the vibrating quartz plate, that added mass is measured. The relationship of the resonant frequency change, df, with mass change, dm, of a quartz plate due to added mass was given by Sauerbrey[4] as

$$df = - K \frac{dm}{A} \tag{4.1}$$

where K is the mass sensitivity or calibration factor of the quartz plate, and A is the area of the quartz plate to which mass is added. Hence,provided K is constant, any change in mass of the quartz plate results in a linear change in resonant frequency.

The resonant frequency of the quartz plate is also affected by changes in the surrounding temperature. Changes in temperature cause a shift in the resonant frequency of the quartz plate according to the relation[5]:

$$\frac{\Delta f}{f'} = a_1 \Delta T + a_2 \Delta T^2 + a_3 \Delta T^3 \tag{4.2}$$

where f' is the resonant frequency, and Δf is the frequency shift corresponding to a temperature change ΔT. The coefficients in Eqn. (4.2) vary widely with the orientation of cut of the quartz crystal plate with respect to crystallographic axes, as shown in Fig. 4.1. By selecting certain cuts, zero or low temperature coefficients can be obtained. The most suitable cut for the microbalance is the AT cut[6], as it has an extremely low temperature coefficient, and is easy to select crystallographically. By choosing slightly different cut angles, one can arrive at a set of crystals with low temperature coefficients over a wide range of temperature.

The quartz crystal microbalance technique has found application in film thickness measurement[7,8], in temperature and pressure measurement[9], in adsorption studies[10], and in chemical reaction studies which included the study of the kinetics of chemisorption of

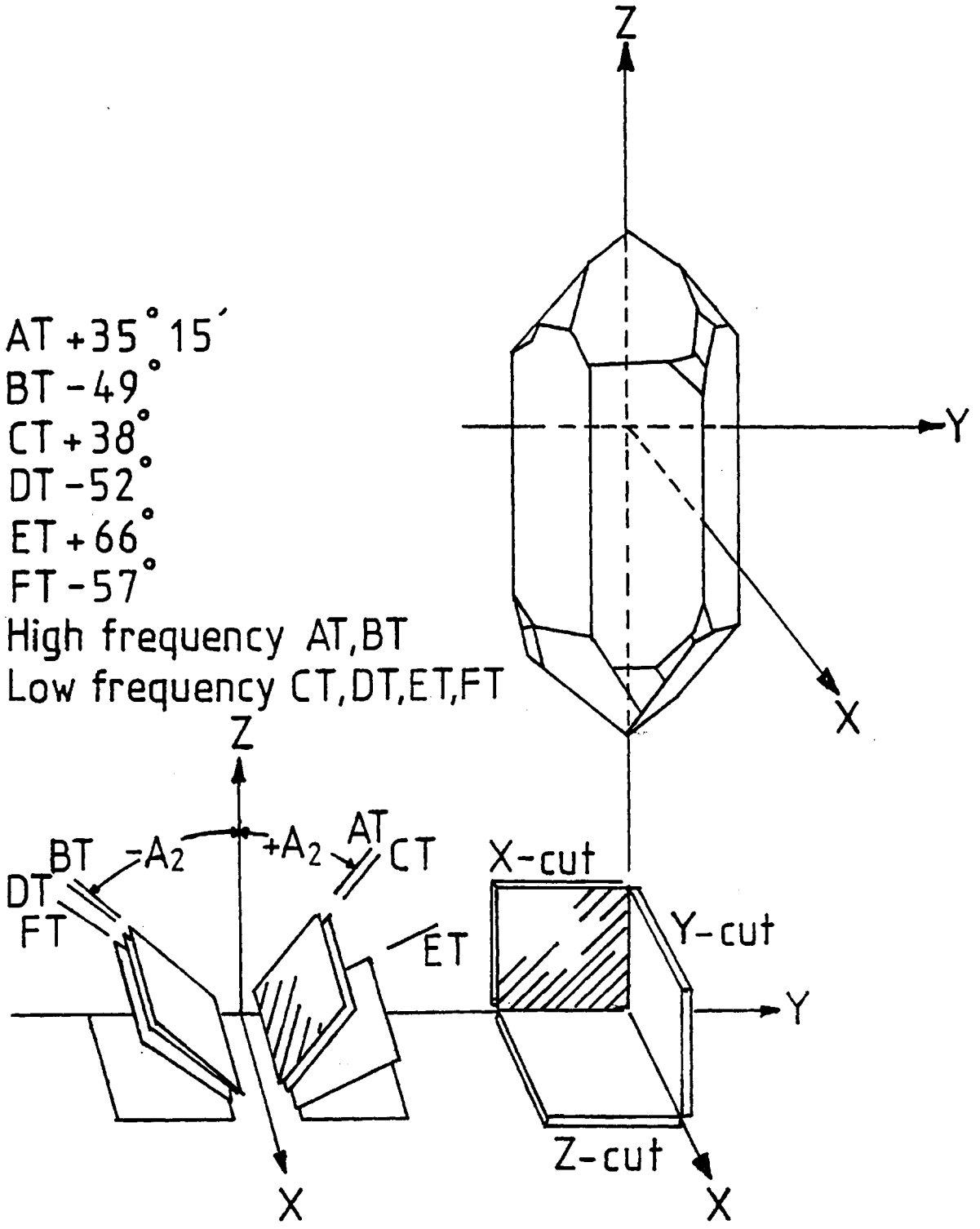

Fig 4·1 Oriented quartz crystal cuts in relation to the natural crystal.

oxygen on aluminium[11], the iodination of copper and lead films[12], and the photolysis of lead iodide[13].

AT cut crystal plates with very low temperature coefficient were used in all our experiments. The 6 MHz crystals were purchased from either ITT Electronics, or Marconi Communication Systems Ltd., to cover the temperature range between 25 and 150°C, over which the photolytic reaction was carried out. A square geometry of 1.27 x 1.27 sq. cm. was found adequate. Gold electrodes were evaporated to the two crystal faces so as to provide electrodes for the excitation of the crystals. In order to eliminate possible sensitisation of the photolytic reaction, quartz of about 2000Å thick was sputtered over the gold electrode area to be exposed to stannous iodide vapour. A substrate temperature of 200°C was found to be suitable during the sputter deposition. The crystal dimensions and coating description are shown in Fig. 4.2. The holder fits into a 'Teflon' plug, which in turn is secured in a copper annular ring.

The frequency change of the quartz crystal substrate either during evaporation, or photolysis, was compared with that of another crystal held outside the vacuum equipment. The difference in their oscillating frequencies was monitored on a commercial digital film thickness monitor, model FTM_3, supplied by Edwards High Vacuum Ltd. This instrument allows either face of the crystal to be earthed, whilst driving the crystal at series resonance, the exposed electrode cannot therefore pick up static charge through, for example, a voltage discharge in the chamber.

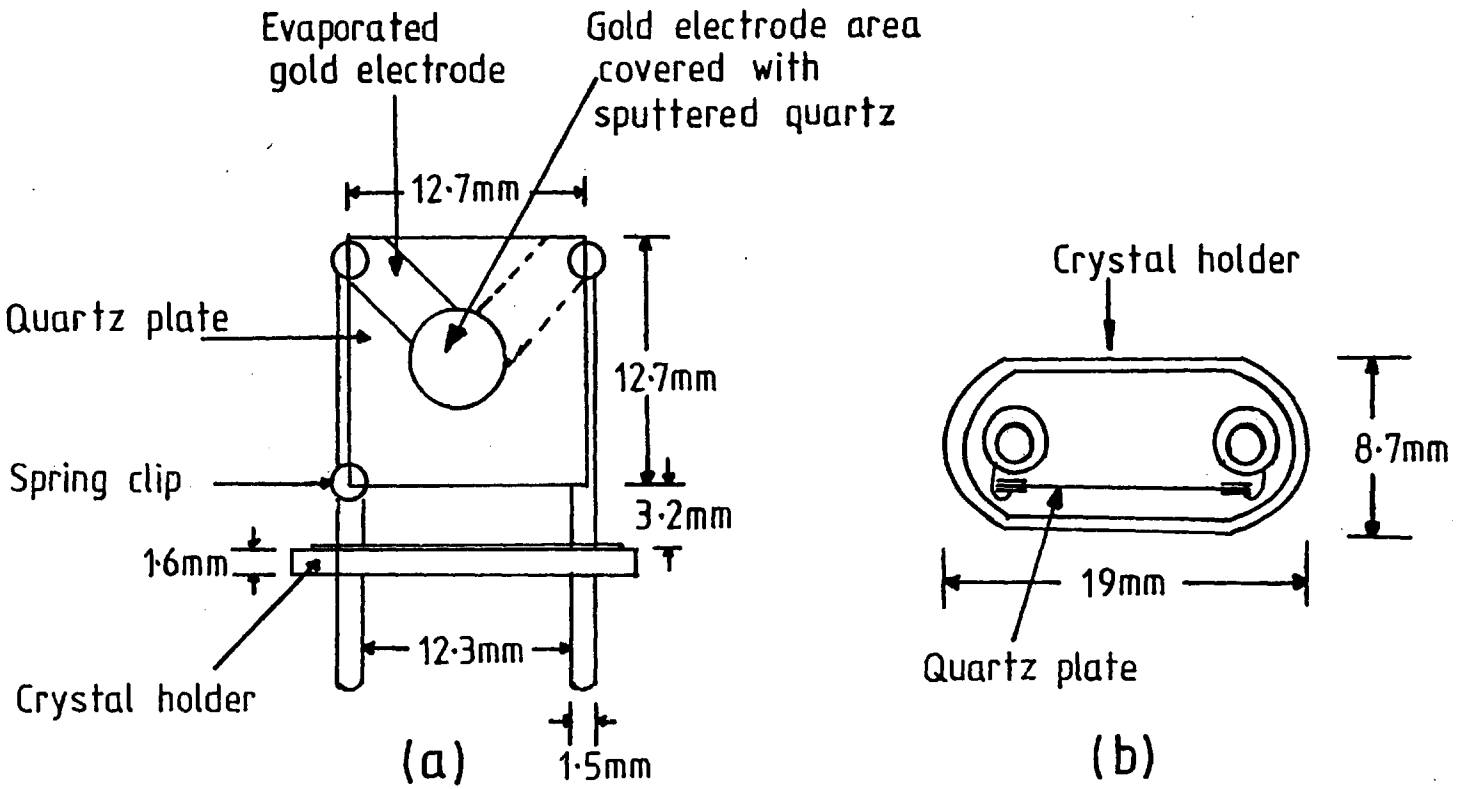

Fig 4·2 (a) Quartz crystal dimensions, and defined gold electrode configuration in holder arrangement. (b) Top view of the arrangement in (a).

4.2 Calibration of the Quartz Crystal Microbalance

The calibration procedure is detailed in Section 3.2. Thin films of stannous iodide were evaporated on masked (metal mask) glass slides, with the quartz crystal plate held next to the glass slide as shown in Fig. 3.2. After evaporation, and with the metal mask removed, gold was uniformly evaporated over the entire surface of the glass slide, thus creating a suitably reflecting surface. The thickness of the SnI_2 film was then conveniently measured on an interferometric microscope. This thickness was correlated to the change in the resonant frequency of the quartz crystal plate. Using the above procedure, K (the mass sensitivity) in Eqn. (4.1) was calculated from different film thickness determinations, and was found to be nearly constant, and approximately equal to 0.82 for all the crystals, with an average error of 2.5% either way. We were able to deduce that for a film area of 0.33 cm^2, 1 Hz change in frequency did correspond to a mass change of 2.7×10^{-9} g, or equivalent to 1.94×10^{13} molecules of SnI_2 cm^{-2}. Thus this enabled the direct determination of film thickness during evaporation, and to follow the rate of the photochemical reaction during the photolysis of SnI_2.

4.3 Temperature Stabilisation

During evaporation of SnI_2, the crystals were shielded from ambient temperature variations by housing them in specially designed ovens. These are of annular construction as shown in Plate 4.1. They consist of an outer copper oven and an inner tin metal oven, which are placed concentrically about the quartz plate. The outer copper oven contained symmetrically arranged heater wires, which could be resistively heated by the use of a stabilised d.c. power supply. Photolysis temperatures between 25 and 150°C were attainable with this system. The inner

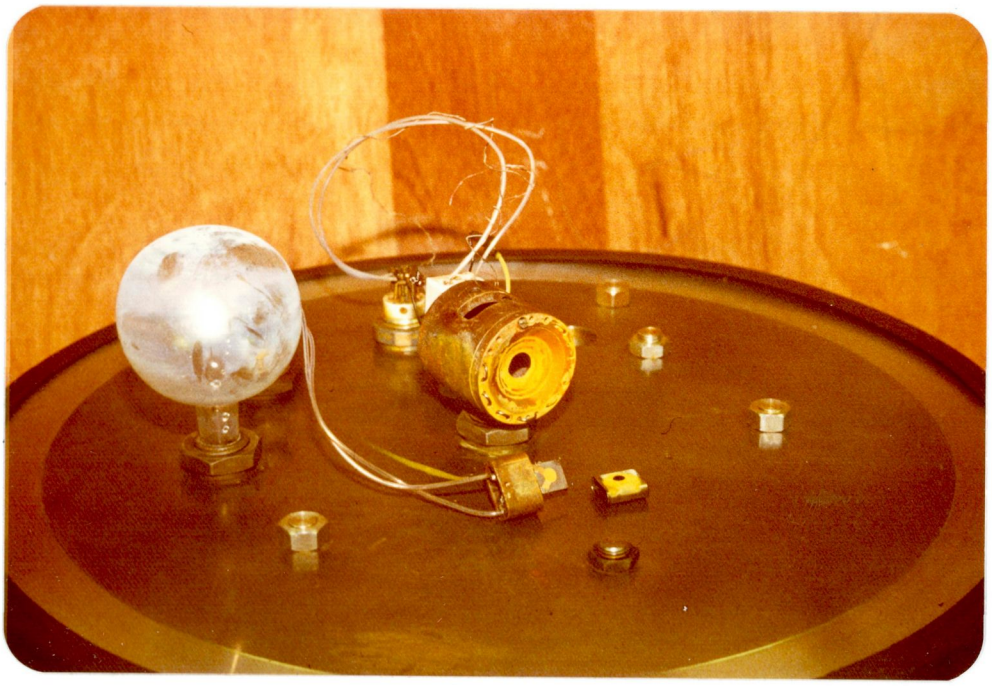

(a)

(b)

Plate 4.1: (a) shows the quartz plate separated from the tin and copper ovens, while (b) shows the arrangement for photolysis. Notice that the outer copper oven is attached to the rotary shaft at the top of the vacuum equipment plate.

tin metal oven was attached to a spring clip holder (Fig. 4.2), and made to fit into the annular copper ring as shown in Plate 4.1. This ring was reproducibly positioned in the outer copper oven with the aid of a screw, which ensured the reproducible positioning of the electrode area of the quartz crystal plate. A hole (0.33 cm^2) drilled on one face of the inner tin metal oven, and directly above the centre of the gold electrodes, allowed the definition of the film on the quartz crystal plate. The outer copper oven had a larger hole of 1.0 cm diameter, drilled at its front face, so as to allow the deposition of the tin diiodide vapour to the quartz crystal plate. Temperature variation within the ovens were measured by three "Chromel"-"Alumel" thermocouples placed differently within the ovens. The variation between the three thermocouples was not more than 1^oC. The outer copper oven was attached to a rotary shaft at the top plate of the vacuum equipment (Plate 4.1), so that the entire arrangement could be turned to face either the evaporation source, or the light source during photolysis.

4.4 Thin Film Production

α-SnI_2 powder, produced as detailed in Chapter 2, has been used as the base material, in the preparation of thin films of SnI_2. As indicated earlier (Chapter 3) the temperature at which the substrate was kept determined the polymorphic type obtained. To produce the β-polymorph (yellow), the substrate was usually left at room temperature, while for the α-SnI_2 (red), the evaporation was on a substrate kept at 100^oC (only about 8^oC less than the transition temperature).

Tin diiodide was evaporated from a silica boat which was really a small test tube as shown in Fig 4.3. The quartz boats were cleaned in detergent, then followed by a subsequent ultrasonic cleaning in

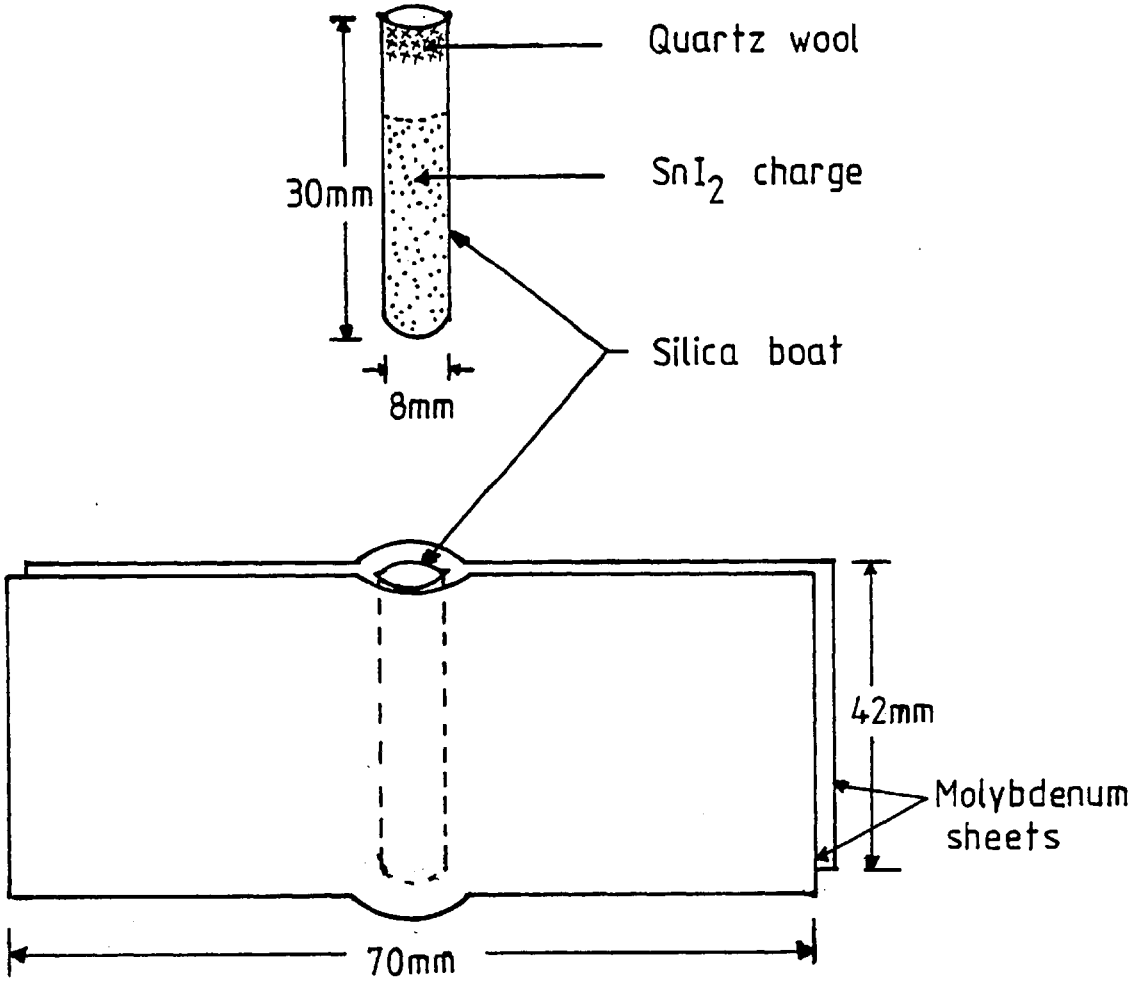

Fig 4·3 Evaporation source arrangement.

distilled water and isopropyl alcohol, and allowed to dry before being filled with a known quantity of SnI_2 powder. The powder was held in position by means of quartz wool. The quartz boat plus charge was then resistively heated via molybdenum sheets concentrically positioned around it as shown in Fig. 4.3. Source temperatures between 350 and 400°C were found to be satisfactory for the evaporation rates required. The rates of evaporation ranged between 30 Hz/sec and 65 Hz/sec (i.e. 275.89 Å/min and 597.76 Å/min). The distance between the source and substrate was fixed at 12.2 cm. The temperature gradient between the two ends of the source boat was small, the variation being about 8°C.

The same arrangement as above was employed during the evaporation of SnI_2 charge doped with any of AgI, CuI, PbI_2 or SnI_4. The vapour pressure of some of these dopants in the same state are as shown in Fig. 4.4, together with that of SnI_2.

Prior to evaporation, the quartz crystal substrate and holder were cleaned in the same manner as the silica boats, plus an additional cleaning in isopropyl alcohol, provided through a Soxhlet extractor. This same cleaning procedure was adopted for the cleaning of glass slides when used as substrates during SnI_2 evaporation.

4.5 Light Source and Optical Filters

The photolysis experiments have been performed by shining a collimated beam of light on the evaporated films of both polymorphs of SnI_2. The source of light was a 650 watts quartz-halogen lamp. This was operated via a stabilised mains supply. The lamp operates as a conventional heated tungsten filament, but whose efficiency is prolonged near the uptimum value via a thermodynamic cycle, created by adding a halogen to the environment inside the quartz envelope. Evaporated

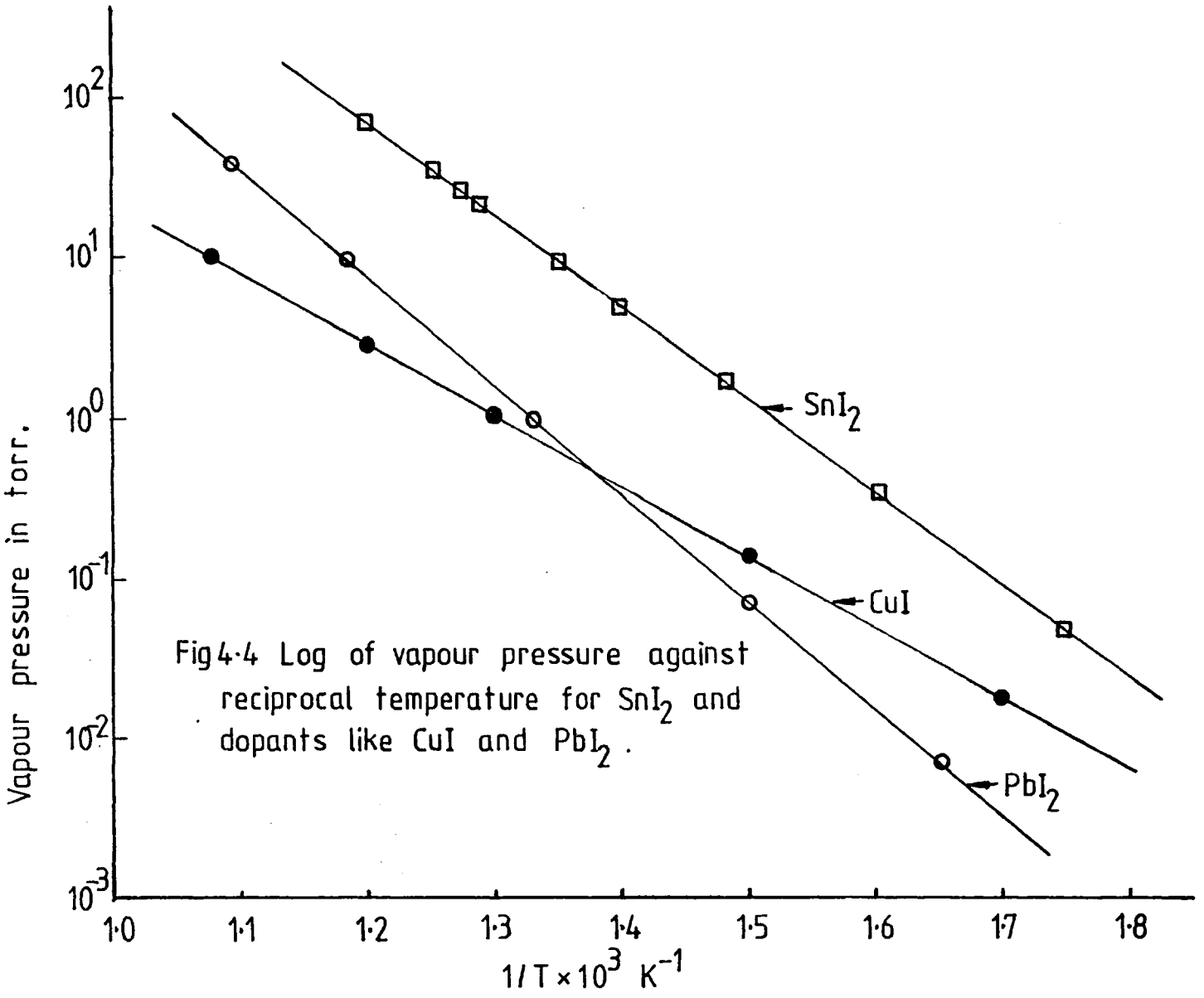

Fig 4·4 Log of vapour pressure against reciprocal temperature for SnI_2 and dopants like CuI and PbI_2.

tungsten reacts at the quartz envelope with halogen to form a tungsten halide, which evaporates from the quartz envelope and decomposes at the tungsten filament. The lamp gives a very intense radiation in the visible as shown in Fig. 4.5.

Most of the experiments reported in Chapter 5 were performed with broad band radiation. A copper sulphate solution (~240 g/litre), placed in an optical cell (1 cm thick), was found to be adequate as a broad band filter, since this has a transmission of almost 100% within the visible region. An experimentally determined spectral variation of the transmission of the copper sulphate solution with wavelength is shown in Fig. 4.6.

To determine the photon efficiency of the photolytic process, and resolve the spectral details of the photolysis more accurately, experiments performed with narrow band radiation were necessary. This was achieved by using narrow band optical interference filters (Barr and Stroud Ltd.). A narrow band interference filter is characterised by four qualities which include the wavelength at the peak transmission, the value of the peak transmission, the bandwidth at half peak transmission, and details of background suppression at wavelengths well removed from the peak transmission. In the present work, peak wavelengths were chosen at 435.8, 492.8, 507.9, 524.5 and 546.0 nm. This allowed continuous selection of wavelengths below the absorption edge of both modifications of SnI_2. Shown in Table 4.1 are the characteristics of the optical filters whose peak wavelengths are stated above.

Fig 4·5 Radiance variation with wavelenght for the 650 Watts Quartz-halogen light source .

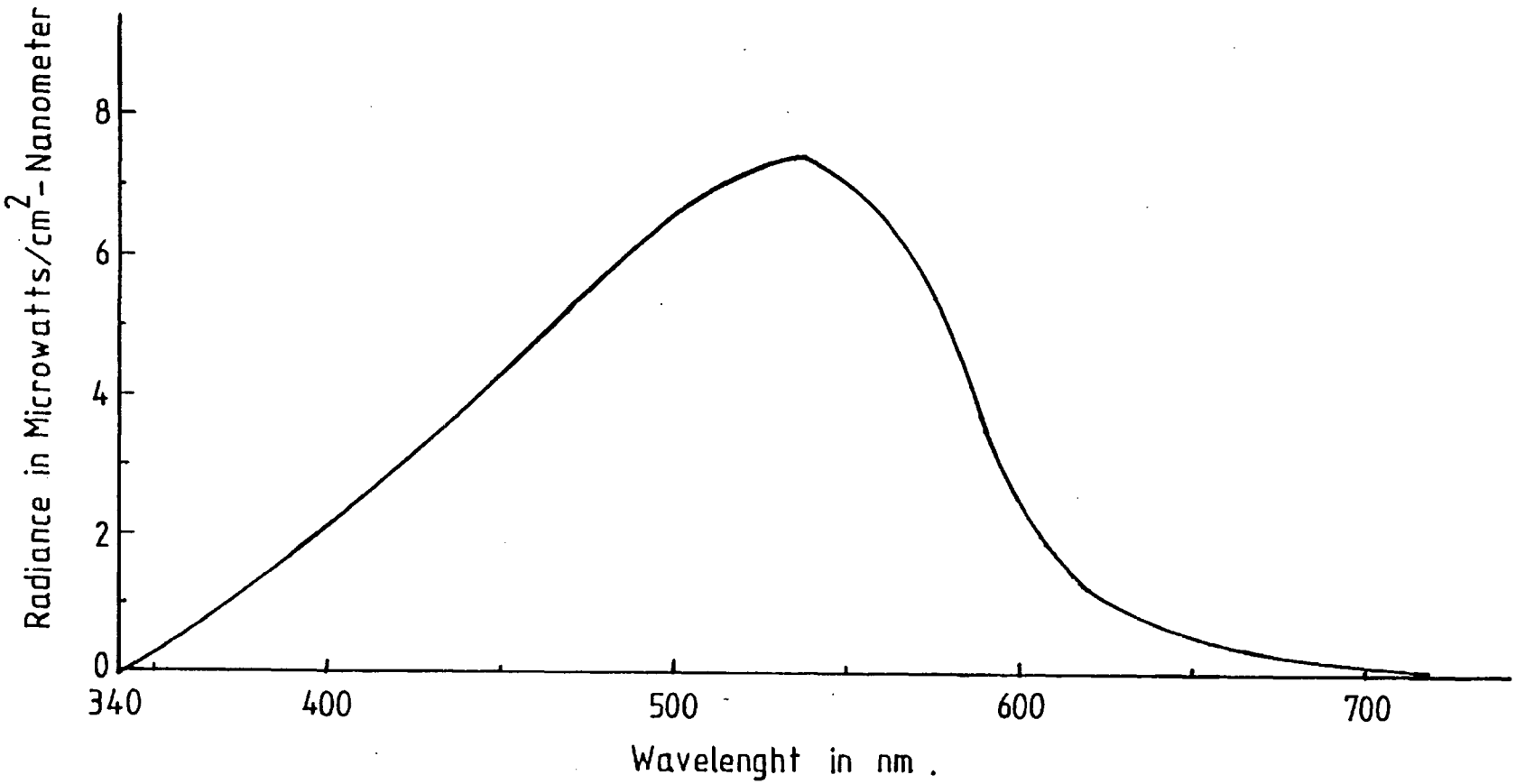

Fig 4·6 Wavelenght dependence of the transmission of the copper sulphate solution (240 g/litre) used as broad band optical filter.

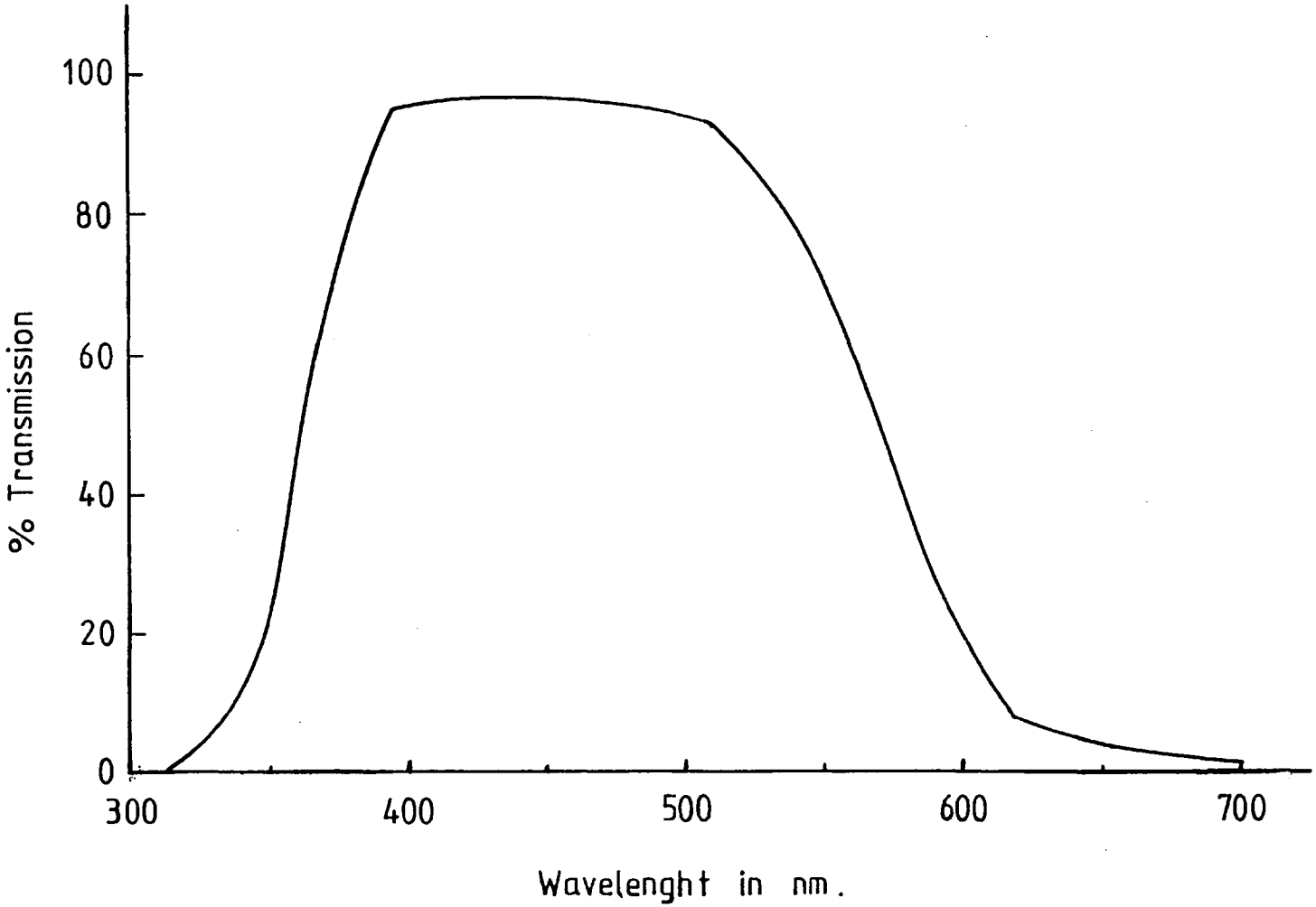

Table 4.1: Characteristics of Optical Interference Filters Type DL8S(Supplied by Barr and Stroud Ltd.)

Peak wavelength (nm)	Band width (nm)	% Transmission at peak wavelength
435.8	3.6	27.5
492.8	2.8	30.0
507.9	2.4	36.5
524.5	2.8	38.0
546.0	4.0	40.1

4.6 Photolysis Arrangement

The source of photolysing radiation was a 650 watts quartz-halogen lamp. The light was passed through a quartz collimating lens, then through an optical filter (either broad band or narrow band), through an optical quartz window in the vacuum system wall, and finally, through a quartz lens in the vacuum equipment, before falling on to the film surface. The optical arrangement is as shown in Fig. 4.7. Light intensities were measured usually after the experiment by putting a silicon photodiode type OSD-50-1, supplied by Centronic Electro Optics Ltd., in the exact position where the film had been during photolysis. The characteristics of the diode are as detailed in Table 4.2. The photo-current, I_{photo}, produced across the diode is linear with incident radiation, and was always determined by measuring the voltage output across the feedback resistor, R_F in the circuit arrangement shown in

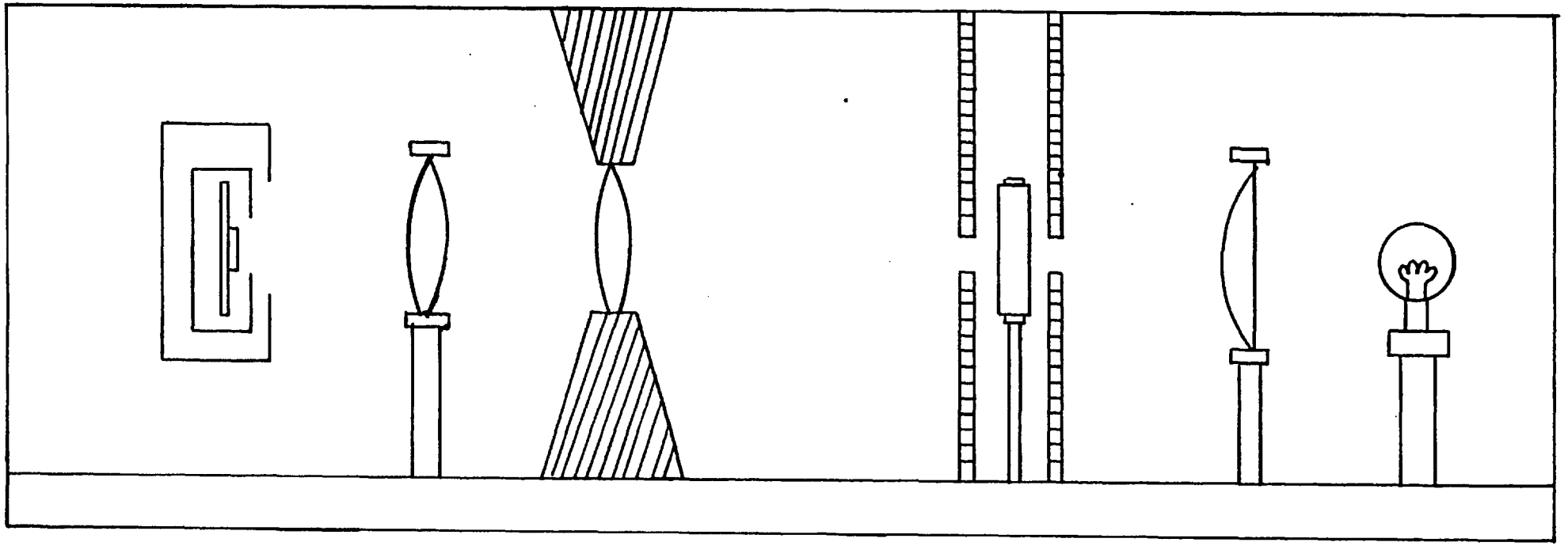

Fig 4·7 Schematic diagram of the photolysis arrangement.

Fig. 4.8.

$$V_o = I_{photo} \times R_F$$

and

$$I_{photo} = Jq\phi A$$

where J is photon flux density efficiency of the photodiode

q is electron charge " " " "

ϕ is average quantum " " " "

and A is the active area of photodiode.

The light intensity obtained from the above diode was usually compared with that of an industry (Centronic) calibrated photodiode of the same type. The spectral characteirstics of the industry calibrated photodiode is as detailed in Table 4.3. The circuit arrangement in Fig. 4.8 affords a linear response, and is low noise due to almost complete elimination of leakage current with zero bias.

Table 4.2: Characteristics of Silicon Photodiode Type OSD-50-1 (Supplied by Centronic Electro Optics Ltd.)

Characteristic	Value
Optimised response	0.25 - 1.15 μm
Maximum voltage, V_R	10 volts
Typical rise time at 0.9 μm	20 nS
Minimum quantum efficiency	40% at 0.43 μm
Typical capacitance (V_R = 10)	80 pF
Typical dark current	0.35 μA
Noise equivalent power at 0.9 μm	5.7×10^{-13} W $Hz^{-\frac{1}{2}}$
Active area	50 mm^2

Table 4.3: Calibration Characteristics for Diode Type OSD-50-1. (Calibrated by Centronic Ltd.)

Wavelength (nm)	Sensitivity (nm)	Quantum Efficiency %
253.7	0.063	31.0
435.8	0.216	61.7
530.0	0.288	67.4
632.8	0.367	72.1
900.0	0.389	53.6

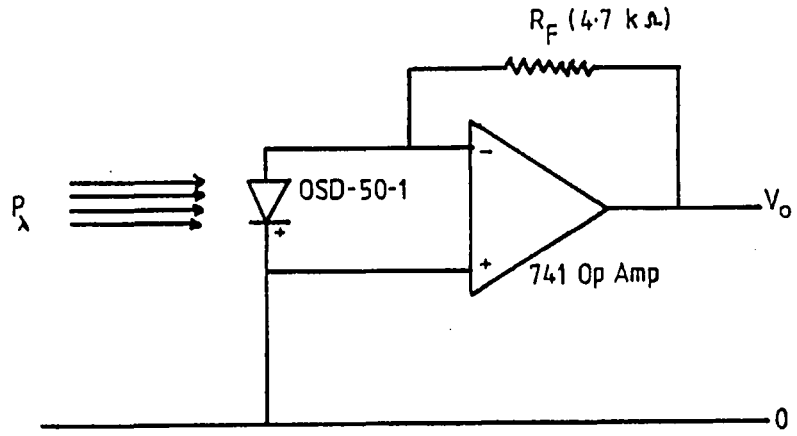

Fig 4·8 Circuit diagram for the measurement of light intensity.

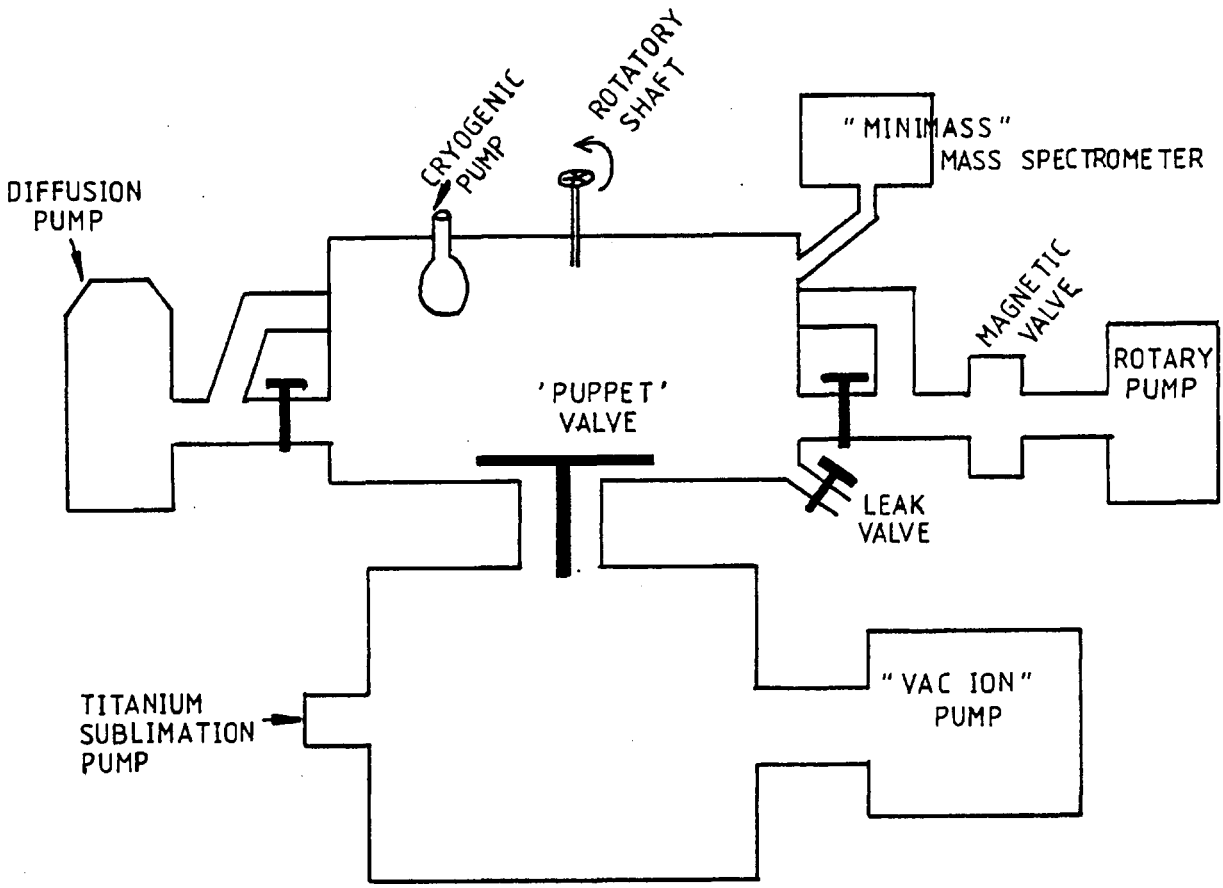

Fig 4·9 Schematic diagram of the vacuum equipment used in the photolysis experiments.

4.7 The Vacuum Equipment

All the evaporation and photolysis experiments were carried out in an Edwards high vacuum equipment, schematically represented in Fig. 4.9, and shown in Plate 4.2. The system was initially "roughed" down with a rotary pump, a roughing pressure of 10^{-3} torr was satisfactory. The system was then opened to the diffusion pump, which usually pulls down the pressure of the system to about 2×10^{-5} torr. Both the titanium sublimation pump and the "Vac-ion" pumps would then be turned on, to give an ultimate pressure of 2×10^{-6} torr. A round bottomed flask attached to the top plate of the vacuum equipment did act as a cryogenic pump when filled with liquid nitrogen. This acted as a very useful pump for the residual water in the system, thus bringing the total pressure to about 1.6×10^{-6} torr. This residual pressure was found to be satisfactory. Lower pressures were attainable by baking out the system. Residual gas analysis was achieved using an AEI Minimass mass spectrometer attached to the system. The system was considered clean with respect to water vapour, oxygen and hydrocarbons; a typical mass spectrum of the residual gas is shown in Fig. 4.10.

As shown in Plate 4.1, the quartz crystal oven was attached to the end of a rotary shaft vacuum seal (Edwards High Vacuum), and located centrally on the top plate of the vacuum equipment, which could be removed completely from the rest of the vacuum system. This allowed the crystal oven to be turned to face either the evaporation source, or the radiation source, during photolysis. This arrangement enabled experiments to be performed in situ. The top plate of the vacuum system was reproducibly positioned by means of three stout locating pins as shown in Plate 4.2.

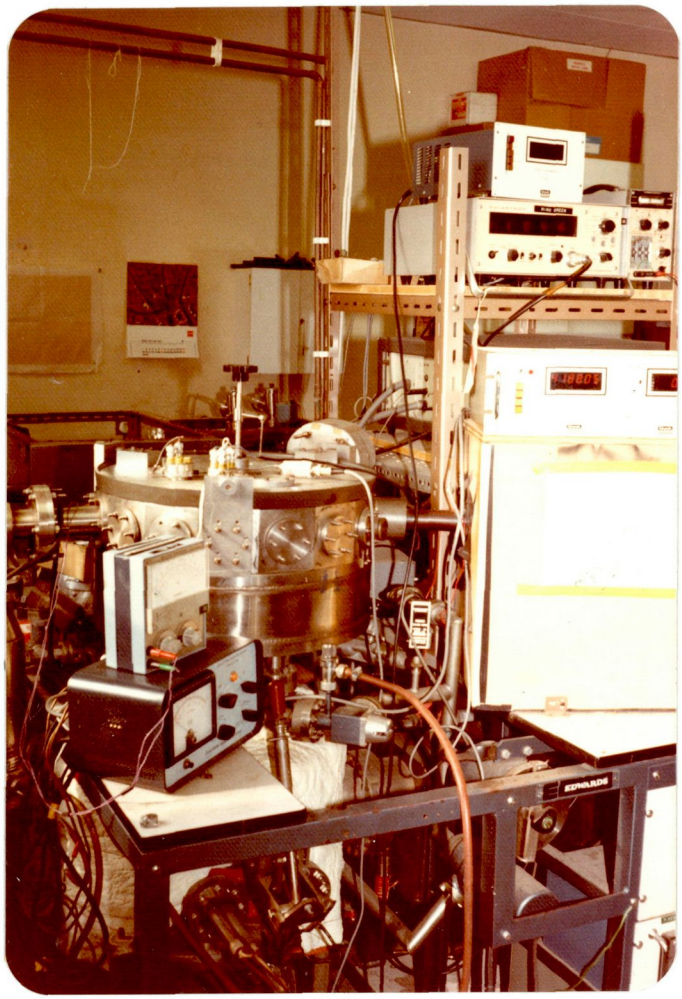

Plate 4.2: The vacuum equipment used in the photolysis experiments

Fig 4·10 Mass spectrometer analysis of ressidual gases in the vacuum equipment for a total ressidual gas pressure of $1{\cdot}6\times10^{-6}$ torr.

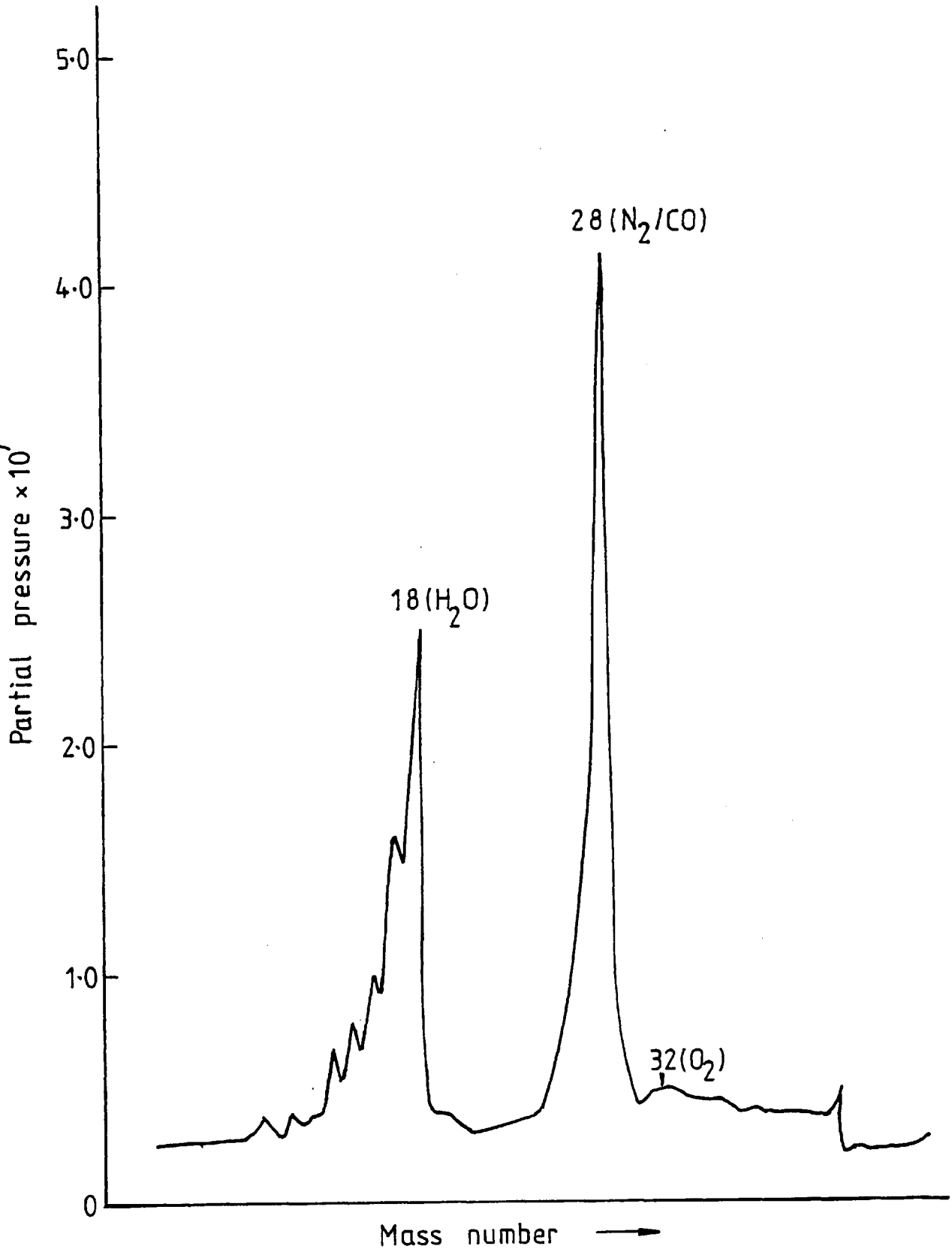

REFERENCES

1. A.W. Warner, "Ultra Micro weight determination in controlled environments". Eds S.P. Wolsky and E.J. Zdanuik, Interscience, N.Y., 1969, p.140

2. W.W. Warner, C.D. Stockbridge, Vac. Mic. Tech. 3, 55, 1963

3. W.G. Cady, "Piezoelectricity", Dover Publications, N.Y., 1964

4. G. Sauerbrey, Z. Phys. 155, 206, 1959

5. E.P.Eeer Nisse, J. Vac. Sci. Tech. 12(1), 564, 1975

6. A.W. Warner, C.D. Stockbridge, Vac. Mic. Tech. 2, 71, 1961

7. W. Steckelnacher, J. English, H.H.A. Bath, D. Haynes, J.T. Holden, L. Holland, Electronic Components 5, 405, 1964; ibid 5, 495, 1964

8. D.C. Fox, M.J. Katz, "Ultra microweight determination in controlled environments". Eds. S.P. Wolsky, E.J. Zdanuk, Interscience, N.Y., 1969, p.465

9. D.L. Hammond, A. Benjaminson, I.E.E.E. Spectrum, p.53, April 1969

10(a) L.L. Levenson, Suppl. Nuovo Cimento 5, 321, 1967

(b) C.E. Bryson, V. Cazcarra, L.L. Levenson, ibid 11 (1), 411, 1974

11. W.H. Wade, R.C. Allen, J. Coll. Int. Sci. 27, 722, 1968

12. M. Shiojiri, J. Electrochem. Soc.: Solid State Sci. Tech. p.698, May 1975

13. M.G. Albrecht, Mino Green, J. Phys. Chem. Solids 38, 297, 1977

CHAPTER FIVE

THE PHOTOCHEMICAL REACTION

There has been no report in the literature of a quantitative determination of the photolysis of SnI_2. The optical density change when light of unspecified intensity was made to shine on SnI_2 (also of unspecified polymorphic type) was interpreted by Kosarev et al.[1] as "ageing", rather than photolysis, even though the change in the optical density of the related lead halide films had been used to follow the kinetics of their photolysis[2,3]. Photochemical studies on $Pb_x\ Sn_{(1-x)}I_2$ films ($0 \leqslant x \leqslant 1$) by Kosarev et al.[4] did indicate that these films were more photosensitive than PbI_2 or SnI_2, but the relative photosensitivities were not quantified.

In this chapter, results are presented on, the identification of the products of photolysis, and the kinetics of the photochemical reaction.

5.1 PRELIMINARY STUDIES

Before embarking on the study of the kinetics of the photolysis of SnI_2, attempts were initially made to characterise the photochemical reaction. Thin films of SnI_2 of both modifications were evaporated on clean glass slides, using the glass substrate holder arrangement shown in Fig. 3.2. The transmission spectrum of the evaporated film was then taken, using the Bechman DK2A double beam spectrophotometer arrangement shown in Fig. 3.3. With the transmission spectrum recorded, the film was returned into the vacuum system and photolysed for some time with unfiltered radiation. The transmission spectrum of the photolysed film

was subsequently taken. Presented in Fig. 5.1 are the transmission spectra of a film of β-SnI_2 (∿ 5000Å thick) before and after photolysis for one hour with unfiltered radiation, at a temperature of 140°C. The extent of photodecomposition was estimated to be about 20% of total SnI_2 molecules in the film. The film was observed to be more transparent (especially on the high energy side of the absorption edge) with photolysis. The transparency observed in Fig. 5.1 for β-SnI_2 films was also typical of α-SnI_2 films.

Thin films of both polymorphs of SnI_2 were also evaporated and photolysed in situ by attaching the glass substrate jig of Fig. 3.2 to the centrally positioned rotary shaft at the top plate of the vacuum system (see plate 4.1). The photolysed films were then x-rayed, using a thin film cylindrical x-ray texture camera arrangement. Equally x-rayed were unphotolysed films of both modifications, of the same thickness, (∿1.45 μm). Shown in Plate 5.1 are the photographs of the x-ray patterns of both the unphotolysed, and photolysed films of β-SnI_2. The photolysis was for four hours, at a temperature of 150°C. The extent of reaction was estimated to be about 35%. More diffraction lines were observed in the photolysed material. Analysis of the diffraction lines for the photolysed films (as shown in Table 5.1) gave characteristic lines due to grey tin. The formation of grey tin at the temperature of photolysis came as a surprise. This will be dealt with in more detail in Chapter 6. This same result was also observed in α-SnI_2 films treated in the same manner. The x-ray results therefore did indicate that the photochemical reaction resulted in the decomposition of SnI_2 to grey tin, while the iodine gas must have been liberated, i.e.

$$SnI_2 \xrightarrow{h\nu} Sn(s) + I_2\,(gas)\uparrow \qquad (5.1)$$

Fig 5·1 Transmission spectra of unphotolysed (xxx) and photolysed (●●●) films of β-SnI_2. Film thickness is 5,000 Å. (Estimated that 20% of SnI_2 molecules were photolysed).

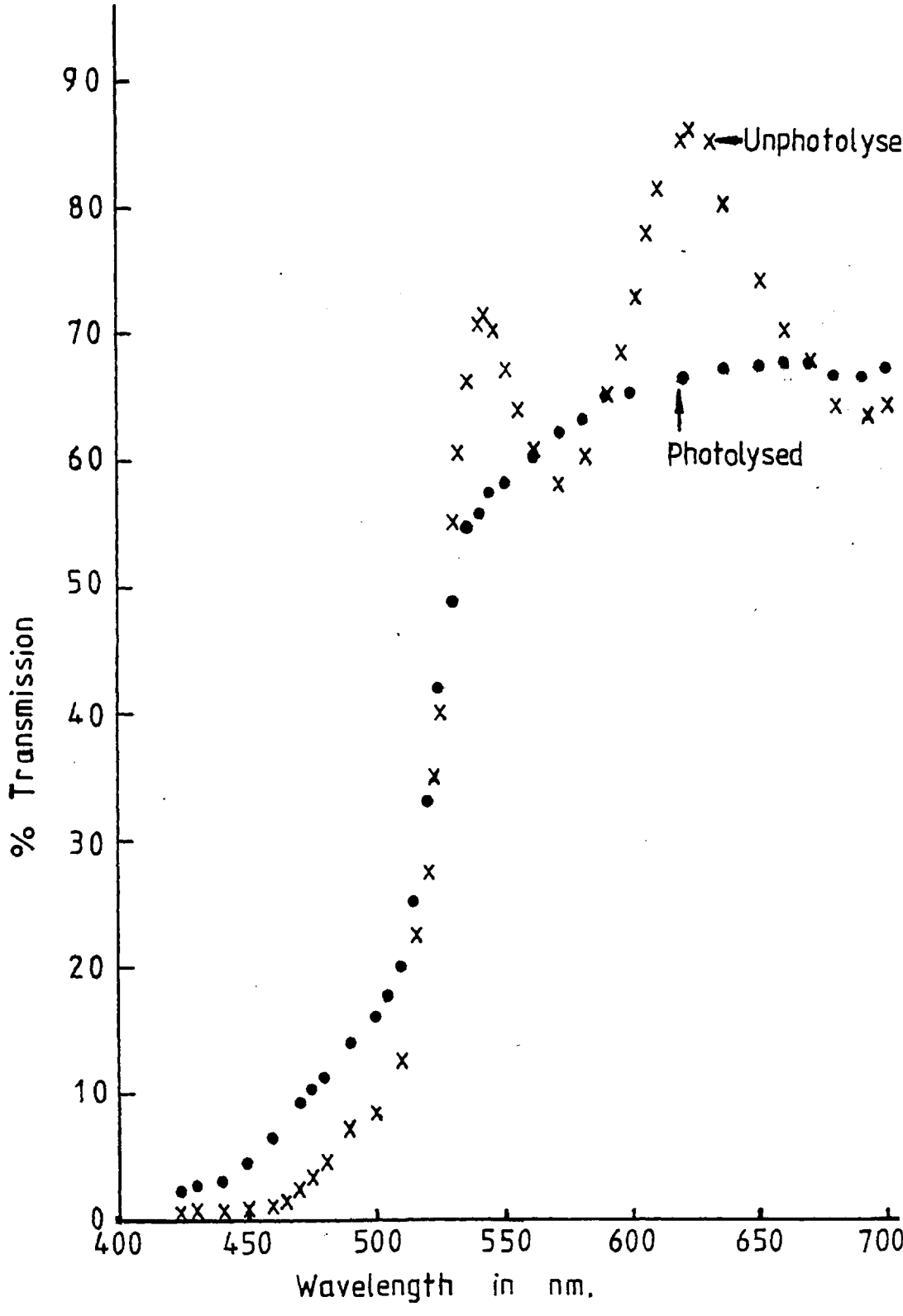

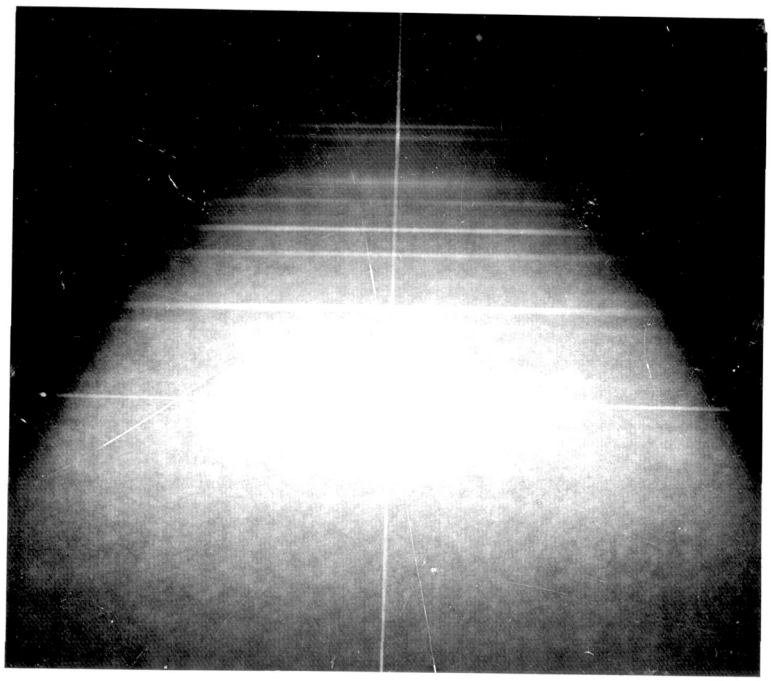

(a)

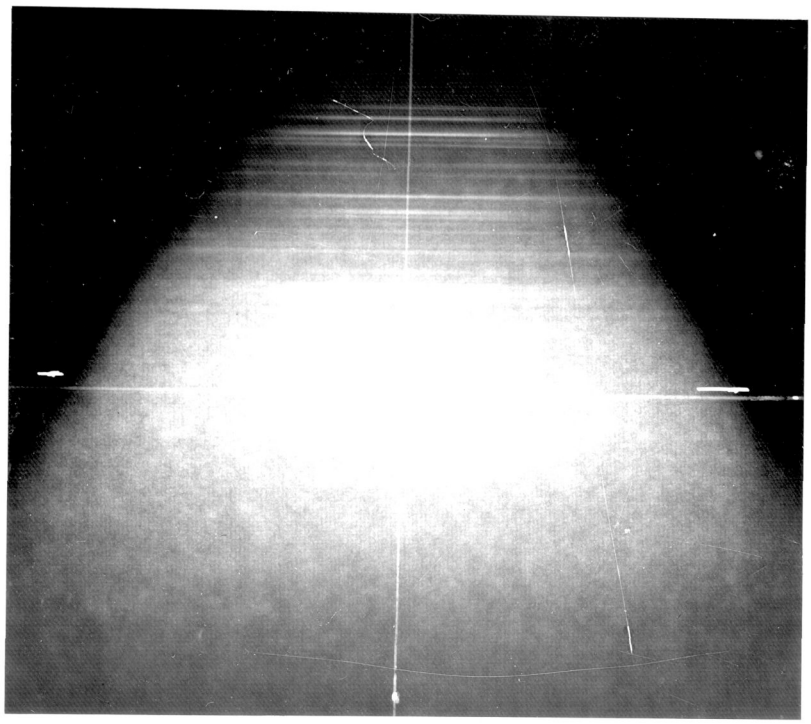

(b)

Plate 5.1: X-ray diffraction pattern for thin films of β-SnI_2 before (a) and after photolysis (b).

(a) Unphotolysed β-SnI_2

Line No.	d(Å)
1	2.661
2	2.360
3	2.299
4	2.230
5	2.029
6	1.924
7	1.847
8	1.773
9	1.649
10	1.407
11	1.323
12	1.152

(b) Photolysed β-SnI_2

Line No.	d(Å)	Features
1	2.360	SnI_2
2	2.294	α-Sn
3	2.230	SnI_2
4	2.203	unknown
5	2.168	SnI_2
6	2.137	unknown
7	2.029	SnI_2
8	1.956	α-Sn
9	1.847	SnI_2
10	1.773	SnI_2
11	1.744	unknown
12	1.705	unknown
13	1.667	SnI_2
14	1.623	α-Sn
15	1.572	SnI_2
16	1.551	unknown
17	1.470	SnI_2
18	1.423	unknown
19	1.392	SnI_2
20	1.323	SnI_2 or α-Sn
21	1.235	unknown

Table 5.1: Features obtained from the analysis of the x-ray patterns of unphotolysed and photolysed β-SnI_2 films

5.2 KINETIC STUDIES

The kinetics of the photochemical reaction were followed by reading the change in the resonant frequency of the quartz crystal microbalance, as registered on an Edward's FTM_3 digital frequency monitor. The calibration of the quartz crystal microbalance was such that 1 Hz change in frequency was equivalent to the photolysis of 1.94×10^{13} molecules of SnI_2 cm^{-2} (for a film area of 0.33 cm^2).

The rate and extent of photolysis of both modifications of SnI_2 have been followed relative to a number of parameters which include time, temperature, wavelength, light intensity, film thickness, substrate type, contamination effect, effect of crystal microstructure, oxygen uptake, and the film ambient during photolysis. The kinetic data are presented as plots of number of molecules of SnI_2 photolysed cm^{-2} (extent of reaction) against time.

5.2.1 Time Dependence of the Photolysis

Kinetic data for the photochemical reaction with time were collected by observing the extent of reaction with time for the two phases of SnI_2. Presented in Fig. 5.2 are the results of the photolysis of thin films ($\sim$ 5000Å) of α-, and β-SnI_2, at 95 and 120°C respectively, with broad band radiation. The initial detail of the reaction was resolved by using narrow band filters. Shown in Fig. 5.3 are the results of α- and β-SnI_2 films photolysed with narrow band radiation employing interference filters with peak wavelength at 507.9 nm, and at temperatures of 95 and 130°C respectively. The extent of reaction against time plots are found to be linear for this part of the reaction. In Fig. 5.4 is presented the result of photolysing a 5171Å thick film of β-SnI_2 at a temperature of 110°C with broad band radiation, for a very long time. A log-log plot of the

Fig 5·2 Time dependence of the photolysis of α- and β-SnI_2

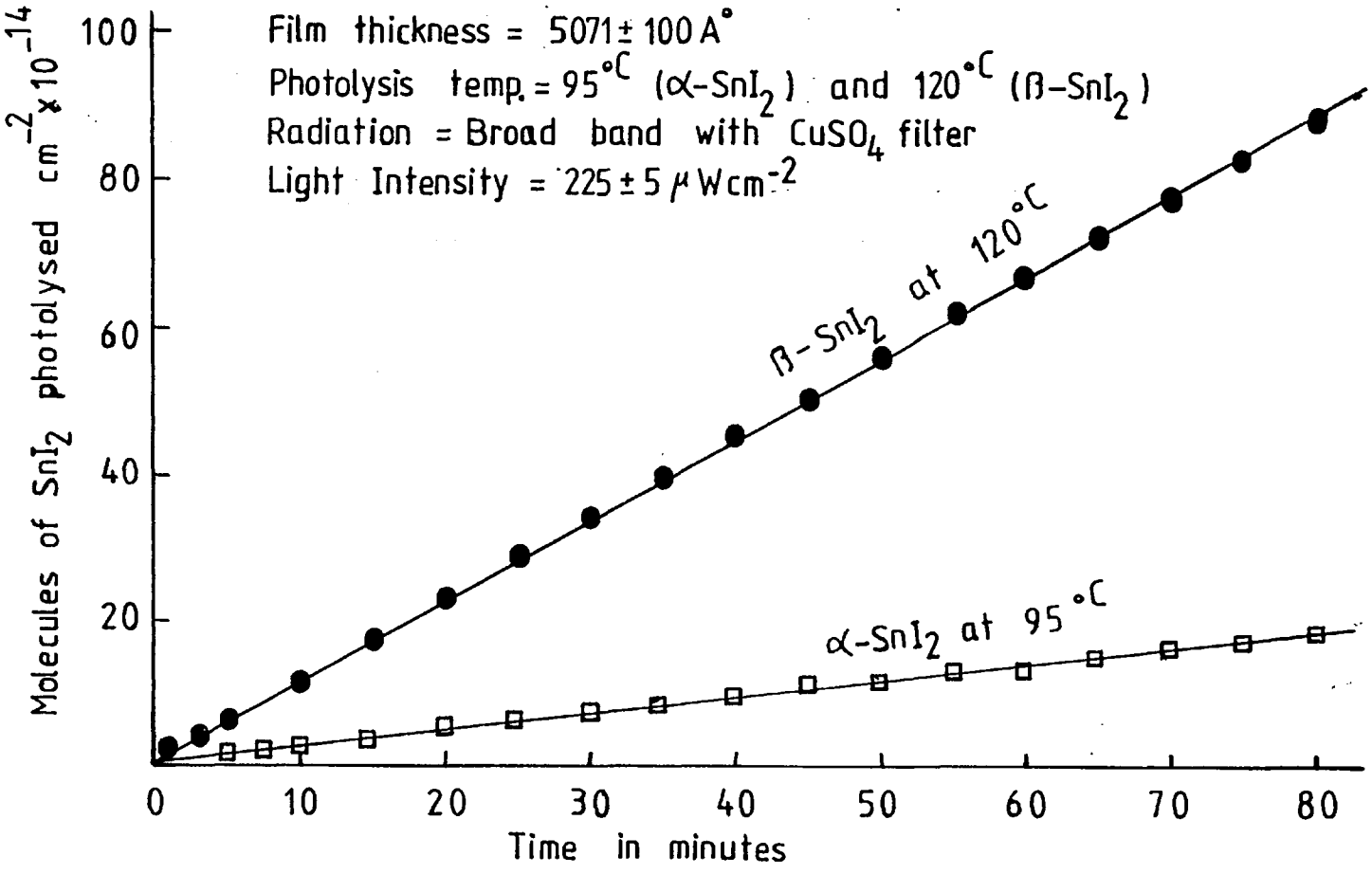

Fig 5·3 Time dependence of the photolysis of α- and β-SnI_2 with narrow band radiation.

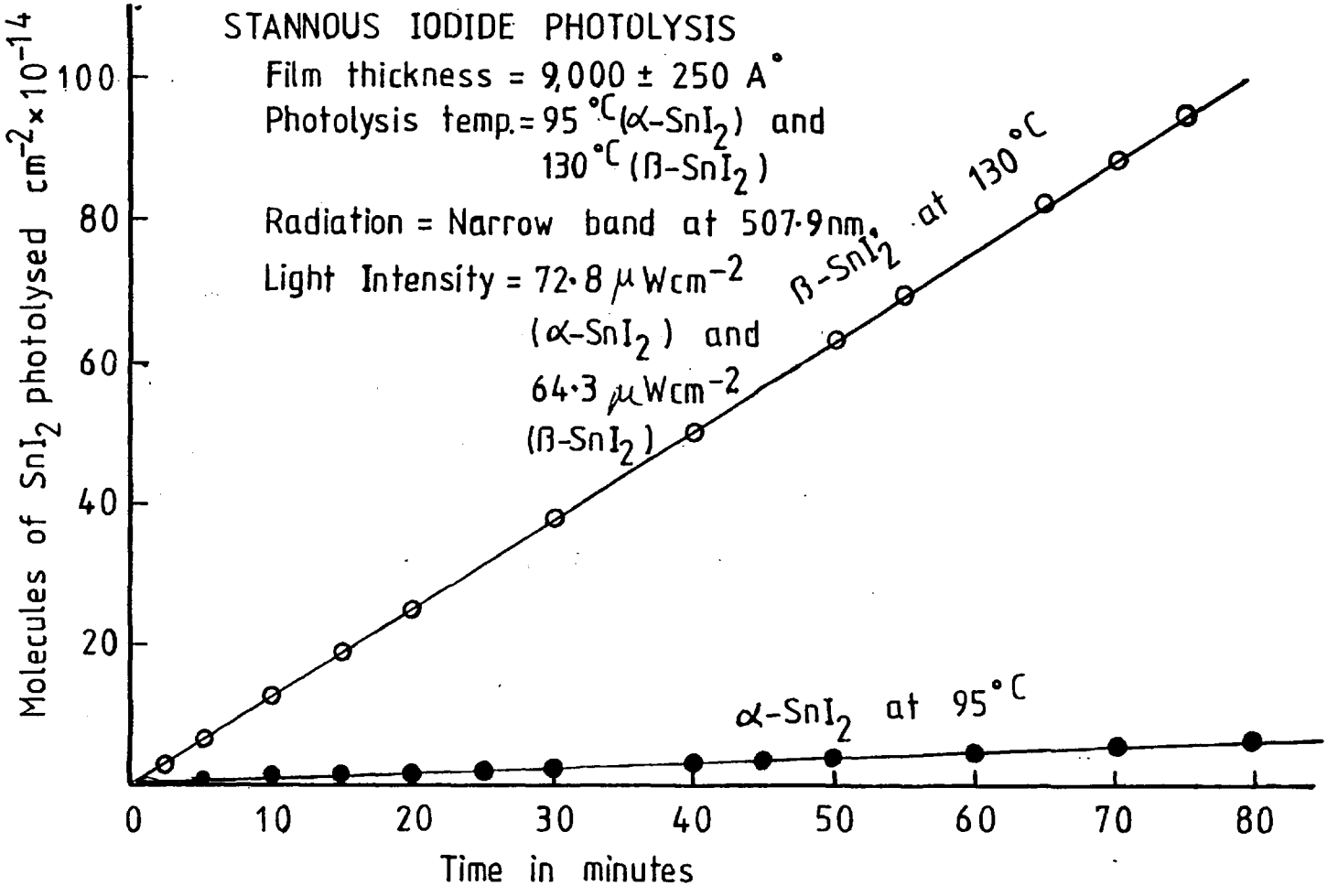

Fig. 5·4 Long time dependence of the broad band photolysis of β-SnI_2.
(~39% decomposition)

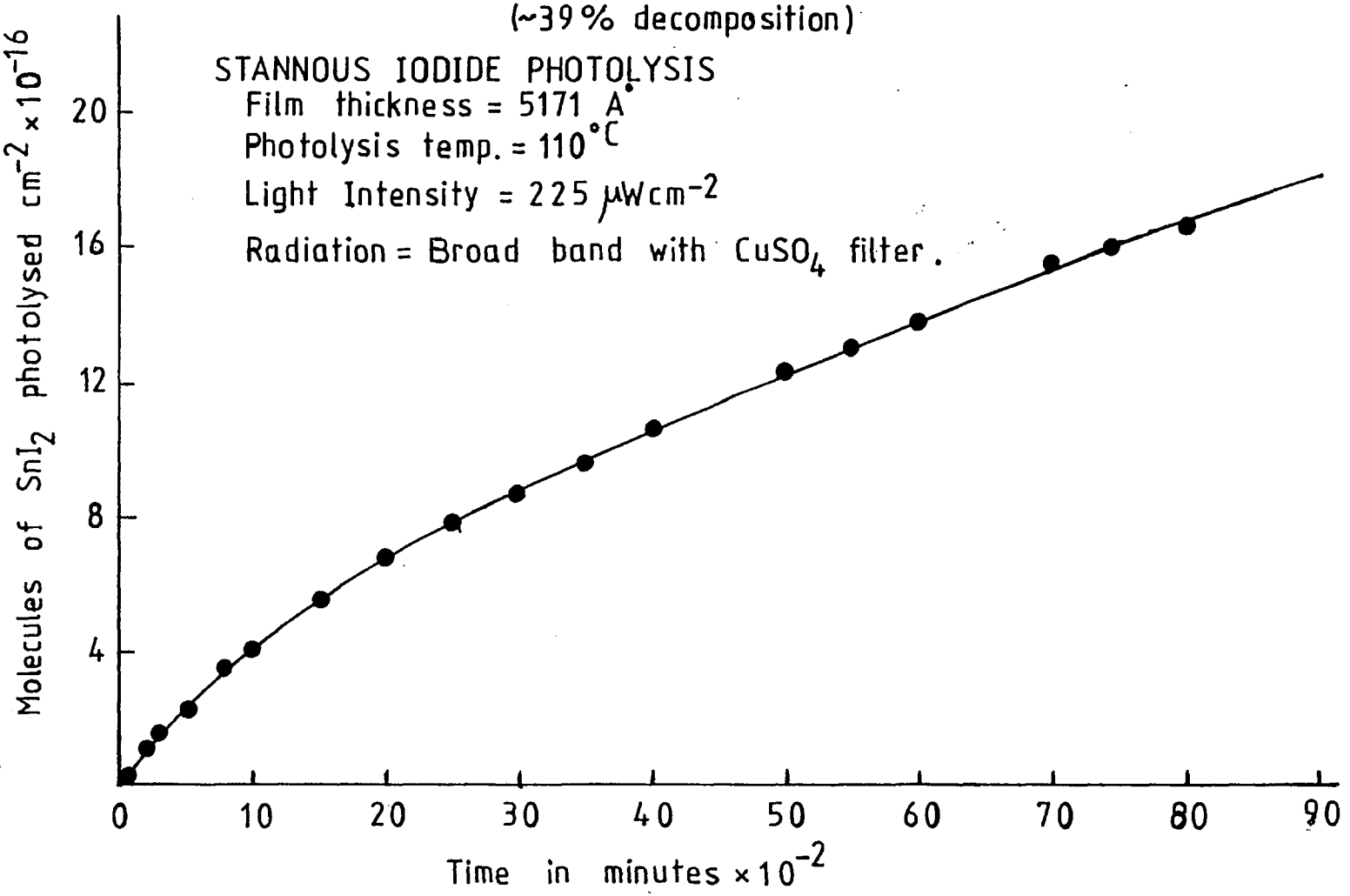

Fig 5·5 Plot of log(extent of reaction) against log(time in minutes) for the data of Fig 5·4. The time dependence of rate is seen to divide into three main regimes of $\frac{dNm}{dt} \propto K$, $\frac{dNm}{dt} \propto t^{-1/4}$ and $\frac{dNm}{dt} \propto t^{-1/2}$

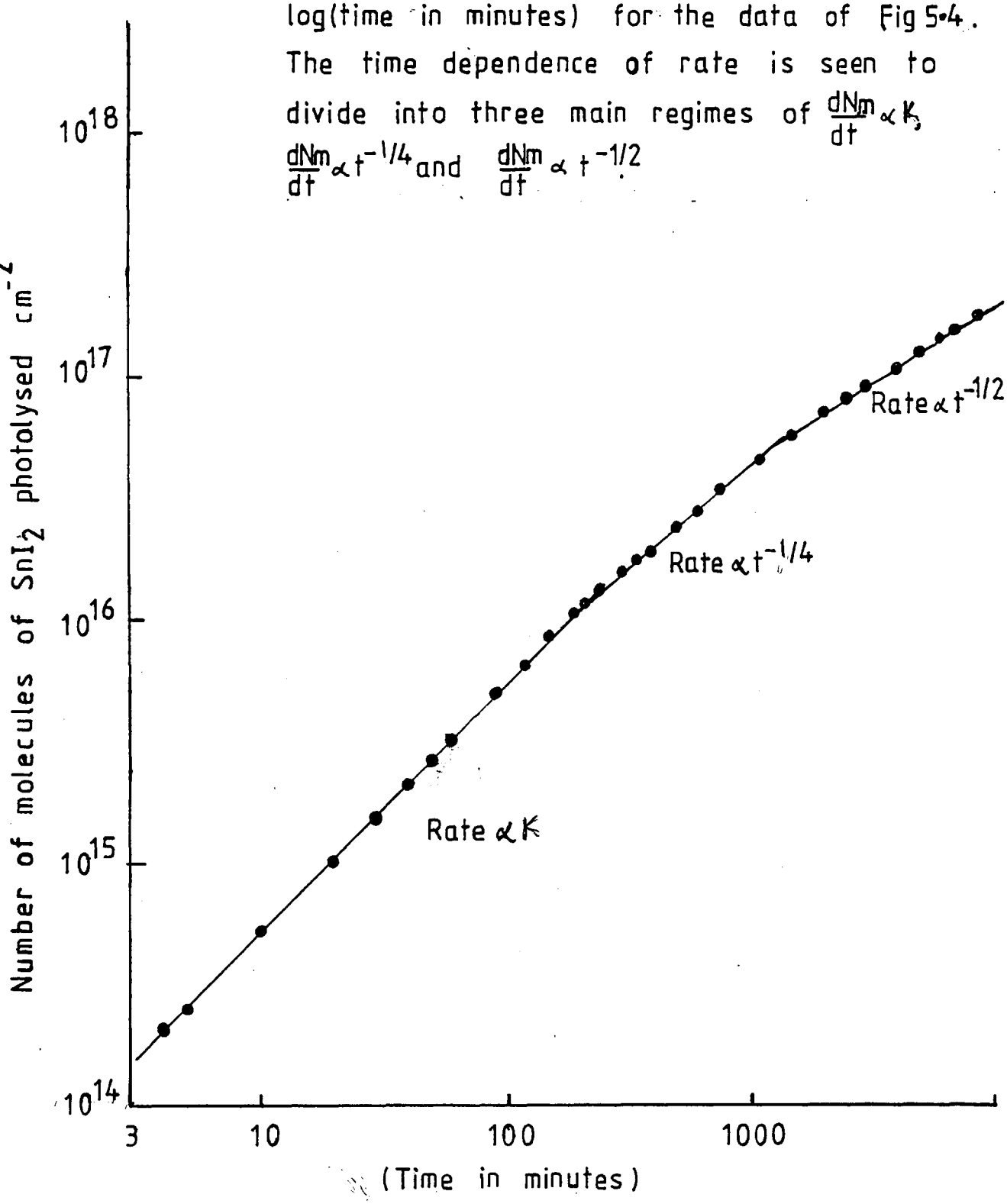

the data in Fig. 5.4 is presented in Fig. 5.5. The time dependence is found to divide into three principal regions, a regime in which extent of reaction is linear with time, t, a $t^{+\frac{3}{4}}$ dependence region, and a $t^{+\frac{1}{2}}$ proportionality regime. The linear regime accounts for about 2.5% of the total possible reaction, while the $t^{+\frac{3}{4}}$ regime accounts for about 8% reaction. The full interpretation of the chemical processes occurring in the three regions are discussed in Chapter 6. The results in Fig. 5.4 are typical of those obtained for α-SnI_2.

The time dependence of the extent of reaction was quite reproducible. Shown in Fig. 5.6 are the results obtained for α-SnI_2 films photolysed at 45°C. The variation between runs is well within ±5%.

At the end of every run, i.e. when the light was shuttered off, there was always observed a small increase in the resonant frequency of the quartz crystal as registered by the digital frequency monitor. This signified a small increase in weight of the quartz plate, and was probably due to the adsorption of some of the iodine gas molecules onto the SnI_2 film surface. This is further discussed in Chapter 6.

5.2.2 Film Thickness Dependence

Photolysis was carried out on films of varying thickness between 400 and 650 nm, for both polymorphs of SnI_2. No significant variation between runs was found, as shown in Fig. 5.7, for α-SnI_2 films photolysed at 90°C. The reactions can, therefore, be said to be thickness independent within the film thickness range employed in this work. The thickness independence can be associated with the very high absorptivity of the films in this wavelength range. As detailed in Chapter 3, the α-SnI_2 film has absorption coefficient in the 10^5 cm^{-1} range, while β-SnI_2 has $\alpha > 10^5$ cm^{-1}.

Fig 5·6 Time dependence of the photolysis of α-SnI_2 for the same film thickness, temperature, and light intensity.

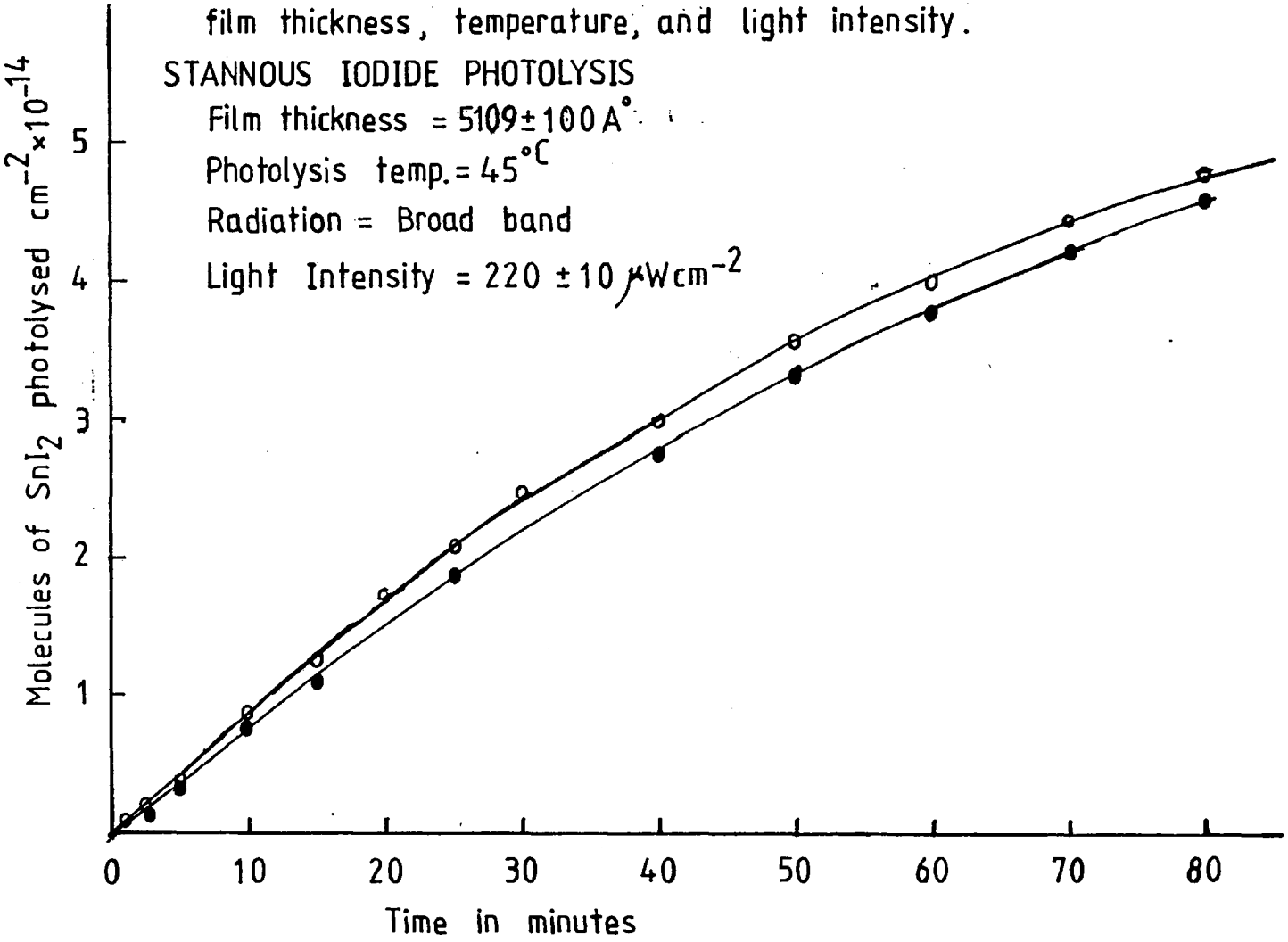

Fig 5·7 Film thickness dependence of the photolysis of α-SnI_2

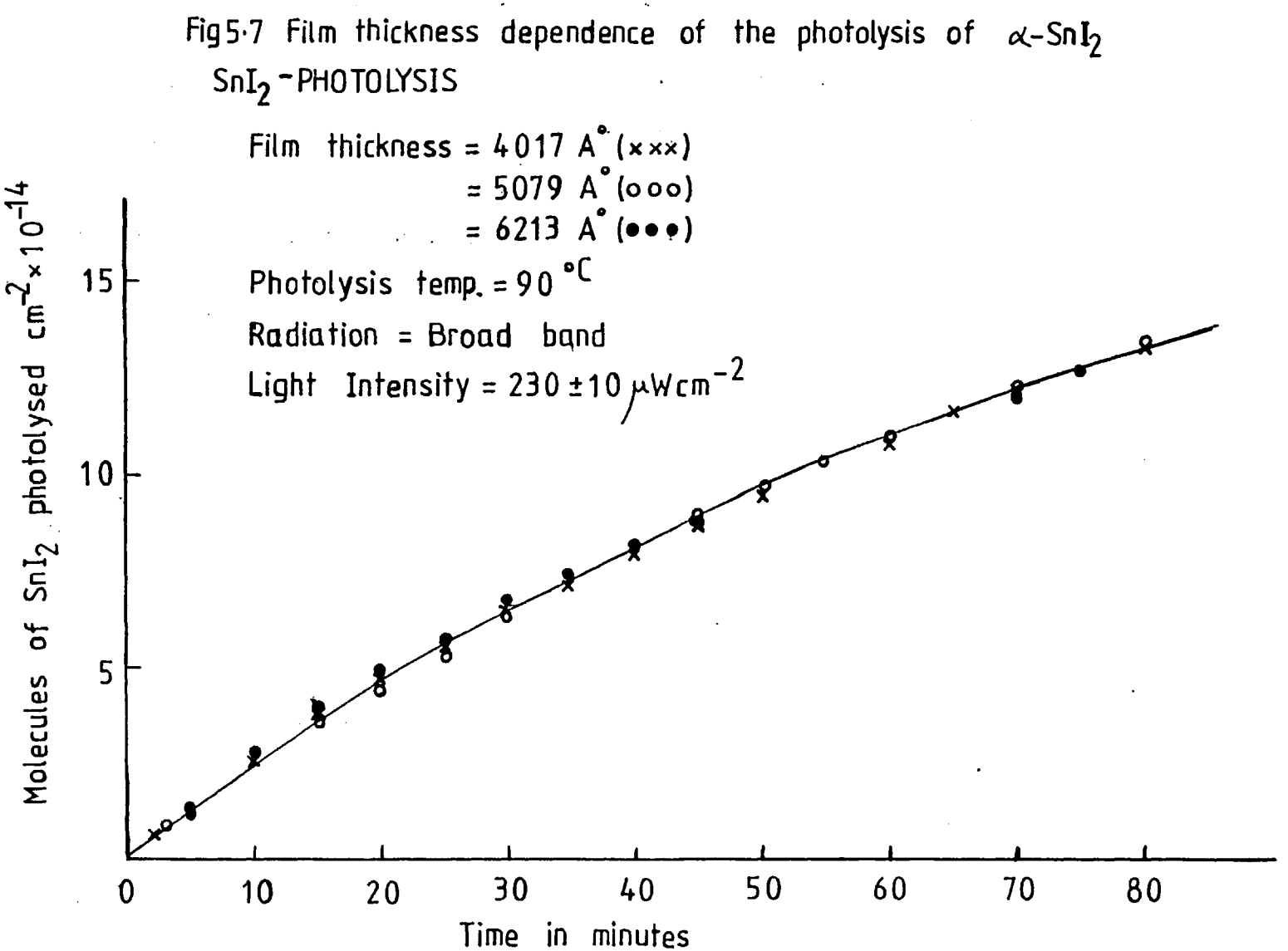

5.2.3 Temperature Effect

Thin films of SnI_2 of the same thickness ($\sim$5100Å) were photolysed with broad band radiation within the temperature range of 45 to 140°C, with the same light intensity ($\sim$230 $\mu W\ cm^{-2}$). The extent of reaction-time plots are as shown in Fig. 5.8. The Arrhenius plot of the rate of photolysis (taken as the reciprocal of the time taken to photolyse a fixed amount of SnI_2) in the linear regime against reciprocal temperature in °K, is indicated in Fig. 5.9. The plot is found to divide into two regions with two different activation energies which are 0.302 ± 0.015 eV for region I and 1.192 ± 0.015 eV for region II. As has been discussed in Chapters 2 and 3, SnI_2 changes modification from the α-(red) to the β-(yellow) modification at a temperature of 108°C. Just as was observed in the resistivity measurements (Section 3.7), the photochemical reaction has trailed after the structure type. The main cause of the difference in the activation energies is taken to be due to the change in the modification type from red to yellow.

5.2.4 Influence of Film Composition (Doping)

The SnI_2 charge was mixed with small amounts of dopants which included AgI, CuI, PbI_2 or SnI_4. Figs. 5.10, and 5.11 show the effect of these dopants on α- and β-SnI_2 films respectively. The first three were found to sensitize the films to faster photodecomposition. The relative difference between the intensification of the reaction by AgI or CuI may be due to a comparative difference in their doping levels, although the films were prepared with source temperatures between 350 and 400°C where

Fig 5·8 Temperature dependence of the rate of photolysis of α-SnI_2 (45−105 °C) and β-SnI_2 (110−130 °C)

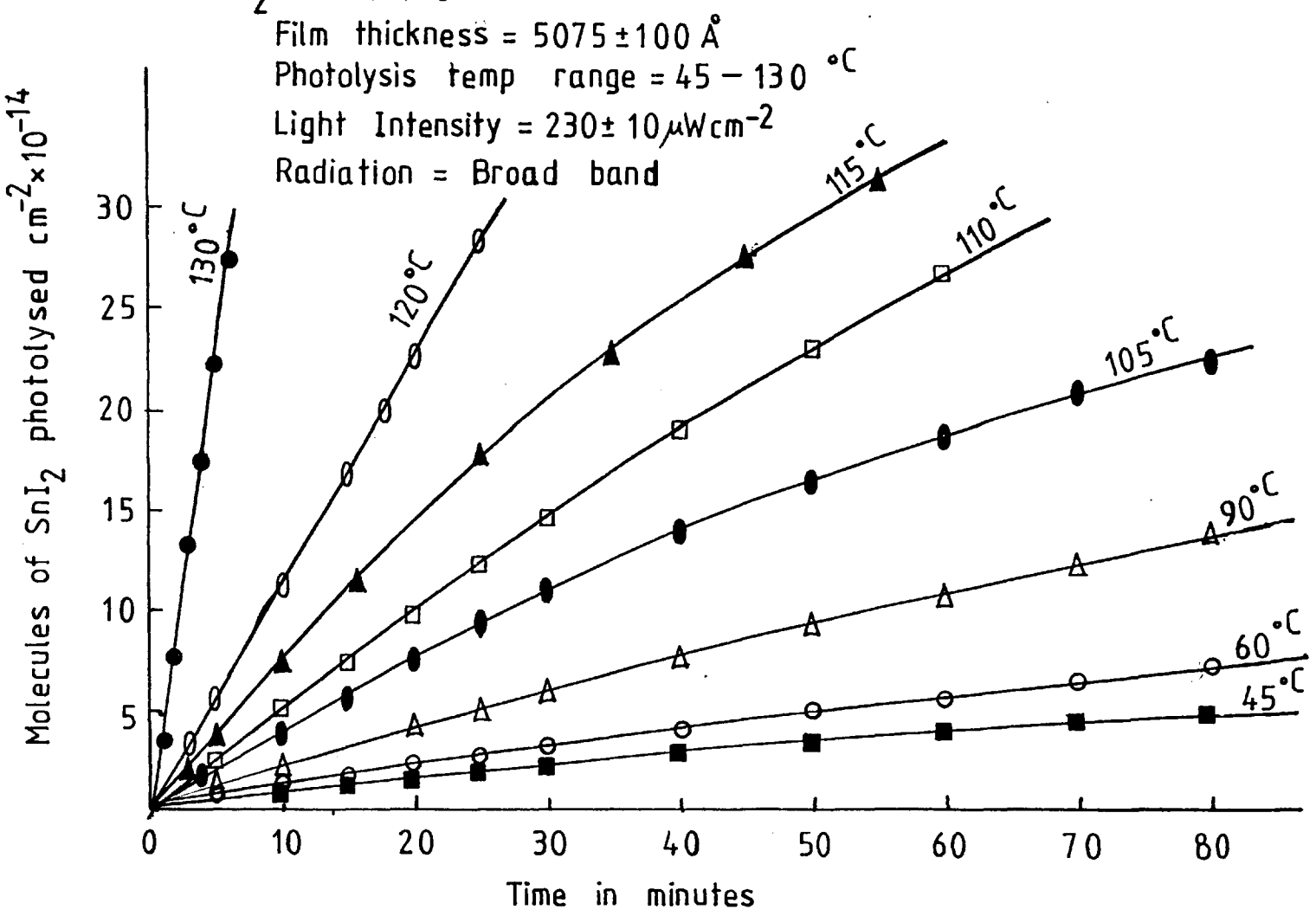

Fig 5·9 Arrhenius plot of log(rate) against reciprocal temperature (°K) of results presented in Fig 5·8 for different extents of reaction. Rate has been taken as the reciprocal of the time to photolyse

(A) $1{\cdot}8 \times 10^{14}$ molecules of SnI_2 cm^{-2}.

(B) $5{\cdot}0 \times 10^{14}$ √ √ √ √

(C) $7{\cdot}95 \times 10^{14}$ √ √ √ √

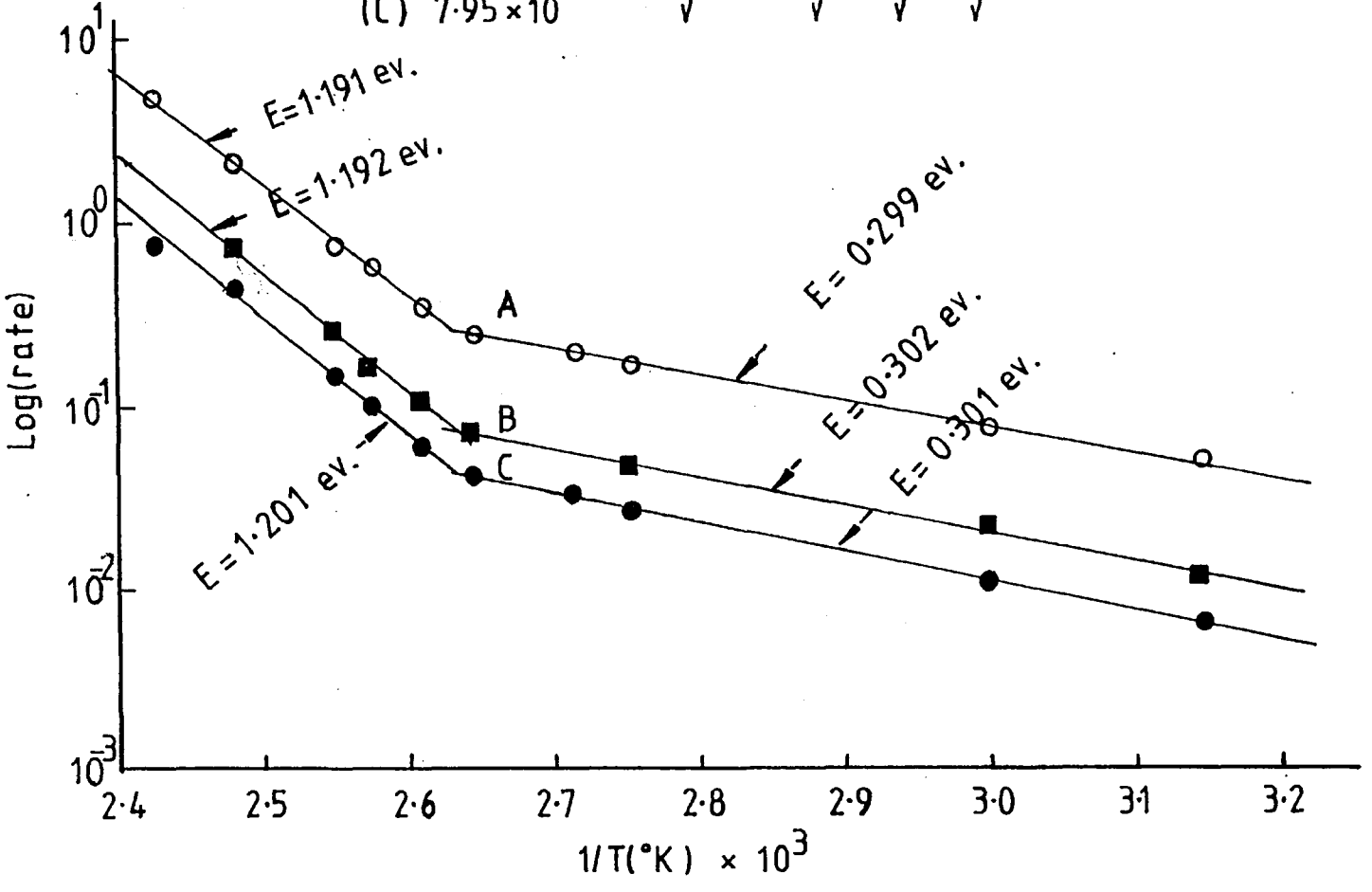

Fig 5·10 Composition dependence of the photolysis of α-SnI_2 on doping with small amounts of SnI_4, PbI_2, CuI or AgI. The effect of Tungsten (W) coated substrate is also shown.

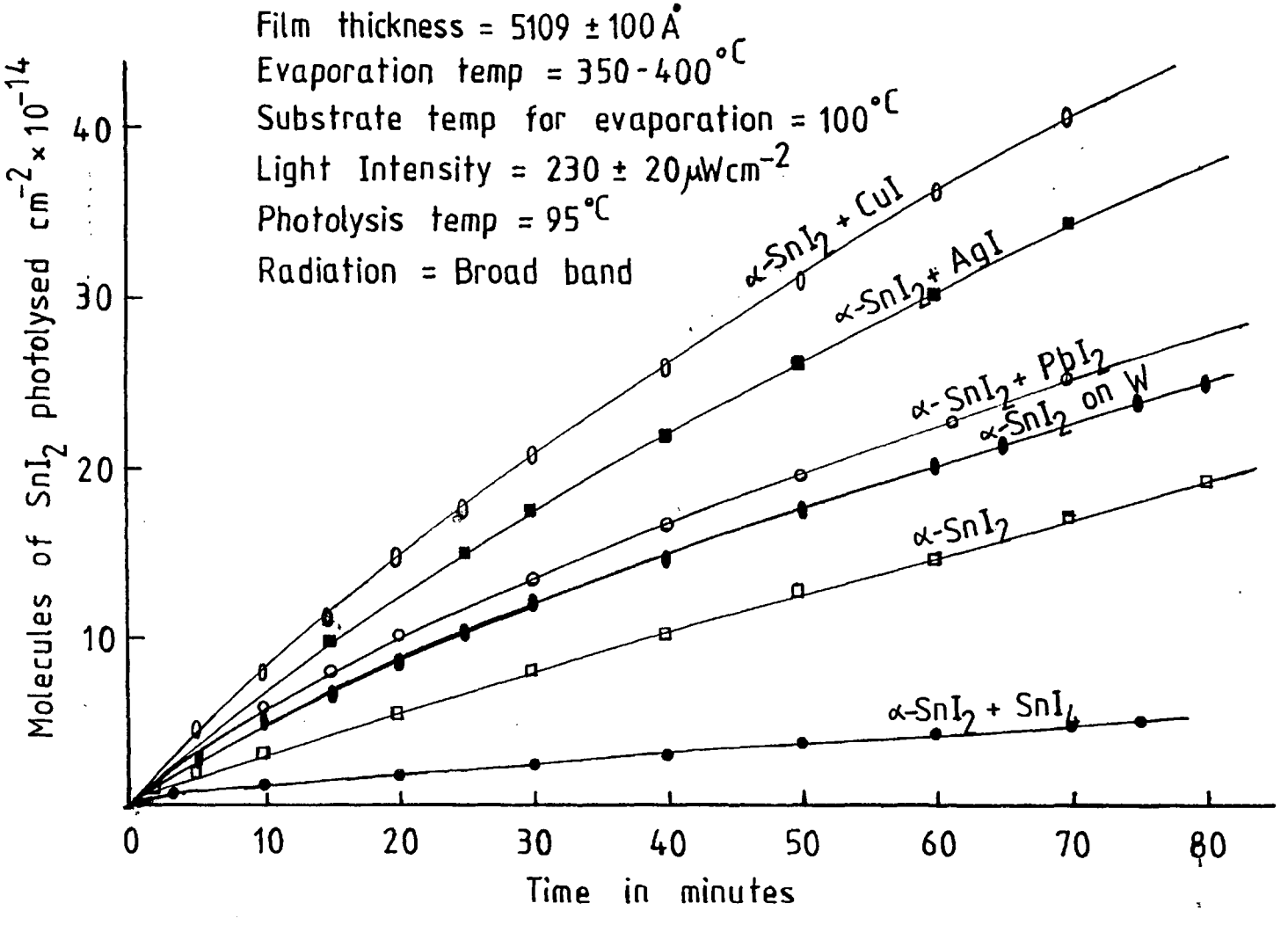

Fig 5·11 Composition dependence of the photolysis of β-SnI_2 on doping with AgI.

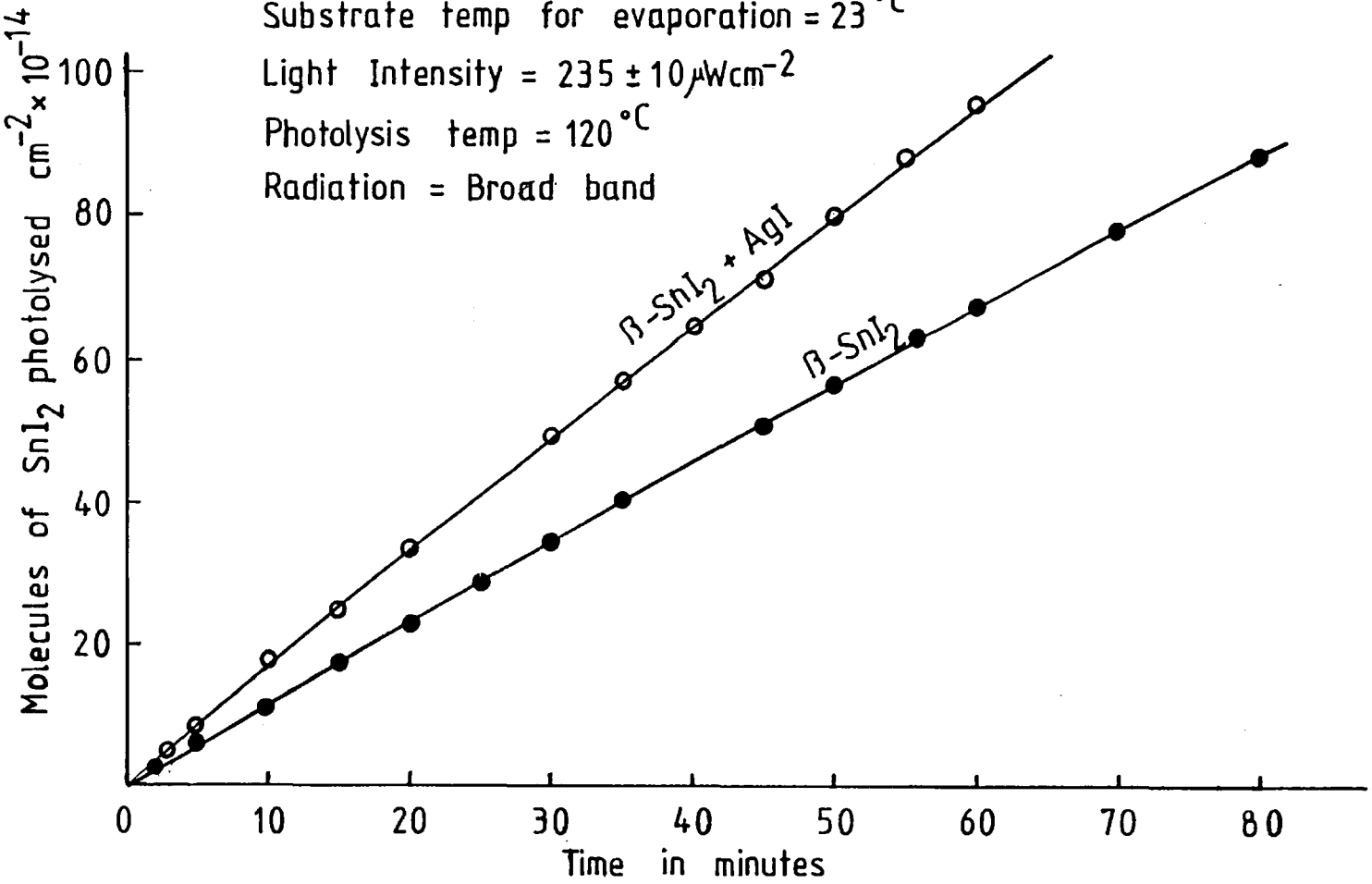

CuI or AgI has very low vapour pressure as shown in Fig. 4.4. The enhancement of the reaction with PbI_2 doping is in conformity with the fact that SnI_2 (possibly both polymorphs) and PbI_2 form continuous solid solutions[5,6], while the mixture has been shown to be more photosensitive than PbI_2 or SnI_2[4]. Stannic iodide, SnI_4, on the other hand repressed the photodecomposition reaction very considerably. These effects are further discussed in Chapter 6.

5.2.5 Substrate Effect

Most of the experiments carried out in this work were on films deposited on quartz crystal plates, with sputtered quartz covering the gold electrode area on which SnI_2 was deposited as shown in Fig. 4.2. The substrate nature was changed by evaporating a thin film of tungsten, W, just above the centrally sputtered quartz, in regions where SnI_2 would be evaporated. The substrates so prepared were used for the evaporation and photolysis of both polymorphs of SnI_2. The photolysis was found to be enhanced on tungsten coated substrates for both polymorphs. Shown in Fig. 5.10 are the results obtained for α-SnI_2 films photolysed at $95^{o}C$ with broad band radiation. The reaction rate was enhanced as is apparently the case for other photosensitive halides[7]. The nature of enhancement is quite similar to those of the monohalides.

5.2.6 Photolysis Ambient

Thin films of both polymorphs of SnI_2 were photolysed in the presence of air or oxygen, at a pressure of about 10^{-5} torr. The results are as shown in Fig. 5.12 for films photolysed at a temperature of $120^{o}C$. The shape of the reaction curve for experiment in oxygen is the same as that of photolysis in the vacuum, and the rate of reaction was observed to be enhanced in this ambient. However in the case of air, the initial

Fig 5·12 Photolysis of β-SnI_2 in low pressure air or oxygen.

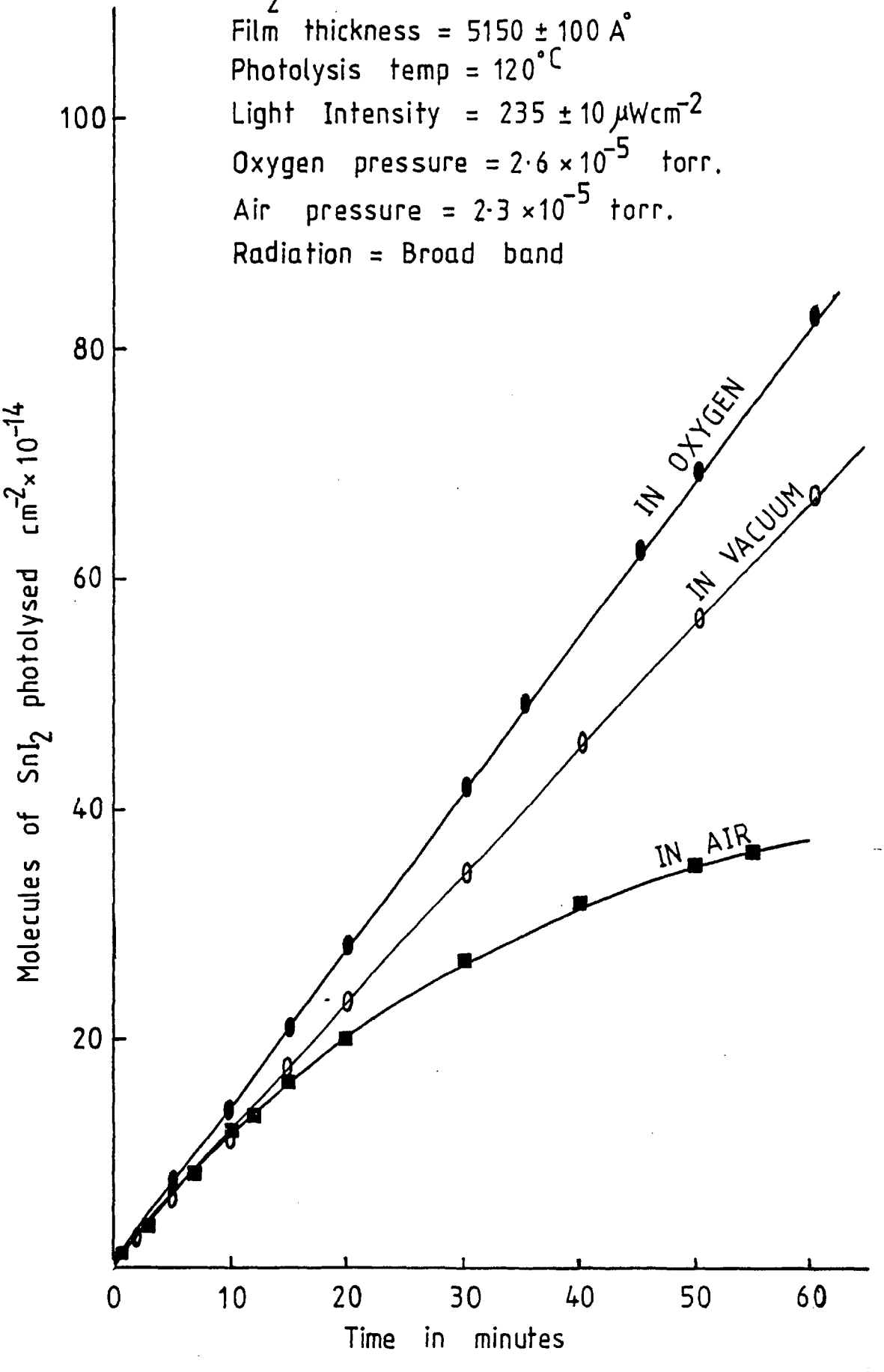

reaction rate was similar to that of vacuum photolysis, but reduced considerably with time. The reduction of the reaction rate in air with time is probably due to the hydrolysis of the films, since SnI_2 is very sensitive to the atmosphere[6].

5.2.7 Oxygen Uptake

Films of α- and β-SnI_2 were photolysed at a temperature of 105 and 120°C respectively for forty minutes before the light was shuttered off. With the light off, oxygen ($\sim 10^5$ torr.) was bled into the photolysis chamber. There was no observable increase in the resonant frequency of the quartz plate that could be read on the digital frequency monitor. This implied that there was no oxygen uptake, and therefore no reaction between the oxygen and the photolytically produced tin metal.

5.2.8 Wavelength Dependence

The spectral variation of the reaction was investigated by photolysing thin films of α- and β-SnI_2 with narrow band radiation, which incorporated the use of narrow band interference filters with peak wavelengths between 438 and 540 nm, which are just beyond the band edge of these compounds. Quantum efficiency, ϕ, was calculated as,

$$\phi = \frac{\text{No. of molecules of } SnI_2 \text{ photolysed cm}^{-2} \text{ in time t}}{\text{No. of photons absorbed by } SnI_2 \text{ film in time t}}$$

Presented in Figs. 5.13 and 5.14 are the results of the quantum efficiency against wavelength obtained for α- and β-SnI_2 respectively. For both polymorphs, the quantum efficiency was observed to be nearly constant in regions where the absorption coefficients are very high, and the photochemical process concentrated in the surface layer region. This would be shown later in Chapter 6 to be due to a rapid recombination of hole-electron pairs at the film surface region. The data in

Fig 5·13 Wavelenght dependence of the quantum efficiency for thin films (~1·0 μm. thick) of α-SnI_2 photolysed at 95°C.

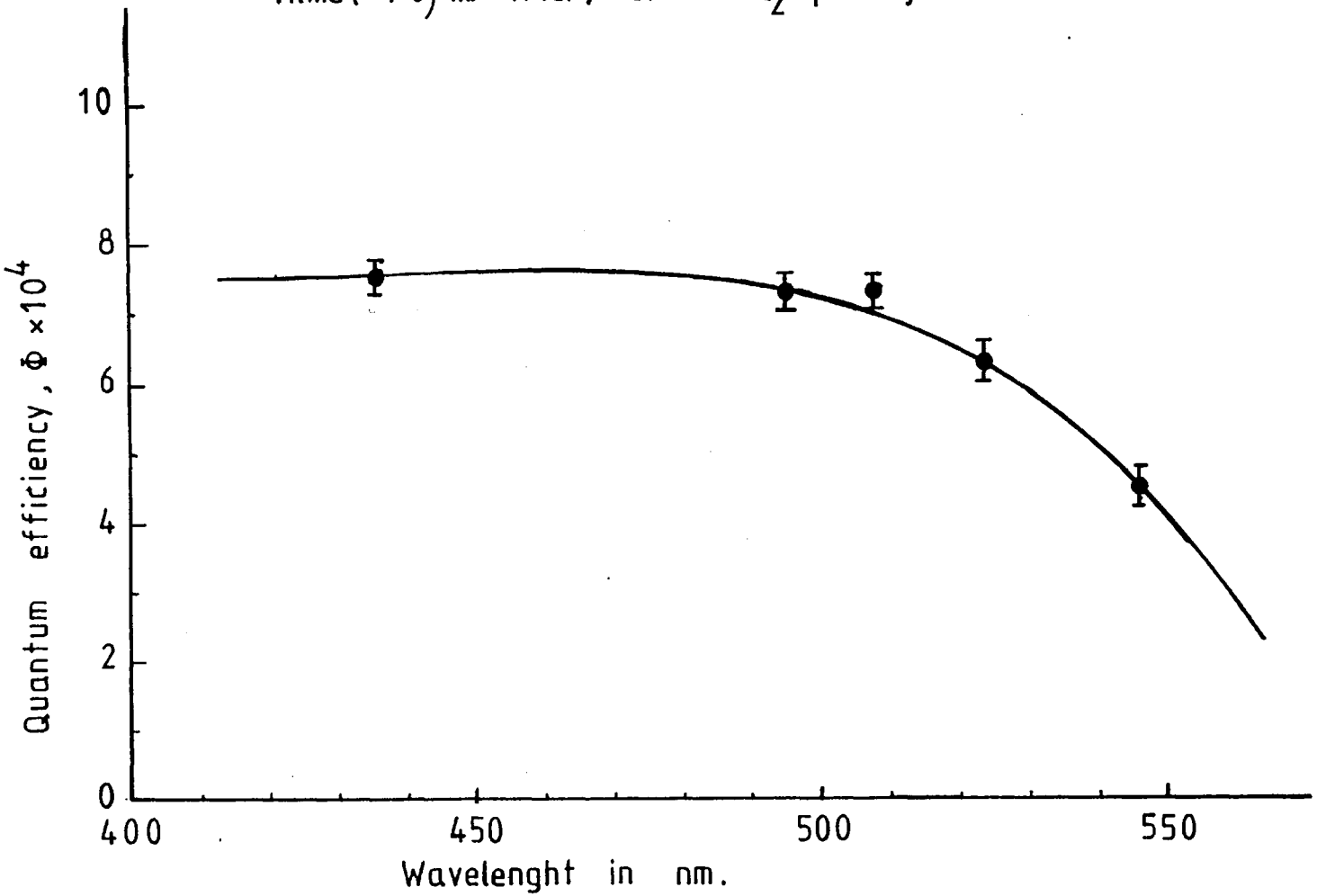

Fig 5·14 Wavelenght dependence of the quantum efficiency, Φ, for thin films (~1·0 m thick) of β-SnI_2 photolysed at 130°C.

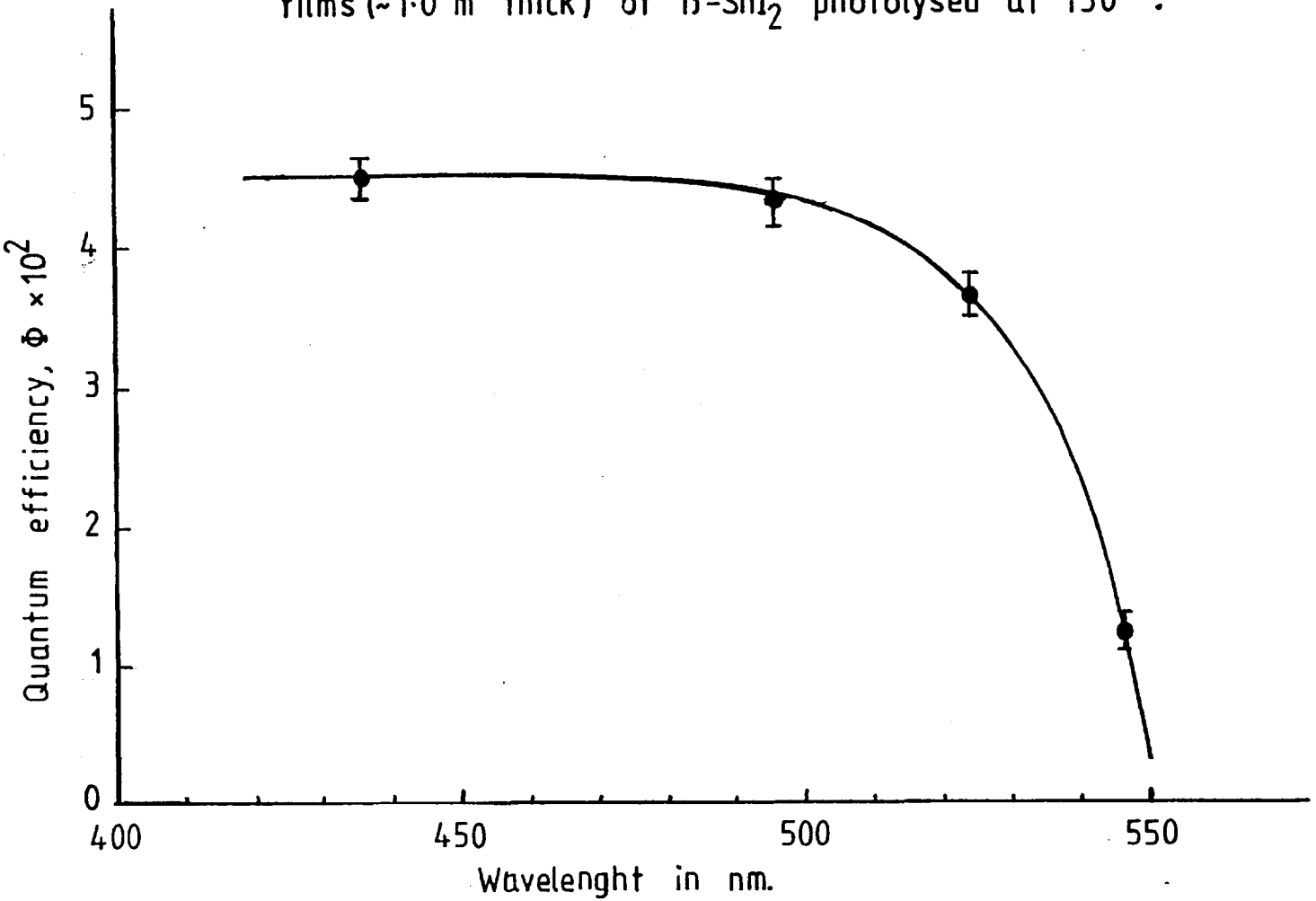

Figs. 5.13 and 5.14 have been corrected for reflection losses from the film surface by using the experimentally determined reflection data at these wavelengths.

5.2.9 Light Intensity

Light intensity dependence of the reaction was determined using the abrupt change technique. This involved photolysing the film at one light intensity for some time, and then changing the intensity to another value, without having to stop the reaction in any manner. The rate of the reaction before and after the intensity change were noted, and their ratio was compared with that of the ratio of the light intensity before and after the change. The light intensities were usually obtained after the experiments, as outlined in Section 4.6. In Fig. 5.15 is presented the results obtained for both polymorphs of SnI_2 photolysed at 95^oC or 120^oC. The ratio of the light intensities before and after the change, as well as the rate ratios before and after the change are presented in Table 5.2. The table covers light intensities between 87 and 650 $\mu W\ cm^{-2}$. All the experiments were with broad band radiation. The reaction rates were observed to be directly proportional to light intensity.

Temp.(^oC)	$R_1R_2 = R$	$I_1/I_2 = I$	I/R
95^oC	0.368	0.359	0.976
	0.4737	0.501	1.058
	2.717	2.786	1.025
120	0.7273	0.7354	1.011
	0.3158	0.3344	1.059
	1.375	1.360	0.989

Table 5.2: Ratios of raction rates, and intensity ratios obtained with the abrupt change technique

Fig 5·15 Light intensity dependence of the photolysis of α, or β-SnI_2 thin films, followed by the abrupt change technique. Photolysis was at 95°C for α-SnI_2 and 120°C for β-SnI_2, at different light intensities indicated in the diagram.

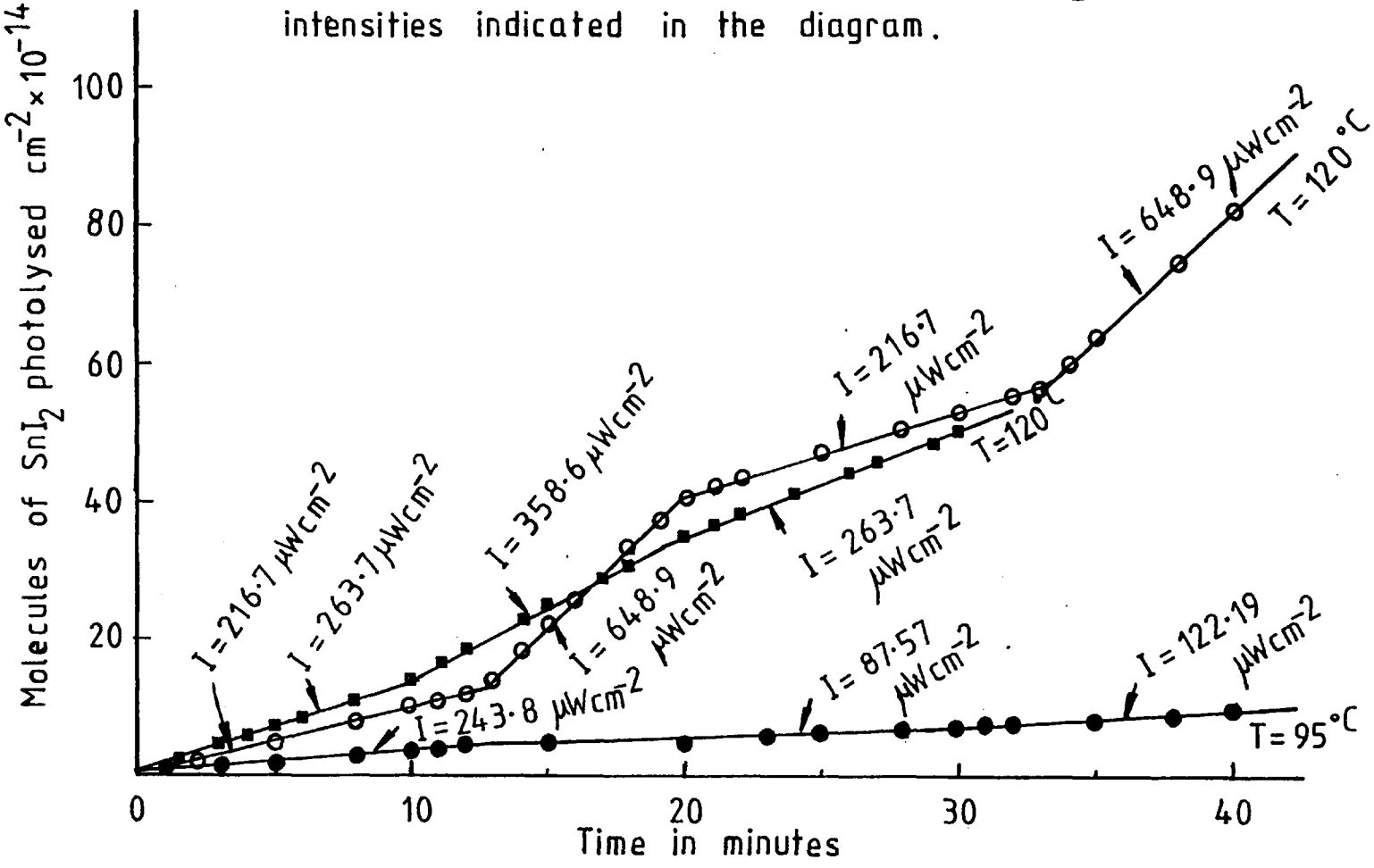

5.2.10 Crystal Microstructure

Most of the α or β-SnI_2 films used in the photolysis work were deposited on sputtered SiO_2 substrates kept at 100°C or room temperature respectively. We investigated the influence of substrate temperature for deposition on the film microstructure by doing some scanning electron microscope study on the prepared films. Prior to electron microscope study, the films were initially etched in 0.025M KI solution, dried, and then covered with gold by vacuum evaporation. Presented in Plate 5.2 are the microphotographs of films deposited at the same deposition rate (350°A/min) on substrates kept at 23 and 120°C respectively. It could be observed that the substrate temperature during film deposition had a considerable influence on the mean grain size of the platelets, being considerably larger at the higher temperature.

We have, therefore, varied the substrate temperature for the deposition of our film so as to determine the effect of microstructure on the extent and nature of our photolysis. Films of α-SnI_2 were consequently deposited on substrates kept at 50°C, while films of β-SnI_2 were deposited on substrates kept at 105°C. The nature of these films at the temperature of deposition as well as that of photolysis are as detailed in Table 5.3. On photolysing these films, no significant difference was observed in the mode as well as the rate of the photodecomposition of the films as shown in Fig. 5.16.

The rate of evaporation of a film was also observed to affect the crystal microstructure, but not as much as the substrate temperature for film deposition. Some films of both polymorphs were therefore prepared

with different evaporation rates. No difference in reaction mode or rate was observed with earlier results when these films were photolysed. It is thus evident that the film microstructure had no influence whatsoever on the rate of photolysis of both polymorphs of SnI_2.

Substrate temperature (°C) for evaporation	Nature of film	Nature of film at photolysis temperature (°C)
25	β-SnI_2	β-SnI_2 (115)
50	α-SnI_2	α-SnI_2 (95)
100	α-SnI_2	α-SnI_2 (95)
105	α-SnI_2	β-SnI_2 (115)

Table 5.3: Variation in polymorphic type of SnI_2 film with substrate temperature

(a)

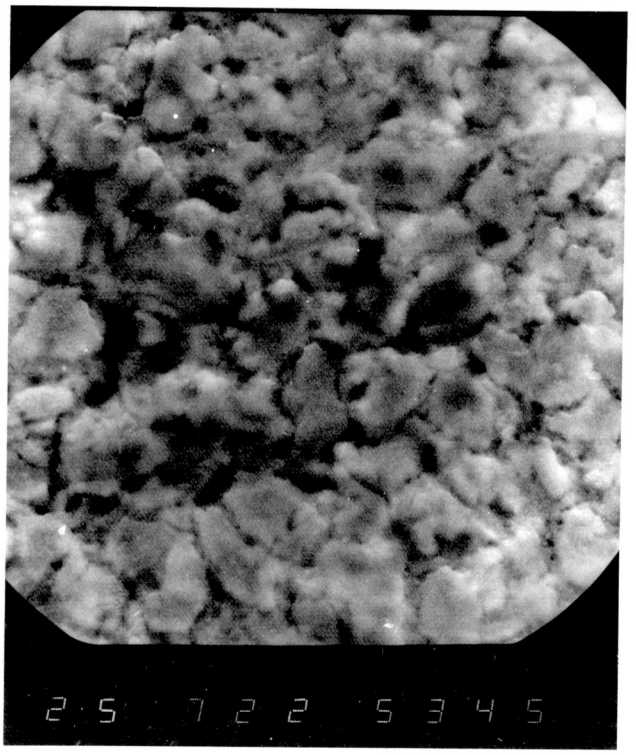

(b)

Plate 5.2: Scanning electron micrographs of etched SnI_2 films; showing the effect of substrate temperature for film deposition on film microstructure. (a) is for a film grown on a substrate kept at room temperature, while (b) is for a substrate kept at 120°C. The magnitication for both pictures is x 7200.

Fig 5·16 The effect of depositing thin films of SnI_2 on substrates kept at different temperatures.

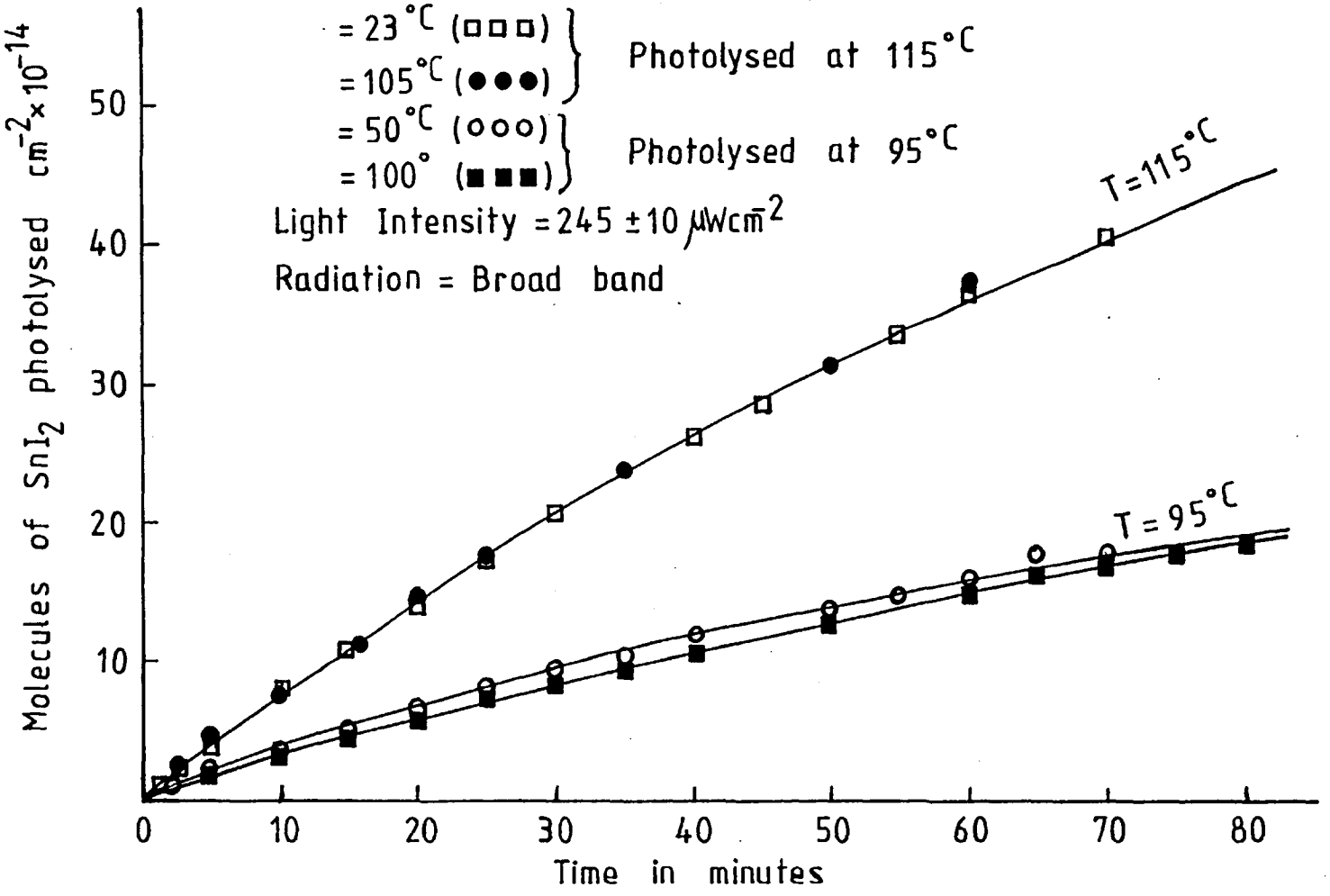

REFERENCES

(1) V.M. Kosarev, V.S. Kostko, and N.N. Karpuk. J. Appl. Spectr. (USA),p.1282, Oct. 1978

(2) J.F. Verwey, J. Schoonman, Physica 35 (3), 386, 1967

(3) J.H. Jacobs, R.A. Corrigan, J. Phot. Sci. 21, 193, 1973

(4) V.M. Kosarev, V.S. Mosttco, A.I. Ivacha, V.F. Nadtochii, T.N. Sushkevich and S.F. Chepur. Zhurn. Prikl. Spectr. 27 (3), 549, 1977

(5) D.P. Belotski, I.N. Antipov, V.F. Nadtochii, and S.M. Dodik. Izv. Akad Nauk SSSR, Neorg Mater. 5 (10), 1852, 1969

(6) R.A. Howie, W. Moser, and I.C. Trevena. Acta Cryst. B, 28, 2965, 1972

(7) M.T. Kostyshin, E.V. Mikhoilorskanya and P.F. Romaneko. Sov. Phys. Solid State 8 (2), 451, 1966

CHAPTER SIX

DISCUSSION OF KINETIC RESULTS

From the kinetic data (Chapter 5), we were able to observe that the time dependence of the photochemical decomposition of α and β-SnI_2 divide into three principal regions, a linear region (i.e. $\frac{d\theta}{dt} \alpha K$), which we would take as the primary step in the reaction process. We would refer to the $t^{-\frac{1}{4}}$ regime as the intermediate reaction step, while the $\frac{d\theta}{dt} \alpha t^{-\frac{1}{2}}$ regime would be referred to as the terminal step of the photochemical process.

In this chapter deductions are made as regards the species that are produced in relation to each of the different time dependent regimes. Insight into each of the regimes is further gained by correlating the results to relevant existing models for photochemical reactions. The mechanism of the photochemical reaction in each of the time dependent zones would also be outlined.

6.1 PHOTOCHEMICAL REACTION SITES

The photolytic process can be described in the following manner. With the absorption of a photon, an electron-hole pair is generated. According to the processes which follow this absorption, we may discern three kinds of event in the photolysis. Firstly, transport to and trapping of photogenerated electrons and holes at defect centres or lattice vacancies. Secondly, in addition to charge transport, there may be mass transport by ionic motion. Thirdly, the removal of some of the reaction products from the surface.

In SnI_2, the photogenerated hole is believed to be trapped at a surface centre, from where it combines with a surface iodine ion, giving an iodine atom, this atom is desorbed either directly or after combination with another atom to form an iodine molecule. The idea of surface desorption is supported by the fact that at the end of every run there was always an increase in the frequency reading ($\sim$2Hz at 110^{o}C) of the digital frequency monitor (i.e. mass increase), that registers the frequency shift (due to mass changes) of the quartz crystal substrate used in the photochemical experiments. This was not the case in a blank quartz crystal plate treated in the same manner. The increase in frequency was a direct registration of mass increase, which we attribute to a possible readsorption of the iodine gas molecules on the film surface. These could easily be accommodated in the surface states created on the film surface during photolysis. A continuous decrease in the frequency reading of the monitor would be expected if the iodine atoms or molecules were bulk generated, as they diffused up to the surface and are lost to the vacuum.

The electrons produced by photon absorption are taken to be trapped at a suitable defect or lattice centre (probably an anion vacancy site), from where they eventually react with the Sn^{2+} ions, thus precipitating aggregates of tin atoms. The tin atoms could either be bulk or surface generated. The lack of oxygen uptake when oxygen was admitted into the reaction chamber at the end of a photolysis run did indicate a lack of reaction between oxygen, and the photolytically produced tin atoms. We can, therefore, infer that the tin atoms are generated below the film surface, i.e. they are bulk generated.

6.2 DEFECT NATURE OF SnI_2

The crystal structure of α-SnI_2 (red) was studied by Howie et al.[1], and showed a distorted octahedral packing of iodine ions between which the tin ions are placed. The tin ions are surrounded by 6 or 7 iodine ions in an octahedral or trigonal prism arrangement respectively, at distances 3.147 to 3.718Å.(see Figs. 1.1, 1.2 and 1.3). Since α-SnI_2 is believed to be a derived structure of the β-SnI_2 polymorph (see Chapter 2), we can safely assume that β-SnI_2 might have a lattice arrangement not too different from the α-polymorph. With the α-SnI_2 lattice arrangement, the iodine ions at 3.718Å will have left enough space to accommodate ions with a radius of at most 0.528Å[2].

The ionic radii of iodine and tin (2+) ions are 2.20 and 0.93Å respectively[3], so we may disregard the occurrence of interstitial iodine or tin ions. We therefore consider anion and cation vacancies to be the only intrinsic point defects in both polymorphs of tin diiodide. Therefore according to a Schottky mechanism, the generation of these vacancies is given by

$$0 \longrightarrow V_{Sn}^{2+} + 2V_I^- \qquad (1)$$

where V_{Sn}^{2+}, V_I^- denote a missing tin ion, at a tin ion site, and a missing iodine ion at an iodine ion site respectively, while 0 denotes the perfect lattice.

If we assume that on doping the foreign ions keep their normal valency states, then doping with monovalent cations Me^+ would lead to a shift in the Schottky equilibrium such that the lattice reaction can be given as

$$MeI \rightleftharpoons Me^{+}_{Sn^{2+}} + V_I^{-} + I^{-} \qquad (2)$$

The electroneutrality condition according to Koch and Wagner system is given by the algebraic equation:-

$$[Me^{+}] + 2[V_{Sn^{2+}}] = [V_I^{-}] \qquad (3)$$

where square brackets denote concentration. Upon doping with monovalent cations in concentrations well above those of the intrinsic lattice defects, the above relation (3) becomes

$$[Me^{+}] = [V_I^{-}] \qquad (4)$$

In the case of doping the SnI_2 charge with AgI or CuI, the foreign ions Ag^{+}, or Cu^{+}, have ionic radii of 1.26 and 0.96Å respectively[3], which are greater than 0.528Å. So in all cases the iodine ion vacancies are to be considered to carry the electrical current in tin diiodide by a diffusion process, as is the case in the lead halides[4].

The anion vacancy diffusion is believed to be an activated process, and dependent on the anion vacancy concentration, n, by the relationship[5]

$$D = \frac{n}{N} \nu a^2 B e^{-E/kT}$$

where D is the diffusion coefficient

n is the number of vacancy sites

N is the number of formular units of SnI_2 molecules per unit volume

ν is a frequency of the order of lattice vibration frequency, usually called the attempt-to-jump frequency

a is the jump length

E is the activation energy for vacancy diffusion

B is a proportionality constant relating to the increased entropy of the system

Increased concentration of anion vacancies would therefore lead to an increased diffusion of these vacancies.

6.3 QUALITATIVE MODEL FOR PHOTOLYSIS IN THE PRIMARY REGIME

The non-dependence of the photochemical reaction on film thickness raises two possibilities as regards the relative lifetimes of the electron-hole pairs generated with photon absorption, and the placement of the photolytic region within the film matrix. The possibilities are:

(1) The bulk lifetime of the electron-hole pairs is long compared with surface recombination process, so that the bulk diffusion length, ℓ_D, is much greater than ℓ, the film thickness.

(2) The light is absorbed in a distance short compared with ℓ. If ℓ_D is less than ℓ, then the photo-carriers are recombined almost where they are generated.

The former case would lead to increased photo-efficiency (since electron hole-pairs would live long enough to photolyse SnI_2) while the latter would be characterised by very low photon efficiency in relation to the total absorbed photon flux. Therefore mechanism (2) is much more enhanced than (1) according to our photon efficiency results. This deduction is butressed by the relatively high ($\sim 10^5$ cm^{-1}) absorption coefficients of the films, which limits the generation of electron hole pairs to the surface region of the films[6], and hence photolysis with light absorption.

6.4 QUANTITATIVE MODEL FOR THE PHOTOLYSIS IN THE PRIMARY REGIME

With the absorption of light, electron-hole pairs are generated some of which react with the material to photodecompose it, while the others recombine either at the surface or in the bulk. In the model which follows, we characterise the surface recombination velocity (at the free surface of the film) as S_r, while the surface recombination velocity at the SnI_2-quartz interface is taken to be zero. The electron-hole pairs in the bulk are characterised by a minority free carrier lifetime, τ. The speed of electron and hole reaction with Sn^{2+}, and I^- ions respectively to effect photolysis is characterised with velocity S_p.

Following a simple semiconductor model by De Vere[7], applied in modified form to photolysis by Albrecht and Green[8], the generation and recombination of carrier pairs in the bulk of a thin slab of material illuminated on one side leads to the relation

$$\frac{d^2n}{dt^2} = \frac{n}{D\tau} - \frac{I\alpha}{D} e^{-\alpha x} \qquad (6)$$

where n is the concentration of photogenerated carrier pairs

D is the pair diffusion coefficient

I is the absorbed photon flux

α is the film absorption coefficient

x is the distance into the slab measured from the film surface

τ is the bulk lifetime of carriers

The above equation is solved subject to two boundary conditions

(a) The flux of electron-hole pairs to the free surface is

$$J_{\text{free-surface}} = D\left(\frac{dn}{dx}\right)_{n \text{ at } x = 0}$$

$$= n_{(x=0)}S$$

(b) The flux at back face is zero because we say S = 0 at the SnI_2-quartz interface.

On solution[8]

$$n_o = \frac{1}{\text{Sinh}(J\ell)} \left\{ \frac{W\alpha}{J} e^{-\alpha\ell} - \left(\frac{n_o S}{JD} + \frac{W\alpha}{J}\right) e^{J\ell} \right\}$$

$$+ \frac{n_o S}{JD} + \frac{W\alpha}{J} + W \qquad (7)$$

where

S is the combined effective surface recombination velocity, i.e. the sum of electron-hole recombination and the consumption of electron hole pairs due to photolysis

ℓ is the slab thickness

n_o is the electron-hole concentration at x = 0

$W = I\alpha/D(J^2-\alpha^2)$

and

$$J = (D\tau)^{-\frac{1}{2}} = 1/\ell_D$$

When all the light is absorbed near the surface, i.e. when $\ell \gg 1/\alpha$, equation (7) can be simplified to the form[8]

$$n_o = \frac{I\alpha\,(1-\alpha/J)}{D(J^2-\alpha^2)(1 + S/JD)} \tag{8}$$

Suppose we assume that the reaction is not activated (which is probably true for the yellow polymorph at very high temperatures, i.e. $T > 140°C$). In this case, all the surface recombination can be associated with photolysis, hence

$$n_o = \phi I/S \tag{9}$$

where ϕ is the quantum efficiency of the photolysis in the non-activated regime.

Substituting eqns. (9) in (8), we have

$$\phi = \frac{\alpha}{(\alpha+J)} \cdot \frac{S/JD}{(1 + S/JD)} \tag{10}$$

We expect S/JD to be much greater than 1. $(JD)^{-1} = (\tau/D)^{\frac{1}{2}}$ is typically 10^{-2} - 10^{-3} cm^{-1}, hence S values greater than approximately 10^{+2} cm sec^{-1} are what we must have for ϕ values greater than approximately 10^{-2}. Eqn. (10) can therefore reduce to

$$\phi = \alpha/(\alpha + J) \tag{11}$$

for a non-activated process.

However, we know from our results that, over the temperature range investigated, the photolysis is activated in both polymorphs of SnI_2. If we assume that α and J are temperature independent, then eqn. (11) can be modified to the form

$$\phi = \left(\frac{\alpha}{\alpha+J}\right) \frac{K(T)}{K(T) + K_r} \tag{12}$$

K(T) is the activation term, and is equal to

$$K(T) = K_p \exp(-\Delta E/kT) \tag{13}$$

where ΔE is the energy of activation for the photochemical reaction

K_p is a constant which is related to the rate constant of the rate determining step in the mechanism of the photolysis

K_r is the equilibrium rate constant for the electron-hole recombination process

We can infer from our experimental results that $K_r >> K_p(T)$

Hence

$$\phi = \frac{\alpha}{\alpha+J} \frac{K_p}{K_r} \exp(-\Delta E/kT) \tag{14}$$

When light is absorbed in a distance short compared with the diffusion length, i.e. $\alpha >> J$, eqn. (12) reduces to the form

$$\phi = \frac{K(T)}{K_r} = K' \tag{15}$$

while if $\alpha << J$, then

$$\phi = \frac{\alpha}{J} \frac{K(T)}{K_r} = \frac{\alpha}{J} K' \tag{16}$$

That is, only light absorbed within a diffusion length of the surface is used for photolysis, while electron-hole pairs more than a diffusion

λ_1(nm)	λ_2(nm)	x 10^{-4} $\alpha_1(cm^{-1})$	x 10^{-4} $\alpha_2(cm^{-1})$	ϕ_1	ϕ_2	$J(cm^{-1})$	ℓ_D(cm)x10^4
450	500	10.22	30.25	0.0445	0.0413	3439.05	2.91
	490		3.26		0.0428	1937.94	5.16
440	490	12.04	3.26	0.0448	0.0428	3690.58	2.71
	500		3.02		0.0413	5522.99	2.84
	510		2.267		0.0392	4126.01	2.42
	520		1.357		0.0358	3970.84	2.52
	530		0.812		0.030	4452.98	2.25
	540		0.549		0.0295	3057.59	3.27
460	490	5.20	3.26	0.0442	0.0428	3027.32	3.30
	500		3.02		0.0413	5622.85	1.78
	525		1.066		0.0333	4795.24	2.09
	540		0.549		0.0295	3247.58	3.08
470	500	4.33	3.02	0.0441	0.0413	8080.23	1.238
	510		2.267		0.0392	6903.71	1.448
	520		1.357		0.0358	5123.70	1.95
	525		1.066		0.0333	5133.44	1.95
	540		0.549		0.0295	3350.76	2.98
490	510	3.26	2.267	0.0428	0.0392	8643.6	1.157
	525		1.000		0.0333	4707.8	2.12
500	515	3.02	1.802	0.0413	0.0378	4778.02	2.09
	520		1.357		0.0358	4319.49	2.32
	540		0.549		0.0295	2942.14	3.40
	530		0.812		0.030	4848.80	2.06

Table 6.1: Calculation of mean diffusion length ℓ_D, using eqn. (12) for the β-polymorph

length from the surface recombine and are lost. The above spectral dependencies of the photolytic process in both polymorphs of SnI_2 were observed : eqn. (15), for higher photon energies, and eqn. (16) at the lower photon energies (i.e. near the band gap).

We were able to determine the diffusion length, $\ell_D = 1/J$, using eqn. (12), and experimental values of α and ϕ, to be $2.480 \times 10^{-4} \pm 0.845 \times 10^{-4}$ cm, at 130°C; for the β-SnI_2 polymorph, as shown in Table 6.1. This value is quite comparable with that obtained by some other methods for compounds that are isoelectronic and have layer type lattice in common with SnI_2[9].

6.5 REACTION MECHANISM

Since iodine is surface generated, there must be a mass transport of iodine ions to the surface where they react with photoholes trapped at suitable surface sites. To generate tin metal in the bulk, there must be a suitable trapping site for electrons in the bulk from where they can react to reduce the tin metal ions. We therefore propose a dynamic reaction mechanism of Verwey[10], which was further developed by Albrecht and Green[8] for lead iodide.

With the absorption of a photon, electron hole pairs are generated

$$0 \rightarrow e^- + h^+ \qquad (17)$$

Since the photolysis is a surface process, the photoholes (h^+), are suggested to be trapped (due to favourable electrostatics) at surface cation vacancy sites (missing Sn^{2+} ion), $V^{\circ}_{Sn,s}$

$$h^+ + V^{\circ}_{Sn,s} \rightleftharpoons V^{+}_{Sn,s} \qquad (18)$$

where s denotes the surface. Because of the relative concentration of the occupied iodine ion sites adjacent to the cation vacancy, the trapped hole can react with an iodine ion in an adjacent site on the surface to produce iodine adatom.

$$V^{+}_{Sn,s} + I^{-}_{I,adj,s} \rightleftharpoons I^{\circ}_{I,adj,s} + V^{\circ}_{Sn,s} \qquad (19)$$

This would lead to accumulation of iodine on the surface. Since iodine is eventually desorbed, we further propose a movement of the iodine atom onto the surface, such that it would be adsorbed on the surface; thus creating a surface anion vacancy.

$$I^{\circ}_{adj,s} \rightleftharpoons I^{\circ}_{(ads)} + V^{\circ}_{I,adj,s} \qquad (20)$$

The iodine atom could desorb either on its own (which is unlikely) or combine with another iodine atom, to form a molecule of iodine which can then desorb as a gas,

$$2I^{\circ}_{(ads)} \rightleftharpoons I_{2(gas)} \qquad (21)$$

The above sequence of steps (18-21) account for the consumption of the photoholes in the production of molecular iodine gas. In the case of the photoelectrons, since these must react in the bulk with tin ions to produce tin atoms, there must therefore be a mechanism by which the electrons are trapped within the film, away from the surface. We propose that the surface anion vacancies $V^{\circ}_{I,adj,s}$, diffuse into the bulk, to enhance the supply of anions to the surface, and generate bulk anion vacancies $V^{\circ}_{I,bulk}$, i.e.

$$V^{\circ}_{I,adj,s} + I^{-}_{I,bulk} \rightleftharpoons V^{\circ}_{I,bulk} + I^{-}_{I,adj,s} \qquad (22)$$

where $I^-_{I,bulk}$ is the iodine ion at an iodine ion site in the bulk.

We further propose that the electron is trapped in the bulk generated anion vacancy sites

$$V^{\circ}_{I,bulk} + e^- \rightleftharpoons V^-_{I,bulk} \tag{23}$$

The electrons trapped at bulk anion vacancy sites can then combine with the tin ions at special tin ion sites in the bulk, $Sn^{2+}_{Sn,bulk}$, to produce tin metal atoms.

$$Sn^{2+}_{Sn,bulk} + 2V^-_{I,bulk} \rightarrow Sn^{\circ}_{Sn,bulk}(s) \tag{24}$$

The inclusion of monovalent dopants (AgI or CuI) enhanced the rates of the photochemical reaction as shown in Figs. 5.10 and 5.11 for both polymorphs of SnI_2. One can therefore infer that anion vacancies generated by the inclusion of these dopants did play a major role in the photolytic process. Monovalent dopants lead to increased anion vacancy concentration (section 6.2), hence if n in eqn. (5) is large, the diffusion of vacancies is further enhanced, therefore increased photodecomposition results. We can therefore assume then that anion vacancy motion into the bulk of the film, from the surface, described by eqn. (22), is the rate limiting process, while reaction steps (18) to (21) are in quasi-equilibrium with the following expressions for the equilibrium constants.

$$K_{(18)} = \frac{[V^+_{Sn,s}]}{[h^+][V^{\circ}_{Sn,s}]} \tag{25}$$

$$K_{(19)} = \frac{[I^{\circ}_{I,adj,s}]\,[V^{\circ}_{Sn,s}]}{[V^+_{Sn,s}]\,[I^-_{I,adj,s}]} \tag{26}$$

$$K_{(20)} = \frac{[I^{\circ}_{(ads)}]\ [V^{\circ}_{I,adj,s}]}{[I^{\circ}_{I,adj,s}]} \tag{27}$$

$$K_{(21)} = \frac{[I_{2(gas)}]}{[I^{\circ}_{(ads)}]^2} \tag{28}$$

From (25),

$$[V^{\circ}_{Sn,s}] = \frac{[V^{+}_{Sn,s}]}{K_{(18)} \cdot [h^{+}]} \tag{29}$$

hence

$$K_{(19)} = \frac{[I^{\circ}_{I,adj}]}{K_{(18)}[I^{-}_{I,adj,s}][h^{+}]} \tag{30}$$

which implies that

$$[I^{\circ}_{I,adj}] = K_{(18)}K_{(19)}\ [I^{-}_{I,adj,s}]\ [h^{+}] \tag{31}$$

On substitution of (31) in (27), we obtain

$$K_{(20)} = \frac{[I^{\circ}_{(ads)}]\ [V^{\circ}_{I,adj,s}]}{K_{(18)}K_{(19)}[I^{-}_{I,adj,s}]\ [h^{+}]} \tag{32}$$

hence

$$[V^{\circ}_{I,adj,s}] = K_{(18)}K_{(19)}K_{(20)}\ \frac{[h^{+}]\ [I^{-}_{I,adj,s}]}{[I^{\circ}_{(ads)}]} \tag{33}$$

From (21),

$$[I^{\circ}_{(ads)}] = \left[\frac{[I_{2(gas)}]}{K_{(21)}}\right]^{\frac{1}{2}} \tag{34}$$

Therefore

$$[V^{\circ}_{I,adj,s}] = K_{(18)}K_{(19)}K_{(20)}K_{(21)}^{\frac{1}{2}} \frac{[h^{+}]\,[I^{-}_{I,adj,s}]}{[I_{2(gas)}]^{\frac{1}{2}}} \qquad (35)$$

If we assume that the surface anion vacancy concentration is much less than the cation vacancy concentration, then we can take the concentration of $I^{-}_{I,adj}$, to be a constant, i.e.

$$[I^{-}_{I,adj,s}] = \text{constant}$$

The readsorption of iodine on the film surface (section 6.1) indicates the presence of a significant vapour pressure of iodine over the film surface, this surface iodine gas concentration is assumed to be a constant, i.e.

$$[I_{2(gas)}] = \text{constant}$$

On the basis of the above assumptions, eqn. (35) then reduces to the form,

$$[V^{\circ}_{I,adj,s}] = K[h^{+}] \qquad (36)$$

This derivation (eqn. (36)) is further strengthened by the relative enhancement of the reaction for films deposited on Tungsten (W) (Fig. 5.10). SnI_2 is a p-type semiconductor, and has a reduced work function compared with tungsten. A depletion region is expected at the W-SnI_2 interface, with W absorbing the electrons from SnI_2 because of the higher work function for W, while holes are created in the SnI_2 as shown in Fig. 6.1. The hole concentration is further increased with photon absorption. Since the anion vacancy concentration is directly related to

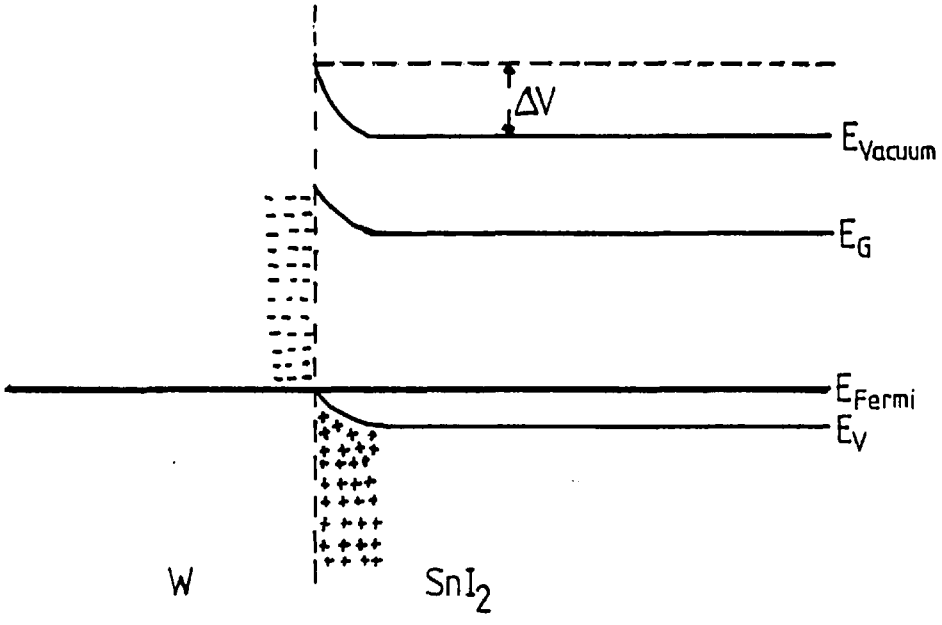

Fig 6·1 Space charge region at the SnI_2-W interface . ΔV is the total potential difference across the p-type space charge region . E_G = 2·358 (α-SnI_2) and 2·495 (β-SnI_2).

the hole concentration (eqn. (36)) increased hole concentration, due to film deposition on W, would therefore enhance the photolytic process. Giving more credence to the above inference is the additional enhancement of the reaction in an oxygen ambient. Oxygen is reputable for absorbing electrons from more electropositive semiconductors, when it is adsorbed on them[11]. We believe oxygen is adsorbed on the SnI_2 film surface, and thus accepts electrons from the SnI_2 at the surface. In this process, holes are created, these therefore influence the reaction with photon absorption when more photoholes are provided. We can therefore conclude that our inference that anion vacancy diffusion into the bulk of the film was the rate limiting process is very valid.

The equations for the electrons, hole and anion vacancy currents perpendicular to the surface can be written as [12].

$$j_h = E_D \mu_h n_h - D_h \frac{\partial n_h}{\partial x} \tag{37a}$$

$$j_e = E_D \mu_e n_e - D_e \frac{\partial n_e}{\partial x} \tag{37b}$$

$$j_v = E_D \mu_v n_v - D_v \frac{\partial n_v}{\partial x} \tag{37c}$$

where the subscripts h, e and v represent the respective quantities for holes, electrons and vacancies respectively.

j indicates the particle current

μ " the mobility of the particles

j_i " the number/cm^2 of species i

E_D " Dember field due to the differences in the diffusion lengths of the species.

D_i " the diffusion coefficient of species i

x " the distance into the film from the free surface

During the photolysis no net particle current flows, hence

$$j_h - j_e + j_v = 0 \tag{38}$$

Due to their consumption in the photolytic process, a complex continuity equation for the holes can be written as[10]

$$\frac{\partial n_h}{\partial t} = - \frac{\partial j_h}{\partial x} + G - R - C \tag{39}$$

where G represents generation of electron-hole pairs

R " the recombination of electron-hole pairs

C " the chemical recombination between holes and iodine ions

The above eqn. (39) can be solved if we assume that we have a steady-state situation in which case $\frac{\partial n_h}{\partial t} = 0$.

Since the reaction is monomolecular, the recombination term R can be related to the concentration and lifetime of electrons and holes and represented as[12]

$$R = \frac{n_h}{\tau_h} = \frac{n_e}{\tau_e} \tag{40}$$

The electron-hole pair concentration is directly related to the light intensity, and their generation rate can be written as[12]

$$G = I \alpha e^{-\alpha x} \tag{41}$$

where I represents the number of photons penetrating the film at $x = 0$, and α is the absorption coefficient of the film.

If we assume that the electrons and holes are only acted upon by the Dember field, E_D, (i.e. no diffusion), and absorption occurs in

a region where $x << \frac{1}{\alpha}$, on substitution of eqns. (40) and (41) in (39), we obtain

$$n_h = I \alpha \tau_h = [h^+] \tag{42}$$

for the linear region, when C is appreciably low.

The anion vacancy motion is mainly due to diffusion, eqn. (37c), therefore reduces to

$$j_v = D \frac{dn_v}{dx}$$

$$= DLn_v \tag{43}$$

where L is an inverse length term.

But

$$n_v = [V^{\circ}_{1,\,adj,s}] \tag{44}$$

$$= K[h^+] \quad \text{from (36)}$$

hence

$$j_v = DLK\,[h^+]$$

$$= DLKI\alpha\tau_h \quad \text{from (42)} \tag{45}$$

The anion vacancy motion is the limiting process in the photolysis mechanism, the anion vacancy current can therefore be equated to the photolysis current, i.e.

$$j_v = j_p = DLKI\,\alpha\,\tau_h \tag{46}$$

The photolytic process is an activated process, eqn. (46) is therefore better expressed as

$$j_p = LI\,\alpha\,\tau_h\,K_p\,e^{-\Delta E/kT} \tag{47}$$

This expression (47), states the direct relationship between the photochemical reaction and light intensity, as obtained in the experimental results (Fig. 5.15) for both polymorphs of SnI_2 in the primary regime.

The pre-exponential factor in eqn. (47) is necessarily different for either polymorph of SnI_2 since the concentration of Schottky defects in the region of phase change (see Figs. 5.9 and 3.16), is not the same on either side of the transition temperature. This change in defect concentration (being higher in the β-polymorph) is believed to compensate for the change in activation energy of photolysis with phase change as observed in Fig. 5.9, since the photolysis current, j_p, must be the same at the phase transition temperature as obtained in Fig. 5.9.

6.6 Model for Photolysis in the Intermediate Regime

The $t^{-3/4}$ regime is believed to be due to the formation of an intermediate product between the linear region (where we have production of discrete tin atoms as outlined in section 6.5), and the $t^{-\frac{1}{2}}$ regime, which is taken to be characteristic of microcrystal (or bulk) tin metal properties (see section 6.7), as was found to be the case for lead in lead iodide[8,13]. The continuous absorption of light and reasonable photon efficiency within this region made us suspect the probable formation of metal clusters. These are inorganic compounds that are covalently bonded together, and have characteristics that are intermediate between simple dimetallic or monometallic covalently bonded compounds and the free metals[14,15]. There is ample evidence of metal cluster formation with light irradiation of silver halides, to give clusters of silver atoms (Ag_n, $n \geq 2$), usually referred to as the latent image[16,17]. There has also been a report of the clustering of tin atoms in KCℓ doped

with $SnC\ell_2$, on β-irradiation[18]. There is some further evidence of the clustering of Sn atoms in the solid state[19-21]. These clusters have tin-tin bonds, which are covalently bonded to each other.

We investigated this idea further by photolysing powder samples of SnI_2 for specific periods, using the experimental arrangement shown in Fig. 6.2. This incorporated the photolysis of SnI_2 samples with unfiltered radiation from a 650W quartz-halogen lamp, using an infra-red lamp as heat source, while photolysis continued with constant passage of oxygen-free-nitrogen gas. The iodine produced as a result of the photolysis was trapped in a 0.25M KI solution (but this was not used for analytical purposes). The powder product of photolysis was subsequently x-rayed, and the x-ray pattern compared with that of an unirradiated powder form. Presented in plate 6.1, are the diffraction patterns of photolysed and unphotolysed red powder samples. The photolysis was for two hours at a temperature of 140°C. The results were similar to those reported in section 5.1 (Plate 5.1), namely more diffraction lines were observed upon photolysis of the sample. An analysis of the diffraction pattern resulting from the photolysed sample (Plate 6.1b and Table 6.2) gave characteristics due to SnI_2, α-Sn (grey tin) and SnO_2. Some extra lines were also obtained, which could not be characterised, and might be due to either Sn_x, or Sn_xO_y; more work would need to be done to be able to characterise these lines.

The production of grey tin is most interesting, if we realise that the experiment was at 140°C, where α-tin should be quite unstable thermodynamically. For the pattern of α-tin to be observed, it means we must have grain sizes of $\gtrsim 40\text{Å}$. Grey tin is a covalently bonded form of tin, and has the diamond structure. It means we must have had isolated pockets of tetrahedrally arranged tin metal atoms, that must

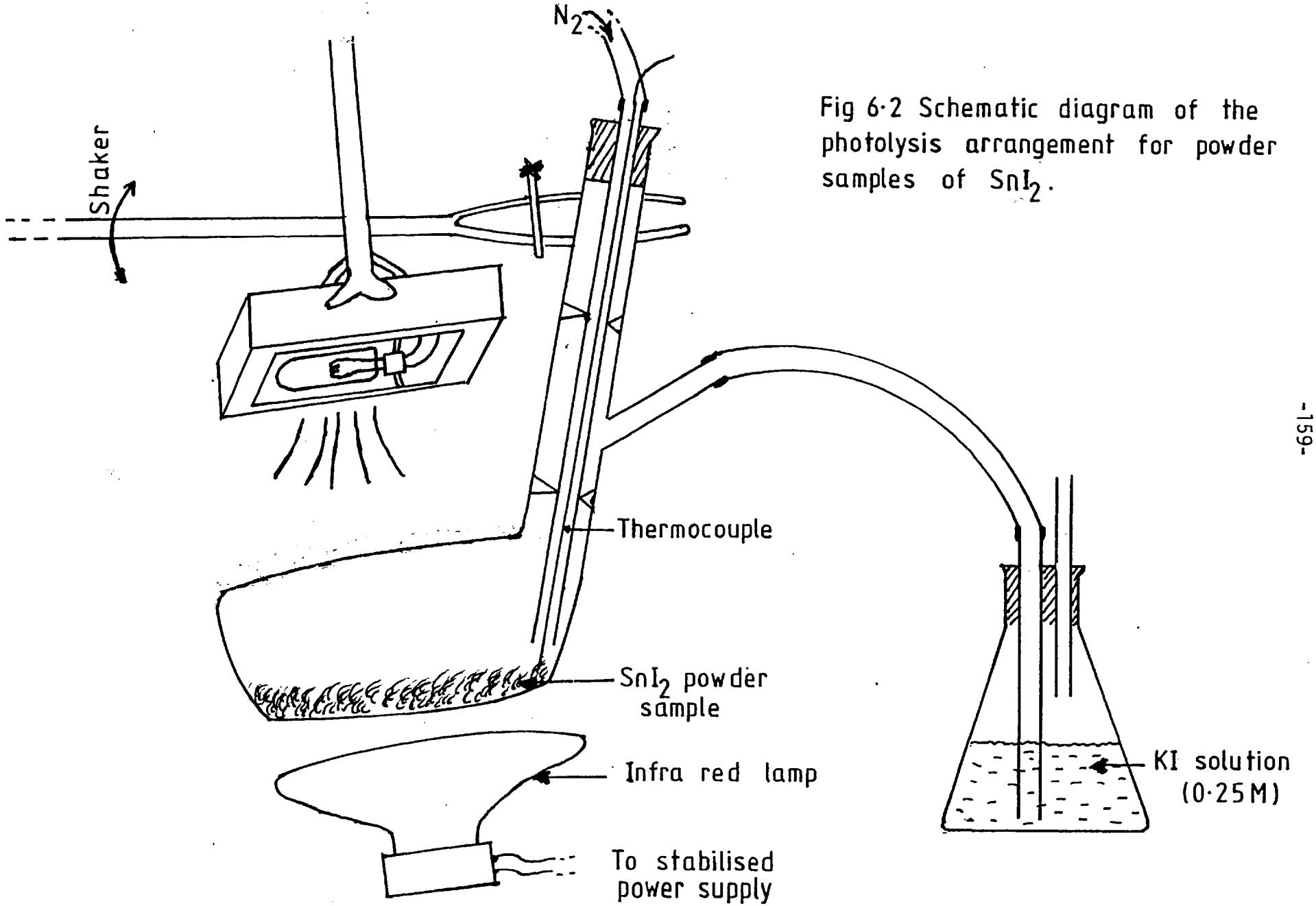

Fig 6·2 Schematic diagram of the photolysis arrangement for powder samples of SnI_2.

Plate 6.1

X-ray diffraction patterns of SnI_2 (α-) powder before (a) and after photolysis (b)

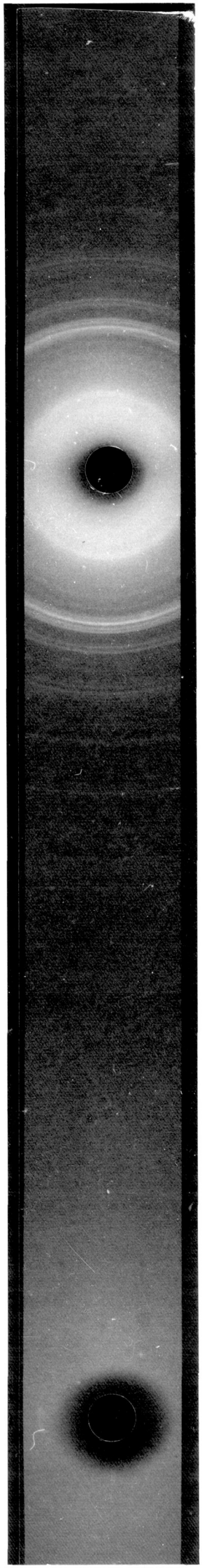

(a)

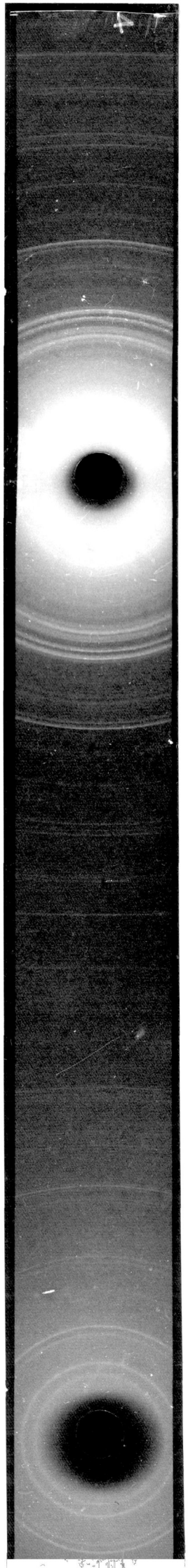

(b)

Line No.	d(A°)	Characteristics	Line No.	d(A°)	Characteristics
1	6.237	?	33	1.998	?
2	5.99	SnI_2	34	1.965	SnI_2
3	5.69	SnI_2	35	1.956	α-Sn ?
4	4.53	Sn_3O_4	36	1.927	SnI_2
5	4.39	SnI_2	37	1.914	?
6	4.21	?	38	1.870	SnI_2
7	3.883	?	39	1.783	SnI_2
	3.753	α-Sn ?			
8	3.651	SnI_2	40	1.681	SnO_2 ?
9	3.540	SnI_4 ?	41	1.664	?
10	3.354	SnO_2 ?	42	1.636	SnI_2
11	3.324	SnI_2	43	1.610	?
12	3.270	SnI_2	44	1.605	SnI_2
13	3.175	SnI_2	45	1.565	SnI_2
14	3.079	SnI_2	46	1.551	SnI_2
15	3.020	SnI_2	47	1.451	?
16	2.867	?	48	1.437	?
17	2.840	?	49	1.423	?
18	2.747	SnI_2	50	1.417	SnO_2 ?
19	2.722	Sn_3O_4 ?	51	1.410	β-SnO ?
20	2.696	SnI_2	52	1.345	?
21	2.682	SnO_2 ?	53	1.329	α-Sn ?
22	2.629	Sn_3O_4 ?	54	1.298	β-SnO ?
23	2.448	SnI_2	55	1.293	?
24	2.295	α-Sn	56	1.278	?
25	2.290	SnI_2	57	1.194	?
26	2.236	SnI_2	58	1.183	SnO_2 ?
27	2.201	?	59	1.174	SnO ?
28	2.165	SnI_2	60	1.169	SnO ?
29	2.137	SnI_2	61	1.165	?
30	2.094	β-SnO ?	62	1.120	?
31	2.071	SnI_2	63	1.105	?
32	2.040	?			

Table 6.2: d(A°) spacings calculated from the diffraction lines of the x-ray pattern of photolysed powder samples

have combined together to give the metal characteristics that we observed in the x-ray pattern resulting from photolysis. We could therefore infer that the production of the grey tin metal must have been through the production of tin metal clusters, Sn_x, which have Sn-Sn metal bonds which are covalent. Sn_x (where $x \geq 2$) could be of any size, ranging from the value of x, but having a basic tetrahedral arrangement of a continuous diamond like structure for $n > 5$. We are therefore able to say (although speculatively) that the photolysis of SnI_2 to achieve bulk metallic properties does go through a transitional tin metal clustering stage.

6.7 MODEL FOR PHOTOLYSIS IN THE TERMINAL STAGE

The $t^{-\frac{1}{2}}$ regime is believed to be due to the observation of bulk metallic properties. It can be taken that the metal clusters have grown to such a size that they tend to behave like bulk metal. We also expect a coalescence of these clusters to bulk metal lattice. A growth of the metal to the surface of the film can therefore be expected.

The low photon efficiency in this region can be rationalised by the fact that not all the incident photons are absorbed by SnI_2, some of them are also absorbed by the tin metal particles generated in the region of the film surface. If the optical absorption coefficient of the tin metal K, as a function of the amount of tin produced, can be represented as[8]

$$K_1 = K_1^{\circ}\phi \tag{56}$$

where K_1° is related to the absorption coefficient at the end of the $t^{-\frac{1}{2}}$ regime, while ϕ is related to the fractional amount of tin produced. ϕ is expected to be equal to 1 ($\phi = 1$) at the end of the $t^{-\frac{1}{2}}$ regime.

If we represent the absorption coefficient of the tin diiodide film by K_2, then the fractional amount of light, I, used in photolysis is

$$I = \frac{K_2}{K_1^{\circ}\phi + K_2} \tag{57}$$

From our results we know that when the concentration of tin atoms is low, the reaction rate is linearly dependent on time (t), and light intensity I_o, i.e.

$$\phi = I_o k' t$$

where K' is a constant.

If we take into account the light lost due to absorption by tin metal particles, we can obtain the following expression for $\phi(8)$

$$\phi = \left[\frac{K_2}{K_1^\circ \phi + K_2}\right] I_o K' t$$

which gives on rearrangement

$$K_1^\circ \phi^2 + K_2 \phi = I_o K_2 K' t$$

thus when $K_1^\circ \phi^2 >> K_2 \phi$, we have

$$\frac{d\theta}{dt} = \frac{(I_o K_2 K')^{\frac{1}{2}}}{K_1^\circ} t^{-\frac{1}{2}}$$

which correlates with what was obtained in our experiment.

REFERENCES

1. R.A. Howie, W. Moser, I.C. Trevena, Acta Cryst. B28, 2965 (1972)

2. A.F. Wells, "Structural Inorganic Chemistry", 4th Edition, Clarendon Press, Oxford, 1975

3. R.C. Weast, "CRC Handbook of Chemistry and Physics", 55th Edition, 1974-75 C.R.C. Press, Ohio

4. J. Schoonman, Solid State Commun. 13, 673 (1973)

5. N.F. Mott, R.W. Gurney, "Electromic Processes in Ionic Crystals", 2nd Edition, Clarendon Press, Oxford, 1948

6. V.S. Vavilov, "Effects of Radiation on Semiconductors", Consultant bureau, New York, 1965

7. H.B. De Vore, Phys. Rev. 102, 86 (1956)

8. M.G. Albrecht, M. Green, J. Phys. Chem. Solids 38, 297 (1977)

9. A.B. Lidiard in "Diffusion"- Americal Society for Metals, Metal Park, Ohio, 1973, chapter 10

10. J.F. Verwey, J. Phys. Chem. Solids 31, 163 (1970)

11. (a) G. Kuwaburg, J. Phys. Soc. Jap. 9, 97 (1954)
(b) R.H. Bube, J. Chem. Phys. 27, 496 (1957)

12. M.D. Tabak, P.J. Warter, Phys. Rev. 148, 982 (1966)

13. J.H. Jacobs, R.A. Corrigan, J. Phot. Sci. 21, 193 (1973)

14. R.B. King in "Progress in Inorganic Chemistry". Edited by S.J. Lipperd, vol. 15, 1972, Willey Interscience, New York

15. E.L. Muetterties, T.N. Rhodin, E. Band, C.F. Brucker and W.R. Pretzer, Chemical Rev. 79(2),91, (1979)

16. G.A. Ozin, H. Huber, Inorg. Chem. 17(1), 155 (1978)

17. E. Mosair, F. Granzer, D. Dautrich, E. Parln, J. Phot. Sci. 25(1), 12 (1977)

18. G.E. Gladyshev, I.B. Dzhelepov, Sov. Phys. Solid State 19(7), 1284 (1977)

19. R.A. Teichman, M. Epting, J. Chem. Phys. 68(1), 336 (1978)

20. J.D. Corbett, P.A. Edwards, J. Chem. Soc. Chem. Commun. 984, (1975)

21. J.D. Corbett, P.A. Edwards, J. Am. Chem. Soc. 99, 3313 (1977)

CHAPTER SEVEN

TECHNOLOGICAL APPLICATIONS OF THE PHOTOLYTIC PROCESS

Apart from our interest in determining the kinetics and mechanism of the photolysis of SnI_2 we have also been interested in any possible potential technological application of this study. Two interests came to mind, these are connected with the production of transparent and semiconducting stannic oxide thin films, and also the delineation of tin metal patterns. Preliminary results in the investigation of these applications are presented in this chapter.

7.1 TRANSPARENT TIN OXIDE FILMS

Stannic oxide SnO_2, is known to be one of several wideband materials which simultaneously exhibit high conductivity. It has found wide application in thin film form as transparent conducting electrodes[1], used for the production of thin film resistors[2], used as transparent heating elements[3], for the production of transistors[4], for transparent antistatic coatings[5], in solar cells [6], in gas sensors[7] and as part of various types of electric equipment where transparency is required[8].

It is generally agreed[1-8] that SnO_2 in its undoped form is a wide band gap n-type semiconductor. Its electrical properties depend largely on deviations from stoichiometry in the material composition and on the presence of unintentionally incorporated dopants in the film. The conductivity is much enhanced when doped with substitutional n-type impurities like Antimony or Indium[8]. Very high conductivities are also obtained when a halogen dopant such as chlorine or fluorine[8] are incorporated in the film.

Several methods have been proposed in the literature for the deposition of thin films of SnO_2. The most promising techniques discussed for thin film formation are:-

(1) sputtering of tin;

(2) vacuum deposition of tin or its compounds;

(3) chemical vapour deposition;

(4) gas phase hydrolysis of stannic chloride, $SnCl_4$, or of other volatile tin compounds;

(5) spraying methods.

Sputtering methods (rf, or dc, reactive or non reactive)[9,10] produce high quality films but the apparatus required is expensive, and their low production rate makes them less useful for mass production. Sputtered films usually need further annealing to stabilise their characteristics[10].

Vacuum deposition methods[6,11] employ either an electron beam or flashing to evaporate the material. They have the same disadvantages for mass production as sputtering methods.

Chemical vapour deposition methods[12,13] produce good quality films. Organometallic compounds are usually employed as the reactants. The deposition set up is rather too expensive to allow mass production of these films.

Gas phase hydrolysis technique involves the precipitation of tin dioxide film from a solution of $SnCl_4$ and water[14]. Annealing at 500°C is usually necessary to lower film resistivity and to stabilise its characteristics. No method has been devised to control the thickness of the deposited film.

Spraying methods[15,16] are based on the pyrolytic decomposition of a tin compound in a liquid mixture sprayed onto a previously heated

substrate. This method also suffers from the relative cost of the equipment needed to make it feasible for mass production. The temperature requirement is too high (∿700°C), the thickness of films has not been adequately controlled.

We have been able to produce highly transparent SnO_2 films by a photolytic process. The method we shall describe is much simpler, and much less costly than those earlier described. The simplicity of the apparatus and process might make mass production feasible.

7.2 PRODUCTION OF SnO_2 FILMS

The production of tin dioxide films in this work is a two step process. The first step involves the evaporation of tin diiodide in a vacuum chamber, while the second step involves the photolysis of the SnI_2 film in air or oxygen ambient.

The set-up for the evaporation of SnI_2 on soda glass substrates has been described in Chapter Three. Source temperatures between 350 and 400°C have been found suitable for the evaporation rates desired (150 - 400 A°/min). The films were condensed on clean room temperature soda glass substrates, and were therefore of the β-polymorph. Thickness of the films was determined by the use of the quartz crystal microbalance method, as also described in Chapter Three.

Thin films of SnI_2,as prepared above, were subsequently photolysed in atmospheric air or oxygen, using unfiltered light from a 650 watt quartz halogen lamp. It has been shown in Chapters Five and Six that the photolysis of SnI_2 was enhanced by carrying out the process in low pressure air or oxygen ambient. The use of much higher light intensities than those employed in Chapter Five and atmospheric air or oxygen pressure has resulted in the tin atom produced (by the photolysis

of SnI_2, see Chapter Five) reacting with the oxygen in the ambient to form SnO_2. The net reaction can therefore be represented as

$$SnI_2 + O_2 \xrightarrow[140\text{-}150°C]{h\nu} SnO_2 + I_2 \uparrow \qquad (7.1)$$

or

$$SnI_2 + 2H_2O \xrightarrow[140\text{-}150°C]{h\nu} SnO_2 + 2HI \uparrow \qquad (7.2)$$

or a combination of both, in the case of air ambient.

The photolytic process has been carried out on films heated to a temperature of between 140 to 150°C. Complete photolysis of the SnI_2 film to SnO_2 was found to be fast, taking about 10 to 12 minutes for a film 1.5 μm thick. The rate of photolysis (time to photolyse a given thickness of SnI_2 film) was found to be independent of the rate of deposition of the films (i.e. no grain size effect). The tin dioxide films were observed to be quite transparent. Films produced in air had a light yellow colour taint, while this was absent in films produced in pure oxygen. The films have been observed to be stable and have good adherence to the glass substrates. They also appear to have appreciable mechanical strength.

7.3 PHYSICAL PROPERTIES OF SnO_2 FILMS

We have examined the optical, electrical and crystallographic properties of SnO_2 films prepared by our method. These have been found to compare favourably with those obtained for SnO_2 films prepared by other methods.

7.3.1 Optical Characteristics

The room temperature optical transmission of our films has been investigated in the wavelength region 0.225 to 0.7 μm, i.e. across

the visible and the ultra violet, using a Unicam Instrument Spectrophotometer. The spectra obtained are as shown in Fig. 7.1 for two films of SnO_2 obtained by the photolysis of SnI_2 in air. The films were found to be appreciably transparent, ~100% in the visible, as have been reported for films of SnO_2 prepared by other methods[1,8]. The results obtained by Arai[17] for SnO_2 films prepared by evaporation techniques are shown for comparison. The absorption edge of our films is quite well defined, with an absorption edge at about 331 nm (3.75 eV), which is comparable with the 3.7 - 3.8 eV characteristic of undoped SnO_2 films[8,18].

The absorption coefficient, α, as obtained from the expression

$$\alpha = \frac{2.303}{x} \log \left(\frac{1}{T}\right) \qquad (7.3)$$

after assuming that the reflection from the surface of the film was negligible. x in the above expression represents the film thickness and T, the transmittance of the film.

A plot of α^2 against photon energy in eV is shown in Fig. 7.2. The optical transition is observed to be allowed direct (see Chapter Three), with direct transition energies lying between 3.76 and 3.78 eV. These values tie up with the value of 3.7 eV obtained by Reddaway and Wright[19] and 3.7 to 3.8 eV obtained by Arai[17], for undoped SnO_2.

7.3.2 Electrical Properties

The resistivity of the SnO_2 films was determined at room temperature and elevated temperatures. The determination was in vacuum. A plot of resistivity against reciprocal temperature for films of SnO_2 are as shown in Fig. 7.3. The films are observed to be quite resistive.

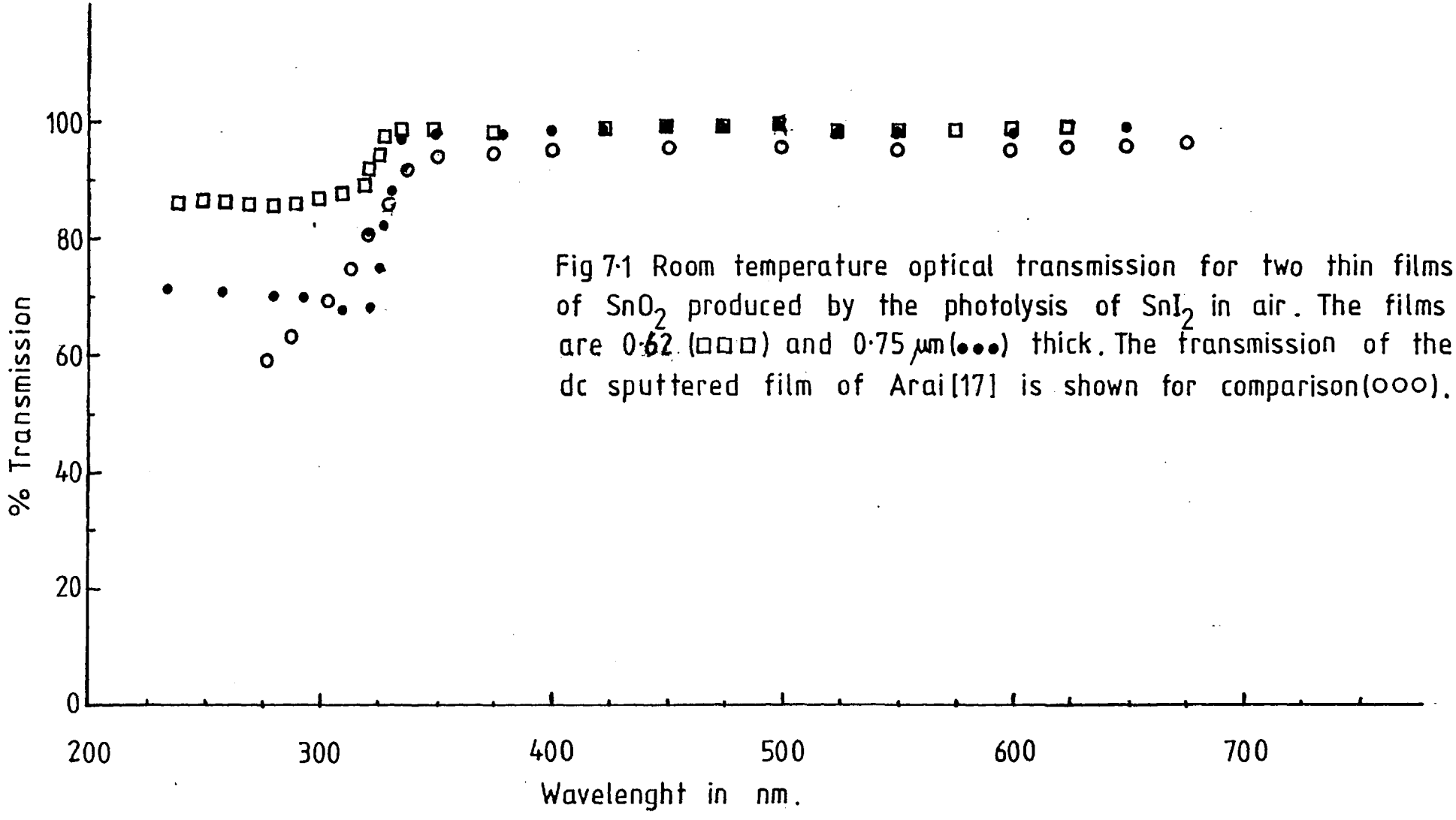

Fig 7·1 Room temperature optical transmission for two thin films of SnO_2 produced by the photolysis of SnI_2 in air. The films are 0·62 (□□□) and 0·75 μm (●●●) thick. The transmission of the dc sputtered film of Arai [17] is shown for comparison (ooo).

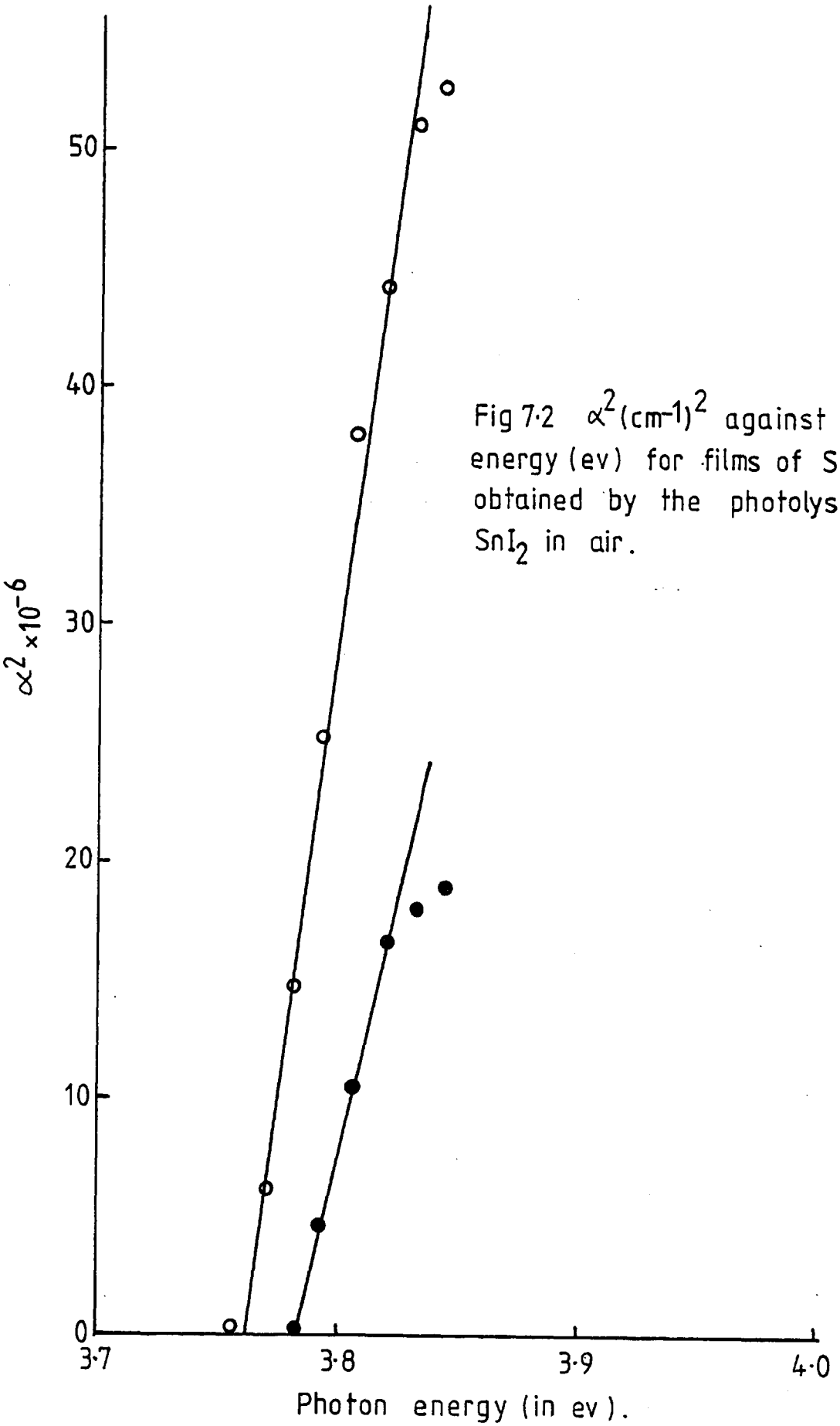

Fig 7·2 $\alpha^2(cm^{-1})^2$ against photon energy (ev) for films of SnO_2 obtained by the photolysis of SnI_2 in air.

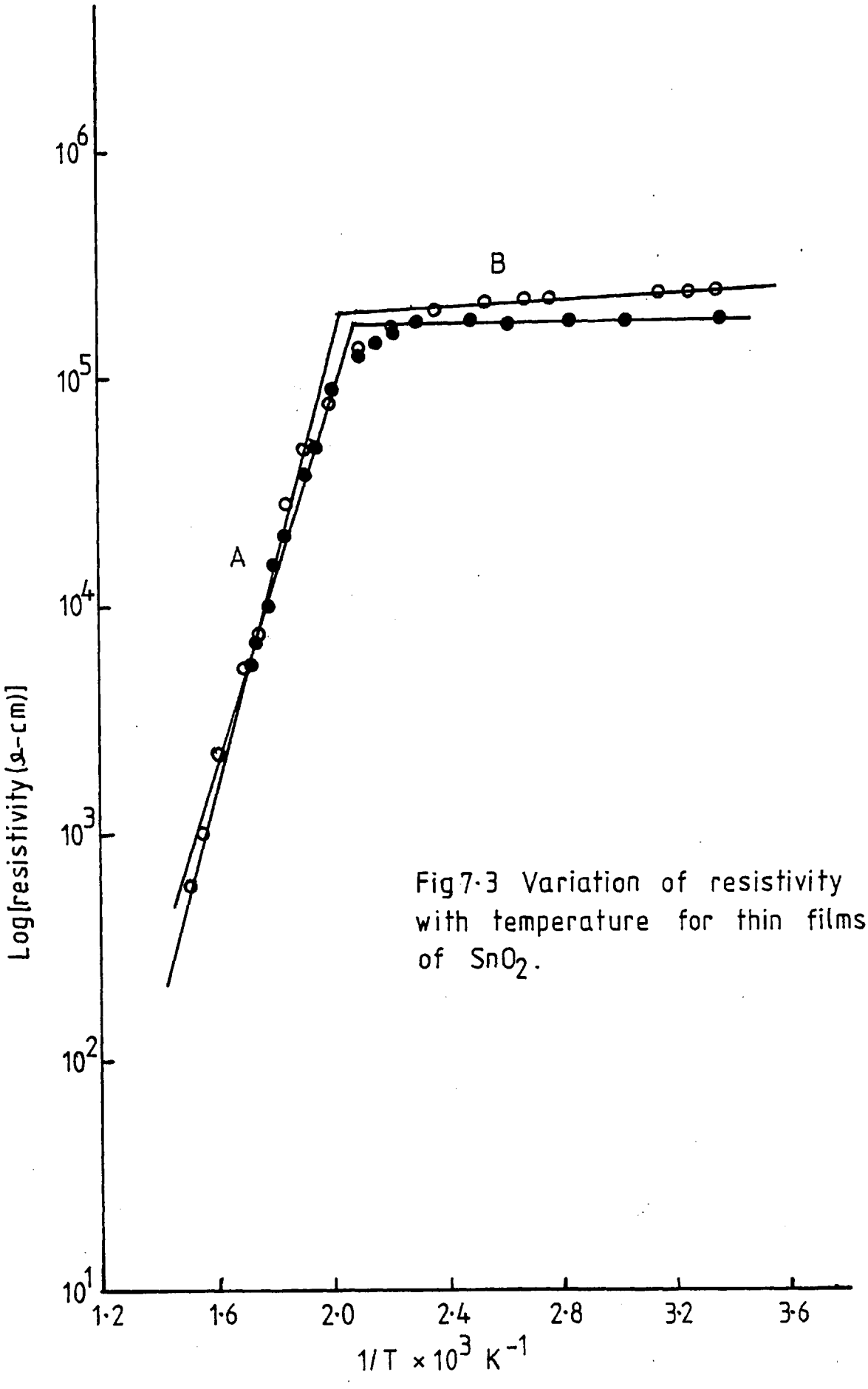

Fig 7·3 Variation of resistivity with temperature for thin films of SnO_2.

The temperature dependence of resistivity is found to divide into two regimes, labelled A and B, with activation energies 1.04 and 0.015 eV respectively. This temperature dependence of resistivity of the SnO_2 films has also been observed by Bartholomew et al[20], Muranoi et al[21] and Arai[17] for undoped SnO_2 films. In region B, the films are appreciably insulating and may therefore be assumed to be due to the stoichiometric nature of the films, even though the resistivity of "stoichiometric" SnO_2 films is reported to be in the neighbourhood of 10^8 Ω cm[1]. The decrease in the resistivity in region A is interpreted to be due to the non-stoichiometry of the films. The resistivity measurement was in vacuum; there is the possibility of loss of oxygen from the film by outdiffusion from the film surface, thus leading to increased oxygen vacancy in the film and consequently increased conductivity. The conductivity of the SnO_2 films in the undoped form has been shown in the literature to be due to the non-stoichiometry of the films[8], while conductivity in doped films has been shown to be due to impurity centres[8,17].

7.3.3 X-ray Analysis

Thin films of SnO_2 prepared by the photolytic process were x-rayed, using a cylindrical texture x-ray camera arrangement. No diffraction lines were obtained for repeated runs on different samples. This would point to the prepared films being fine grained polycrystalline or amorphous: this was as expected. All our films were prepared from photolytic reactions that took place on a glass substrate kept at a temperature between 140 and 150°C. For films deposited by the spraying method[16], or the chemical vapour deposition method[21], or the sputtering method[22], x-ray studies have revealed that films grown on substrates kept below 350°C were found to be structureless while those

grown on substrates kept above 350°C were polycrystalline[16,21,23]. The amorphous nature of films grown below 350°C was confirmed by electron microscopy[16] which means that fine grained polycrystalline films can be excluded as an alternative to amorphous.

7.3.4 Discussion

No attempt has been made in this work to follow the kinetics of the formation of tin dioxide films from the photolylic decomposition of SnI_2 in oxygen or air. We have only investigated the possibility of producing thin films of SnO_2 by photolytic means at considerably reduced temperature, from those that obtain by the use of other methods. It is possible however that the kinetics would divide into two time regimes, an initial short time regime in which the iodine anion vacancy motion from the surface of the SnI_2 film to generate I_2 (which can then desorb as postulated in Chapter Six) is rate limiting. The adsorption of oxygen on the film surface has been observed in Chapter Five to influence anion vacancy notion, since the oxygen makes the SnI_2 film more p-type, and thus leads to faster photodecomposition with photon absorption, to produce tin atoms and iodine gas molecules. However as the reaction proceeds, the diffusion of oxygen atoms into the SnI_2 film to react with the bulk generated tin atoms may become rate limiting. It is likely that the oxygen atoms move into the SnI_2 film through the grain boundaries to react with tin atoms, thus precipitating SnO_2. The iodine is still generated at the surface either as distinct iodine molecules or as HI molecules or as oxyiodides.

With this process, it has been possible to produce transparent and semi-insulating SnO_2 films at fairly low temperatures (140-150°C) unlike other preparative methods which require temperatures in excess of 250°C. The thickness of the film is determined by that of the SnI_2 film,

so is the grain size, except this can be improved upon by annealing at higher temperatures (>150°C).

We are of the opinion that the conductivity of the films can be increased by doping the SnI_2 charge with suitable photosensitive dopants like SbI_3, InI_3 or CuI etc before photodecomposition. The photolytic characteristics of these dopants are not known in detail, but their incorporation into the SnI_2 film is quite feasible.

7.4 METAL FILM PRODUCTION

The increasing density of integrated circuits has put a greater demand on the method of laying metal patterns on these devices for interconnection purposes. Metal patterns have been delineated on these devices by a variety of methods which include electroless plating[23], lithographic methods (x-ray[24], electron beam[25], and photolithography[26]) which also involve dry etching techniques[27], and the lift-off technique[28]. Some other alternative methods of depositing conductive metal patterns have already been described in the literature[29-31]. The method described in this section is similar to that employed by Green and Albrecht[29] in the deposition of conductive lead patterns.

The process involves the photolysis of tin diiodide. The production of tin metal patterns by the photolysis of SnI_2 is a four stage process. The first two stages have already been described (section 7.2) in connection with the production of SnO_2. These involve the evaporation of SnI_2 in vacuum, and subsequent photolysis in air or oxygen ambient. The only modification to the above process is that glass or metal masks are used during the photolysis stage. The last two stages in the process step involve the re-evaporation of unphotodecomposed regions of SnI_2 (protected by the mask) in a vacuum equipment, and the subsequent reduction of the tin dioxide pattern to tin metal

STAGE ONE — Evaporation of SnI_2 on soda glass.

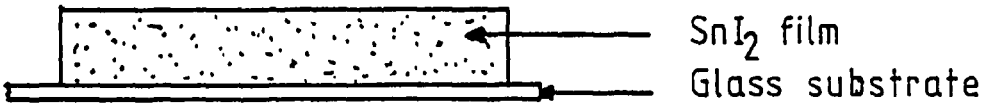

STAGE TWO — Photolysis of SnI_2 film through a Chrome glass plate contact mask.

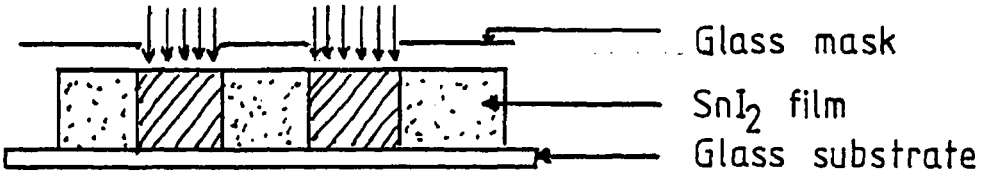

STAGE THREE — Re-evaporation of unexposed SnI_2 regions in the vacuum.

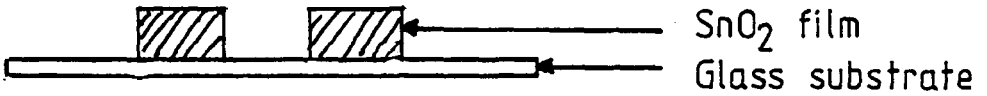

STAGE FOUR — Reduction of SnO_2 film in a plasma of atomic hydrogen to generate tin metal.

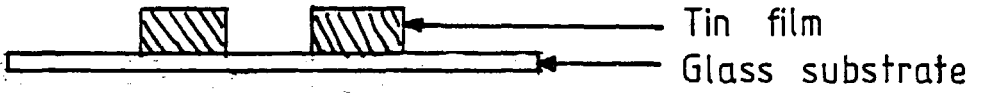

Fig 7·4 The process stages for the production of tin metal patterns by the photolysis of SnI_2 in air or oxygen.

patterns, in a plasma of atomic hydrogen, produced in a microwave discharge cavity. The process steps are as shown in Fig. 7.4.

7.4.1 Evaporation of SnI_2

Thin films of SnI_2 were evaporated as detailed in Chapters Three and Four. Films were evaporated on clean soda glass substrates. The rate of evaporation was 400 to 600A°/min; this was needed to ensure the growth of small grain size platellets (needed to avoid light scattering due to roughness). Films were grown on room temperature substrates, and the thickness varied between 0.7 and 4.0 μm.

7.4.2 Photolysis of SnI_2 Films

The films prepared as indicated above were irradiated with unfiltered collimated beam of light from a 650 watt quartz halogen lamp. A chrome glass plate contact mask was placed on the film and the film irradiated through this mask. Metal masks were also employed for the oxydation. Most of the photolysis was carried out at 150°C. The film in the path of the light was usually completely converted to SnO_2, so as to eliminate undercutting that may result with the re-evaporation of some of the SnI_2 lying under the SnO_2 cap, during the next stage of the process. A film of about 1.5 μm in thickness would be completely converted to SnO_2 in 10 to 12 minutes, at a photolysis temperature of 150°C.

7.4.3 Re-evaporation of SnI_2 Films

After photolysis, the film was usually returned into the vacuum system and placed in a jig similar to that of Fig. 3.2. The film is heated to a temperature of between 200 and 300°C so as to re-evaporate the SnI_2 from the regions of the film protected by the mask during the photolysis stage. Too severe a heat off was avoided, so as to avoid local thermal decomposition of the SnI_2, as was observed to be the case in

PbI_2[32]. A uniform heating of the film is also necessary, as a temperature gradient across the film might result in a region of the film re-evaporating faster than the other regions. For a typical run, a film 2.5 μm thick would re-evaporate completely in about one hour at a temperature of 250°C. Shown in Plate 7.1(a) is the picture of a re-evaporated film of SnI_2. The width of the lines are as indicated in thou (1 thou = 25 μm). The lighter regions represent areas of re-evaporation, and the darker regions, the SnO_2 film.

7.4.4 Reduction of SnO_2 Pattern to Sn Pattern

The next stage is to reduce the SnO_2 pattern on the soda glass substrate to metallic tin. This is achieved by a dry chemical reduction process. The reduction is accomplished in a plasma of atomic hydrogen generated in a microwave cavity. The set-up for the reduction process is as shown in Plate 7.2. We have employed a "Microtron 200" microwave power generator (supplied by Electro Medical Supplies Ltd.) to excite the hydrogen discharge. The film to be reduced is placed in a glass envelope in the gas discharge cavity. Flasks of pure hydrogen and pure nitrogen gas were directly connected to the sample chamber (see Plate 7.2). The set-up is initially pumped down to a pressure of about 10^{-2} torr by means of a rotary pump.

Prior to plasma generation, the sample holder and the column of glass connecting the sample holder to the gas flasks are heated to a temperature of between 80 and 100°C, so as to preheat the gas and the sample before the reduction is carried out. This is to prevent film rupture such as that observed when the films were reduced at room temperature.

The "Microtron 200" microwave power generator has an output power of between 20 and 200 watts, at an operating frequency of 2450 megacycles (12.5 cm). An output power of about 70 watts was found to be

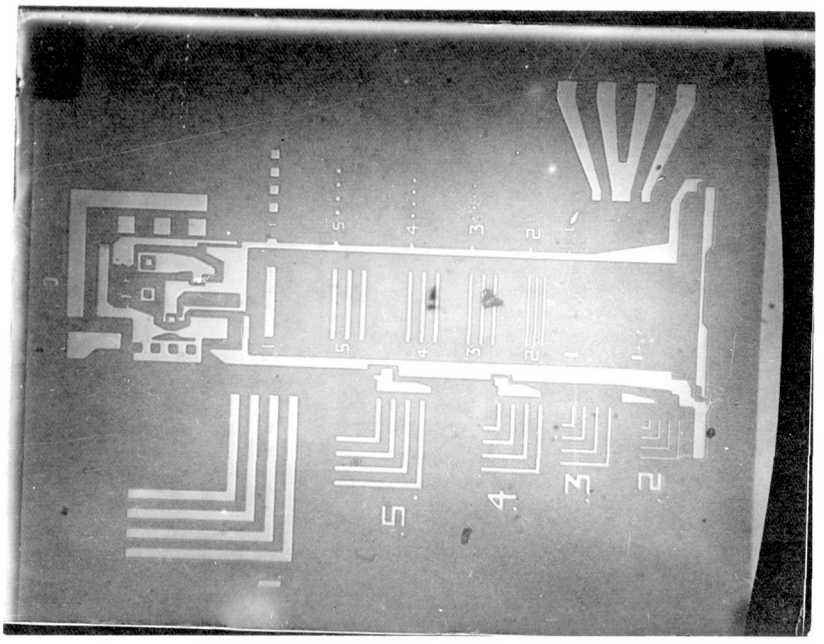

(a)

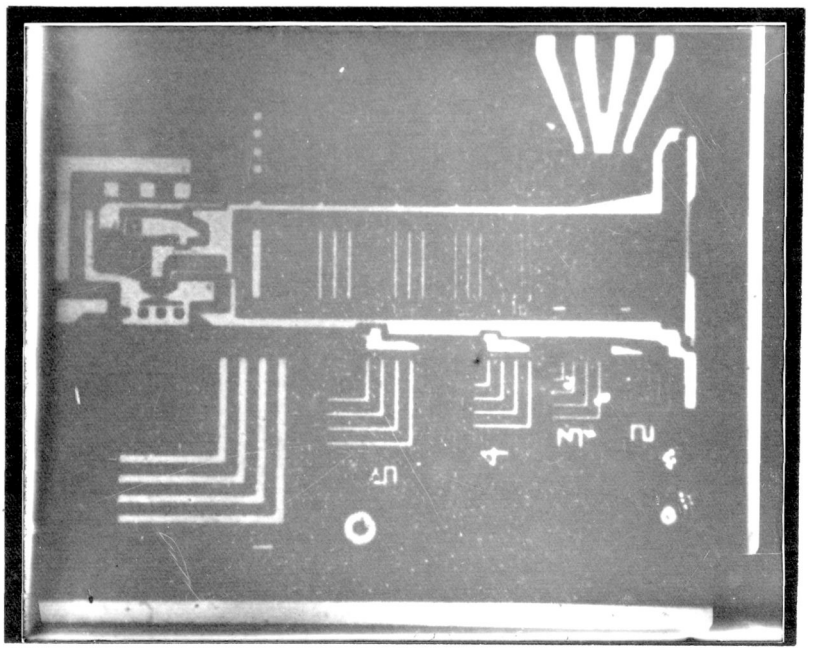

(b)

Plate 7.1: Photographs of patterns generated on soda glass. (a) is for a film that has undergone the processes of photolysis and re-evaporation of SnI_2, while (b) is for a film that has gone through all the four process stages.

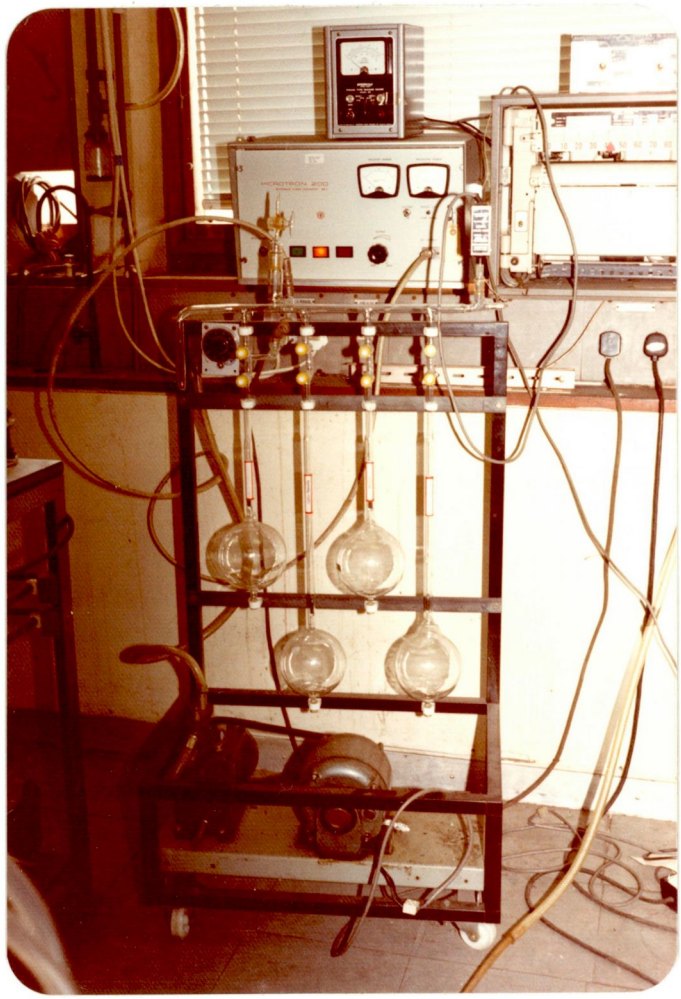

Plate 7.2: The experimental set-up for the reduction of SnO_2 film to Sn film. The Microtron 200 microwave power supply is in the top left-hand corner, while the Quick-Fit glass assembly, used as the sample holder, is just in front of the power supply. The sample holder fits into the the microwave discharge cavity. The glass flasks contained the H_2 and N_2 needed for the process.

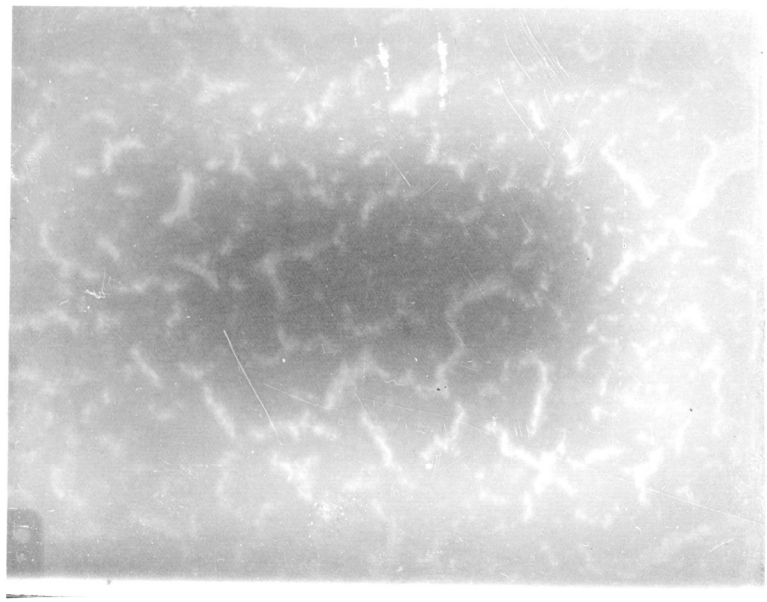

Plate 7.3: The grainy nature of the Sn film prepared by our process (x 450).

Film thickness is 1.8 μm and the film resistivity is 3.8×10^{-2} Ω cm

sufficient for our application. This was needed to maintain the gas ionisation after an initiation of the ionisation of the hydrogen gas by the use of a "Tesla Coil". A film 1.5 μm thick would be completely reduced in 20 minutes at a temperature of 90°C. Presented in Plate 7.1(b) is the reduced pattern resulting from a film that had gone through all the four processing stages already described. The dark parts are the tin metal patterns, while the white lines represent areas where SnI_2 had been re-evaporated in the preceding process stage. It can be seen that little or no resolution is lost from this stage when compared with that of Plate 7.1(a).

7.4.5 Discussion

The tin metal patterns produced from the process steps outlined above have been observed to be grainy, as shown in Plate 7.3. They are however reasonably conductive with a typical room temperature resistivity of 0.42 Ω cm for an initial SnI_2 thickness of 1.57 μm. The resistivity improved with initial SnI_2 film thickness, with a typical value of 4.7×10^{-3} Ω cm for a SnI_2 film thickness of 3.55 μm. The bulk resistivity of grey tin is $\sim 1 \times 10^{-5}$ Ω cm[33].

The metal films were observed not to flake off, the adhesion between the film and the substrate is quite appreciable (which cannot be said for Pb produced in this way).

It is believed that resolutions in the sub micron range are possible with this process because of the special advantage that the SnI_2 film can be completely oxidised by photolysis to tin dioxide, which has good adhesion characteristics to the glass substrate (section 7.2). From the work of Green and Albrecht[32] on PbI_2, they observed that it was the sidewise evaporation of PbI_2 (under the PbO cap) during the re-evaporation stage that affected the resolution obtainable. This effect is eliminated when complete photolysis is carried out.

This technique might find useful application in the microelectronics industry, and more so in the production of fine tin microstrip lines for Josephson junction applications which is presently being developed[34-36]. Annealing the films at temperatures >150°C should give films suitable for the above applications.

REFERENCES

1. R.E. Aitchison. Australian J. Appl. Sci. 5, 10 (1954)

2. L. Maissel in L. Maissel and R. Glang (eds) "Handbook of Thin Film Technology". McGraw-Hill, New York (1970), p.18-23

3. J.W. Ward, Appl. Ind. 16, 408 (1955)

4. A. Aoki and H. Sasakura. Japan J. Appl. Phys. 9, 582 (1970)

5. L. Holland and G. Siddal, Vacuum 3, 375 (1953)

6. T. Feng, A.K. Ghosh, C. Fishman. J. Appl. Phys. 50 (12), 8070, (1979)

7. M. Nitta, S. Ohtani and M. Haradome. J. Electron. Mater. 9 (4), 727, 1980

8. Z.M. Jarzebski and J.P. Marton. J. Electrochem. Soc.
123(7), 199C,(1976)
123(9), 299C,(1976)
123(10),333C,(1976)

9. E. Giani and R. Kelly. J. Electrochem. Soc. 121 (3), 394 (1974)

10. E. Leja, T. Pisarkiewicz and A. Kolodziej. Thin Solid Films 67 (1), 45 (1980)

11. J.C. Manifacier, M. de Murcia and J.P. Fillard. Thin Solid Films 41, 127 (1977)

12. Yar-Sun Hsu, S.K. Ghandhi. J. Electrochem. Soc. 127 (7), 1592 (1980)

13. O. Tabata and T. Tanaka. Surf. Sci. 86 (2), 230 (1979)

14. G.N. Advani, A.G. Jordan, C.H.P. Lupis and R.L. Longini. Thin Solid Films 62, 361 (1979)

15. J.C. Manifacier, L. Szepessy, J.F. Bresse, M. Perolin and R. Struck. Mater. Res. Bull. 14, 109 (1979)

16. J.S. Maudes, T. Rodringuez. Thin Solid Films 69, 183 (1980)

17. T. Arai. J. Phys. Soc. Japan 15, 916 (1960)

18. W. Spence. J. Appl. Phys. 38 (9), 3767 (1967)

19. S.F. Reddaway and D.A. Wright. Brit. J. Appl. Phys. 16, 195 (1965)

20. R.F. Bartholomew and H.W. Garfinkel. J. Electrochem. Soc. 116, 1205 (1969)

21. T. Muranoi and M. Furukoshi. Thin Solid Films 48, 309 (1978)

22. E. Giani and R. Kelly. J.Electrochem. Soc. 121, 394 (1974)

23. L.K.H. van Beek. Philips Tech. Rev. 33, 1 (1973)

24. K.D. Kolwicz and M.S. Chang. J. Electrochem. Soc. 127 (1), 135 (1980)

25. G.A.C. Jones, H. Ahmed. New Electron 13 (6), 34, 40, 42, 46 (1980)

26. T.F. Deutsch, D.J. Ehrlich and R.M. Osgovel, Jnr. Appl. Phys. Lett. 35 (2), 175 (1979)

27. R.L. Maddox. Microelectronics Journal 11 (1), 4 (1980)

28. L.M. Ephrath, T.H. Ning. IBM Disclosure Bull. 22 (8B), 3869 (1980)

29. M. Green and M.G. Albrecht Thin Solid Films 37, L57, (1976)

30. S.M. Metev, S.K. Savtchenko and K.V. Stamenov. J. Phys. D. 13 (4), L75 (1980)

31. V.M. Koleshico, B.S. Reznikov and E.A. Utkina. Inorg. Mater. (USA) 15 (5), 612 (1979)

32. M.G. Albrecht. Ph.D. thesis, Imperial College London, 1975

33. J. Donaldson. Tin Research Institute Information Booklet, 1970

34. V.N. Gubankov, V.P. Koshelets and G.A. Ovsyannikov. Sov. Phys. Tech. Phys. 24 (4), 481 (1979)

35. L.N. Smith. J. Low Temp. Phys. 38 (5-6), 553 (1980)

36. M. Octavio and W.J. Skocpol. J. Appl. Phys. 50 (5), 3505 (1979)